Turkish Journal of REMOTE SENSING

Türkiye Uzaktan Algılama Dergisi

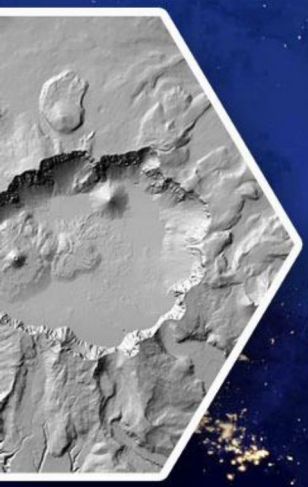

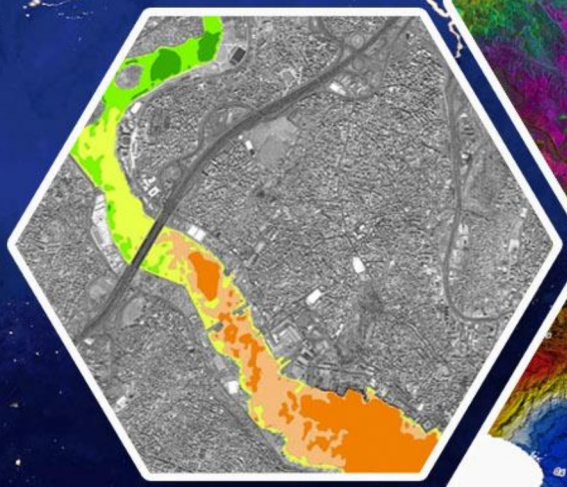

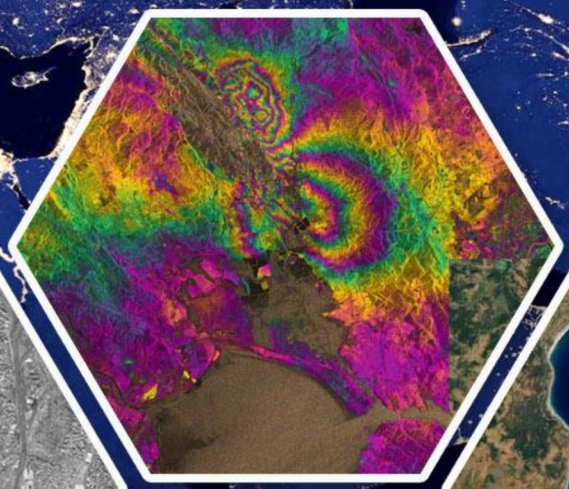

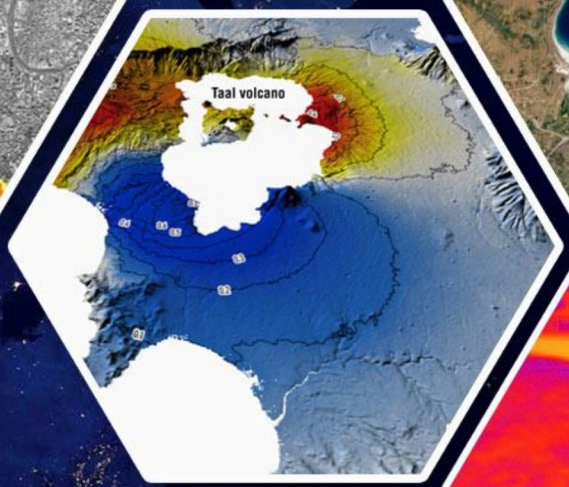

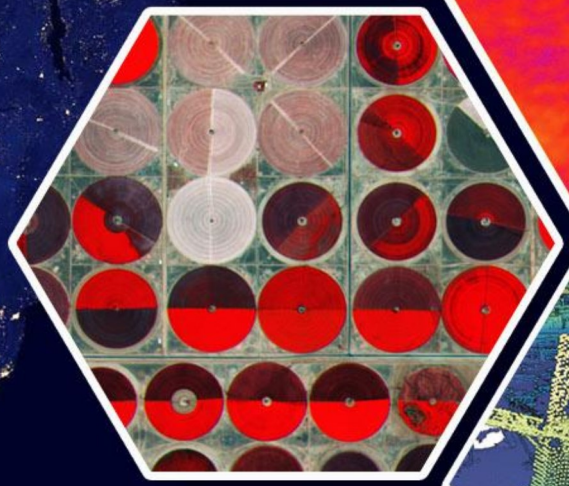

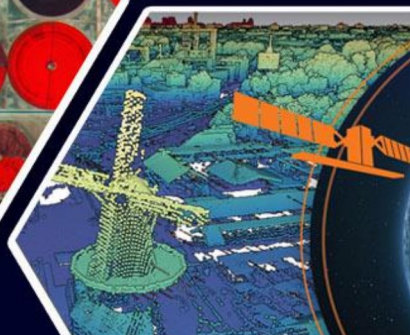

Vol/Cilt:6
Issue/Sayı:1
June/Haziran, 2024

e-ISSN: 2687-4997

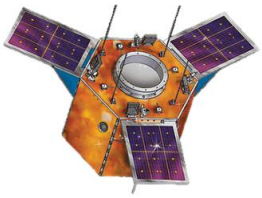

Türkiye Uzaktan Algılama Dergisi

Dergi Hakkında

Türkiye Uzaktan Algılama Dergisi (TUZAL) bilim ve teknolojideki gelişmelere paralel olarak Uzaktan Algılama alanındaki yeniliklerle ilgili yapılan çalışmaları yayınlayan ve Uluslararası İndeks ve Veri tabanlarında taranan bir dergidir.

Amaç & Kapsam

TUZAL Dergisi,

- Uzaktan Algılama alanında ulusal ve uluslararası gelişmeleri Harita, jeoloji, Çevre, Elektrik ve Elektronik, Bilgisayar vb. mühendislik alanı ile ilgilenen bilim insanlarının bilgisine sunmak,
- Konu ile doğrudan veya dolaylı etkinliklerde bulunan bilim insanları, araştırmacılar, mühendisler ve diğer uygulayıcılar arasındaki bilgi ve deneyim paylaşımını güçlendirecek ve hızlandıracak, kolay erişilebilen, geniş katılımlı bir tartışma ortamı sağlamak ve bunları yayma olanağı yaratmak,
- Türkiye'nin teknolojik ve ekonomik kalkınmasında rol oynayabilecek Uzaktan Algılama teknolojisine ilişkin sorunların daha etkin bir şekilde çözüme kavuşturulması açısından büyük önem taşıyan kurumlar arası işbirliğinin başlatılmasına ve geliştirilmesine katkıda bulunmak,
- Türkçe`nin Uzaktan Algılama alanında bilim dili olarak geliştirilmesini ve yabancı sözcüklerden arındırılmasını özendirmek amaçlarına sahiptir.

Dergisinin kapsamı;

Temel Uzaktan Algılama Uygulamaları,

RADAR/SAR/LIDAR,

Hiperspektral uzaktan algılama,

Görüntü sınıflandırma ve analiz yöntemleri,

Radyometrik düzeltme için atmosferik modellemenin geliştirilmesi,

Uygu verilerinden elde edilmiş parametrelerin modellenmesi

Küresel modelleme, izleme ve sürdürülebilir kalkınma için küresel veri tabanı ve değişim göstergelerinin belirlenmesi,

Laboratuvar ve yerinde test yöntemleri kullanarak veri ve bilginin kontrolü,

Uzaktan algılama ve CBS yöntemlerinin entegrasyonu,

CBS Uygulamaları,

İnsansız Hava Araçları (İHA) ve Yersel Lazer Tarama ile gözlem uygulamaları,

Havasal ve Uzaysal Uzaktan Algılama

Afet ve risk etkilerinin azaltılması için bilgi desteği: erken uyarı sistemleri, etki değerlendirmesi, izleme, esneklik ve risk azaltma çalışmaları,

Çevre kirliliği: değerlendirme ve etki çalışmaları,

Jeoloji, Jeomorfoloji ve Pedolojide Yeryüzü Bilimi Uygulamaların ile uzaktan algılanmış girdilerin entegrasyonu,

Sürdürülebilir tarımsal üretim ve tarımın korunması için tarım ürünlerinin büyümesinin çok boyutlu izlenmesi,

İklim değişikliği çalışmaları,

Arazi kullanımı/örtüsünün küresel ve bölgesel dinamikleri, biyo-çeşitlilik, bozulma,

Çölleşme ve kuraklık çalışmaları,

Topraklar, bitki örtüsü ve iç, kıyı ve okyanus sularında karbon akıları,

Su kalitesi çalışmaları vb.

Yayınlanma Sıklığı Yılda 2 sayı(Haziran-Aralık)

ISSN 2687-4997

WEB https://dergipark.org.tr/tr/pub/tuzal

İletişim osmanorhan@mersin.edu.tr / tuzaldergisi@gmail.com/ osmanorhan44@gmail.com

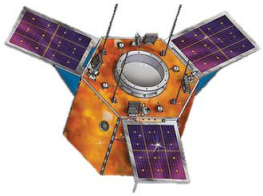

Turkish Journal of Remote Sensing

About Journal

Turkish Journal of Remote Sensing publishes studies related to innovation in the field of Remote Sensing parallel to the developments in science and technology and indexed in the International Index and database.

Aim & Scope

The Journal,

- To present to the knowledge of National and international developments in the field of Remote Sensing to scientists related with Geomatics, Geology, Environment, Electric and Electronic, Computer etc. engineering fields.
- To provide an easily accessible, broadly attended discussion environment that will strengthen and accelerate the sharing of knowledge and experience between scientists, researchers, engineers and other practitioners who engage in direct or indirect activities with the subject, and create an opportunity to disseminate them,
- Turkey's technological and economic development in the problems related to remote sensing technology that can more effectively play a role of great importance in terms of inter-agency cooperation to be initiated and resolved to contribute to the development,
- It has the aim of encouraging the development of Turkish as a scientific language in the field of Remote Sensing and to be free from foreign words.

Scope of The Journal;

- ✓ Basic remote sensing applications,
- ✓ RADAR/SAR/LIDAR,
- ✓ Hyperspectral remote sensing,
- ✓ Image classification and analysis methods,
- ✓ Development of atmospheric modelling for radiometric correction,
- ✓ Determine global database and alteration indicator for global modelling, monitoring and sustainable development,
- ✓ Data and information control using laboratory and in-situ tests,
- ✓ Integration of remote sensing and GIS methods,
- ✓ CBS Uygulamaları,
- ✓ İnsansız Hava Araçları (İHA) ve Yersel Lazer Tarama ile gözlem uygulamaları,
- ✓ Havasal ve Uzaysal Uzaktan Algılama
- ✓ Information utility for reducing disaster and risk effects: Early warning systems, impact evaluation, monitoring, flexibly and risk reducing studies,
- ✓ Environment pollution: Evaluation and effect studies,
- ✓ Integration of Earth science applications in Geology, Geomorphology and Pedology with remote sensing data
- ✓ Multidimensional monitoring of growth of agricultural goods for sustainable agricultural production and protection of agriculture
- ✓ Climate change studies,
- ✓ Land use/ Dynamics of global and regional land, biodiversity, deterioration,
- ✓ Carbon amount in Earth, plant cover and in shore, ocean waters,
- ✓ Water quality studies etc.

Publication frequency Biannual (June-December)

ISSN 2687-4997

WEB https://dergipark.org.tr/tr/pub/tuzal

Contact osmanorhan@mersin.edu.tr / tuzaldergisi@gmail.com/ osmanorhan44@gmail.com

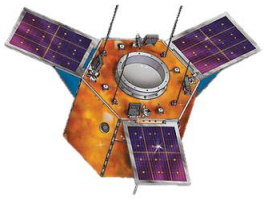

Turkish Journal of Remote Sensing

Türkiye Uzaktan Algılama Dergisi
Turkish Journal of Remote Sensing
Cilt/Volume 6
Sayı/Issue 1 *Haziran/June, 2024*

İçindekiler
Contents

Araştırma Makaleleri;
Research Articles;

Araştırma Makalesi/Research Article
https://doi.org/10.51489/tuzal.1394585

2024; 6(1); 01-11

Turkish Journal of Remote Sensing

https://dergipark.org.tr/en/pub/tuzal

e-ISSN 2687-4997

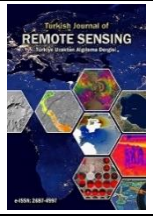

A Case Study of the Impact of University Establishment on Urbanization in Turkey's Medium-Sized City of Osmaniye

Ceren Yağcı*[1], Dilşah Erkek[2], Fatih İşcan[2]

[1]Osmaniye Korkutata University, Faculty of Engineering, Geomatics Engineering, Osmaniye, Turkey
[2]Konya Technical University, Faculty of Engineering, Geomatics Engineering, Konya, Turkey

Keywords:
Land Cover / Use
Urban Growth
Medium-Sized City
Change Detection

ABSTRACT

The rapid increase in the urban population increases the space requirement of the cities and this situation causes the growth of them. As cities grow, problems such as agricultural lands, irregular settlements and destruction of natural areas arise. City managers respond to these problems with various political solutions and new technologies. Developments in computer technology are very important in analyzing the rapid changes in land use and ensuring sustainable and planned land use. In this study, the change in land cover/ use during the process of the establishment of Osmaniye Korkut Ata University in the province of Osmaniye is examined. This situation revealed that the most important dynamic that accelerates urbanization in the region is the university. The study area is Osmaniye city center and the land use change according to years in the university region (Fakıuşağı district) has been discussed. For this purpose, a pixel-based controlled classification technique was applied to satellite images of 1999 - 2009 - 2019. The city areas triggered by the university and the amount of changing land cover in the province of Osmaniye were revealed spatially and spatially with the help of satellite images of each year. It was observed that the settlement class in both Osmaniye and Fakıuşağı districts has increased considerably. While the settlement class in Osmaniye province increased 2.5 times from 1999 to 2019, the increase in Fakıuşağı district increased approximately 10 times from 1999 to 2019. It has been observed that the establishment of the university, apart from the natural population increase, increased the migration to the city and led to the opening of new zoning areas in the determined 20-year period. In this process, it has been concluded that while settlements have expanded, agricultural lands have decreased, and pastures and forests have been destructed in recent years.

Türkiye'nin Orta Ölçekli Kenti Osmaniye'de Üniversite Kuruluşunun Kentleşmeye Etkisi Üzerine Bir Vaka Çalışması

Anahtar Kelimeler:
Arazi Örtüsü Kullanımı
Kentsel Büyüme
Orta Ölçekli Kent
Değişiklik Tespiti

ÖZ

Kent nüfusundaki hızlı artış, kentlerin alan kullanım ihtiyacını artırmakta ve bu durum kentlerin büyümesine neden olmaktadır. Kentler büyüdükçe, tarım arazileri, düzensiz yapılaşmalar ve doğal alanların tahrip edilmesi gibi sorunlar ortaya çıkmaktadır. Kent yöneticileri, bu sorunlara çeşitli politik çözümler ve yeni teknolojilerle karşılık vermektedir. Bilgisayar teknolojisinde yaşanan gelişmeler arazi kullanımındaki hızlı değişimleri analiz etmek, sürdürülebilir ve planlı arazi kullanımını sağlamak açısından oldukça önemlidir. Bu çalışmada, Osmaniye iline Osmaniye Korkut Ata Üniversitesi'nin kurulmasıyla yaşanan süreçte arazi örtüsü/kullanımındaki değişimi incelenmektedir. Bu durum bölgede, kentleşmeyi hızlandıran en önemli dinamiğin üniversite olduğunu ortaya koymuştur. Çalışma alanı Osmaniye il merkezi olarak ve üniversite bölgesi özelinde (Fakıuşağı Mahallesi) yıllara göre arazi kullanımı değişimi ele alınmıştır. Bu amaçla 1999- 2009- 2019 yıllarına ait uydu görüntülerine piksel tabanlı kontrollü sınıflandırma tekniği uygulanmıştır. Belirlenen her yıla ait uydu görüntüleri yardımıyla Osmaniye ilinde, üniversitenin tetiklediği kent alanları ve değişen arazi örtüsü miktarı alansal ve konumsal olarak ortaya konmuştur. Hem Osmaniye hem de Fakıuşağı Mahallesi'ndeki yerleşim sınıfının oldukça arttığı

Article Info

Received: 23/11/2023
Accepted: 21/12/2024
Published: 30/06/2024

Citation:

Yağcı, C., Erkek, D. & İşcan, F. (2024). A Case Study of the Impact of University Establishment on Urbanization in Turkey's Medium-Sized City of Osmaniye. Turkish Journal of Remote Sensing, 6 (1), 01-11.

***Corresponding Author:** Ceren Yağcı, cerenavciyagci@gmail.com, +90 328 827 10 00 (3629)

gözlenmiştir. Osmaniye İl'indeki yerleşim sınıfı 1999 yılından 2019 yılına yaklaşık 2.5 katına çıkarken, Fakıuşağı Mahallesi'ndeki artış 1999 yılından 2019 yılına yaklaşık 10 katına çıkmıştır. Belirlenen 20 yıllık süreçte doğal nüfus artışının dışında üniversitenin kuruluşunun, kente olan göçleri arttırdığı ve yeni imar alanlarının açılmasına sebep olduğu gözlenmiştir. Bu süreç içerisinde yerleşim yerleri genişlerken tarım arazilerinin azaldığı, mera ve ormanlıkların da son yıllarda tahrip edildiği sonucuna ulaşılmıştır.

1. INTRODUCTION

After the industrial revolution, the rapidly increasing population and the initiation of migration from rural areas to cities accelerated urbanization. Cities that experience the urbanization process rapidly, in order to benefit more from the unit area; have started to consume natural resources and turn the areas that cannot be used economically into new economic activity areas. This situation also accompanied the problem of unintended land use (Zhang & Song, 2003). The increase in non-purpose land use destroys agricultural areas, ecosystems, water resources and land cover, which adversely affects environmental plans (Caniberk et al., 2015). Changes in land cover use occurred especially in agriculture and forestry areas. Agriculture and forestry areas have turned into residential areas under the pressure of urbanization. The growing settlement areas have started to negatively affect the life in the cities along with the economic, social and political change processes (Sönmez, 2011). This process experienced in cities has revealed the necessity of renewal and planning of the city (Breuste, 2004). Geographical Information Systems (GIS) and Remote Sensing (RS) technologies have been widely used in urbanization studies in recent years in order to stop unplanned cities, to prevent wrong land use and offer solutions. Thanks to the developments in these technologies, it has become possible to obtain data on the earth quickly and with high precision. In addition, it was very useful to obtain and process periodic data kept at regular intervals in order to detect land use change in order to observe change in cities. In brief, by processing satellite images with the Remote Sensing method and using them as a base map. In Geographical Information Systems, it enables the analysis, interpretation and developing solution proposals of many urbanization problems (Masser, 2001). Many academic studies prepared with the integrated use of GIS and Remote Sensing techniques in determining the land cover change are encountered. These studies have been evaluated under three different headings. These are the studies of misuse of agricultural lands (Hadeel, AS, Jabbar, & Chen, 2011;Dengiz & Turan, 2014; Bayar, 2018; Çolak & Memişoğlu, 2018; Köse, 2023) misuse of natural resources such as forests and pastures (Tucker, et al., 1985; Genç & Bostancı, 2007; Safari, et al., 2017; Aydın & Durduran, 2021) and the dynamics that accelerate urbanization process (Aydın, 2009; Başer, 2019; Çelikoyan & Şeker, 2005; Green, et al., 1994; Gülersoy, 2013; Kara & Karatepe, 2012; Özdemir & Bahadır, 2008; Treitz, et al., 1992; Weng, 2002). With these studies, land use changes in cities were determined. Providing effective positional awareness about the development of the city to decision-makers on land use is a very important step in ensuring sustainability in the city. In this way, it becomes possible to determine the dynamics that trigger urbanization. Identifying these dynamics in cities is very important in order to produce effective solutions in areas under the pressure of urbanization. In general, industrial facilities, foreign migration, health institutions, transportation networks, tourism and educational institutions accelerate urbanization. Universities established in cities in recent years have become one of the most important dynamics of the city over time. As in many countries such as England, Australia, Finland and the USA, it has been observed that universities in Turkey are important for urban development and affect the city economically directly or indirectly (Armstrong et al., 1994; Bleaney, et al., 1992; Borland, et al., 2000; Çayı, & Yapraklı, 2014; Görkemli, 2009; Huggins & Cooke 1997; Öztürk, et al., 2011; Penn State Extension & Penn College-MSETC, 2012; Serel, & Kaşlı, 2008; Tavoletti, 2007; Tösten, et al., 2013; Tiuzbaian, 2003; Newland, 2003). In addition, universities are institutions that play a role in the formation of urban areas and contribute to major developments in the fields of commerce, arts, health, education, economy, tourism and science as a result of collaborations with the state and industry (Andersson, et al., 2009). For this reason, universities are seen as extremely important economic factors. It is an undeniable fact that especially universities established in low-populated Anatolian cities bring socio-cultural as well as economic dynamism to cities (Arslan, 2014).

The impact of Bartın University in Bartın, Mehmet Akif Ersoy University in Burdur province, Çankırı Karatekin University in Çankırı, Kilis 7 Aralık University in Kilis, Kütahya Dumlupınar University in Kütahya, Muş Alparslan University in Muş and Sivas Cumhuriyet University in Sivas province on the city, urban dwellers, population, economic growth, construction and employment opportunities in Sivas province has been revealed by the researches (Arslan, 2014; Ceyhan, & Güney, 2011; Çayın & Özer, 2015; Dalğar, et al., 2009; Demireli & Taşkın, 2013; Ergün 2014; Erkekoğlu, 2000; Sönmez & Başkaya, 2013). However, in these studies, the impact of universities on urbanization has not been addressed. Especially, small and medium-sized cities in Turkey with universities can enter a rapid growth process (Ergün, 2014). It has been observed that in these

cities, big dynamics such as the university, especially urbanization in the environment where the university campus is located, and the increase in unplanned growing areas have been observed to be more affected than the big cities.

This study addresses a critical research gap by investigating the impact of recently established universities on the status of small and medium-sized cities, with a specific emphasis on Osmaniye. The research aims to elucidate the developmental trajectories of these cities, particularly focusing on the influence of Osmaniye Korkut Ata University on urbanization, analyzed through Remote Sensing and Geographic Information System.

The study's findings unveil substantial changes in land use within Osmaniye province subsequent to the establishment of Osmaniye Korkut Ata University. The analysis, centered on the Fakıuşağı neighborhood, encompassing the university campus, signifies a noteworthy acceleration in residential area expansion. Concurrently, a reduction in pasture and agricultural areas within the study scope is evident.

These observations affirm the proposition that medium-sized cities, driven by the presence of universities, experience a rapid growth process. The study contributes to a nuanced comprehension of the transformative effects of higher education institutions on urban landscapes in regions like Osmaniye.

2. MATERIAL AND METHOD

2.1. Material

The basic material of the study consists of the satellite images taken in 1999-2009-2019 to examine the land use change in Osmaniye province and the neighborhood border data taken from the Osmaniye municipality. To determine land use classes basic data set in the United States Downloadable Landsat-5 TM and Landsat 8 satellite images with low cloud rate and 30 m terrestrial resolution were selected by the Geological Survey (USGS) for the years 1999-2009-2019 (URL-1). These images (174 Path, 34 Row) were processed in an area of 100 thousand square meters determined in the ArcGIS environment to cover the city center of Osmaniye and Fakıuşağı. Following this, supervised classification of satellite images for each year within the same software was created of four distinct land use classes (Table 1).

2.2. Study Area

Osmaniye Province is located in the east of them Mediterranean Region and Çukurova. It is surrounded by Gaziantep in the east, Hatay in the south, Adana in the west, and Kahramanmaraş in the north. Osmaniye, which had been made a district in 1933 and connected to Adana, gained its new administrative structure as the 80th province of Turkey on 24.10.1996 (URL 2). The area of the province is 3222 square kilometers, 121 m above sea level and 20 km from the Mediterranean Sea. Osmaniye is the 67th largest city of Turkey in terms of geographical area. Osmaniye is located between 35°52'-36°42 'east longitudes and 36°57'-37°45' north latitudes in the northern hemisphere (Fig. 1).

Figure 1. Study area

Osmaniye is a medium-sized city. Although there is no complete explanation about the concept of medium-sized cities, settlements with a population of at least 50,000 and a maximum of 750000 are considered to be medium-sized urban areas (Üzmez, 2012). People earn their livelihood primarily from livestock and agriculture. The main agricultural products are peanuts, oranges and cotton. There is a total of 40,000 decares of meadow pasture in the province. Most of the meadow pasture areas in the province are bottom and irrigable areas. Irrigation possibilities of pasture areas on medium

and slightly inclined slopes are insufficient. Pasture areas in the base lands are generally used as cattle pasture. (URL-2)

According to the general population census data in the TUIK database, the population of Osmaniye was 438,372 in 1997 and 471,804 in 2009. In 2019, it reached 538,759. An increase of 100,387 was observed from the year it reached the provincial status until 2019 (URL-3). The population chart by years is given in Figure 2. The reasons for the increase in population are the proximity of the province of Osmaniye, especially to the ports of Ceyhan and Iskenderun, and accordingly the settlement of Iskenderun Iron and Steel Factory workers in Osmaniye, the opening of various trade centers, the city's providing employment opportunities at a good level and the establishment of the university.

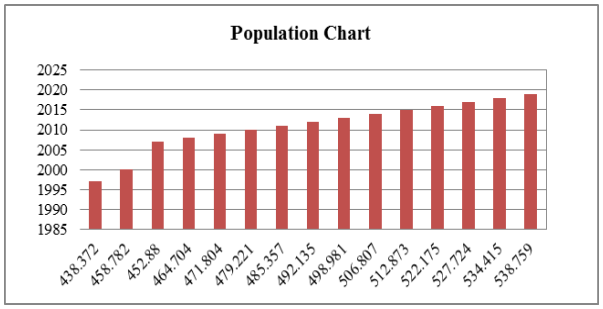

Figure 2. Population chart

2.3. Method

Today, Remote sensing is benefitted to detect land use changes. Remote sensing technology provides data to the Geographical Information System. GIS analyzes, interrogates and visualizes the digital data which it obtains. With the development of science and space technologies, the rapid development of spectral and spatial characteristics of sensors in satellites has intensely increased R.S applications. It has provided the opportunity to easily transfer digital data to the GIS environment and to provide analysis opportunities to users, in other words, the integration of Remote Sensing and Geographical Information Systems. R.S and GIS integration are used in a wide variety of areas such as forest, coastal destruction, urban, environmental and ecological changes (Figure 3).With such an integration, it provides convenience in determining, analyzing, planning and managing temporal change (Dengiz & Turan 2014).

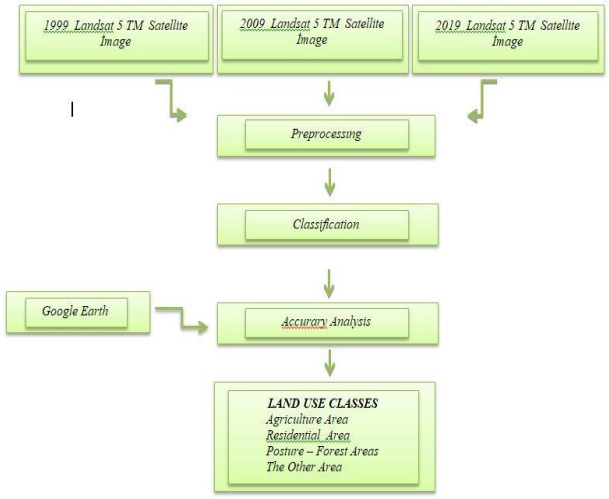

Figure 3. Flow chart

In the process of processing satellite images of the province of Osmaniye and obtaining land use maps, firstly, satellite images were obtained and the land classes to be used were designed. These classes are; settlement, agriculture, pasture and forest areas and others.

The process of determining the feature group of each pixel value in an image and assigning pixels with similar spectral characteristics to the feature groups for the selected bands is defined as classification (Gürbüz et al., 2012; Balçık et al., 2011; Dhanaraj & Angadi, 2022). For this purpose, first of all, controlled classification process was performed on Landsat satellite images. After the field classes are determined, the first stage of the controlled classification, the training part, is carried out. Training part means collection of sample regions. The collection of sample regions is the stage where it is applied by taking samples with an even distribution from the pixels that they know approximately which class they represent on the land. Landsat satellite images were used as a base for the sampling areas. After this stage, the supervised classification of the image was completed using the maximum likelihood algorithm with the reference of the samples taken. After the accuracy analysis of the thematic maps where the supervised classification process was applied, the land cover uses of each three years were obtained.

Accuracy analysis was applied to the classified images and the land use change of the study area in 1999-2009-2019 was tested. In addition, the land use change in the district of Fakıuşağı, where Osmaniye Korkut Ata University is located, in the province of Osmaniye has been examined.

3. RESULTS

3.1. Land Use Change

Land use maps obtained by using Landsat 4-5 TM satellite image are given in Figure 4 for the years 1999, 2009 and 2019. Accuracy values obtained by

controlled classification of satellite images are 80%, 85% and 87.5% for the years 1999, 2009 and 2019, respectively.

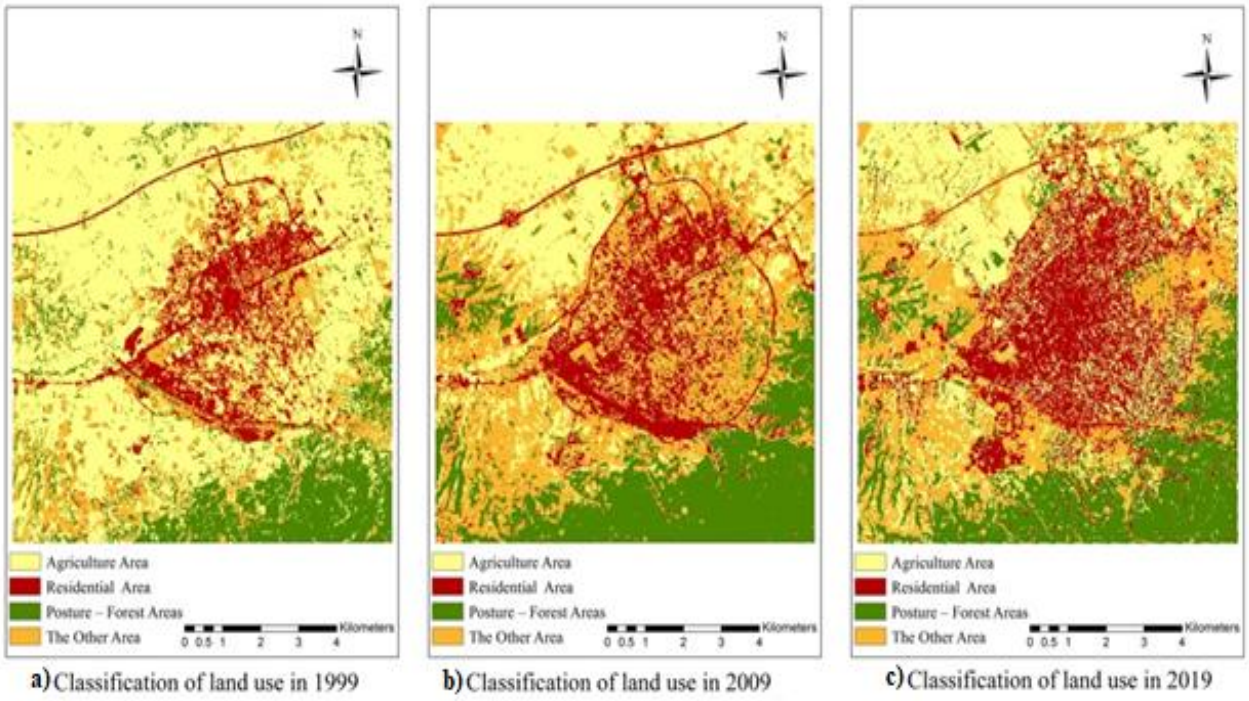

Figure 4. Controlled classification of satellite images, respectively; (a)1999-year (b)2009-year (c) 2019 year

Land use maps obtained by using Landsat 4-5 TM satellite image are given in Figure 4 for the years 1999, 2009 and 2019. Accuracy values obtained by controlled classification of satellite images are 80%, 85% and 87.5% for the years 1999, 2009 and 2019, respectively. Within this period, the residential area increased by 1814.84 ha, while the other (unusable infertile soils, bare surfaces) area also increased by 633.61 ha. It was determined that one of the least land losses was pasture and forest areas with an area of 532.79 ha (Table 1).

Table 1. Area of land use classes

Osmaniye of Province	**1999**		**2009**		**2019**	
Land use classes	**Area (Ha)**	**Percent (%)**	**Area (Ha)**	**Percent (%)**	**Area (Ha)**	**Percent (%)**
Agriculture Area	5514.89	55.15	3083.9	30.84	2533.65	25.34
Residential Area	1083.20	10.83	1466.42	14.66	2898.04	28.98
Pasture and Forest Areas	1454.56	14.55	2187.83	21.88	1987.35	19.87
The Other Area	1947.35	19.47	3261.85	32.62	2580.96	25.81
Total Area	10000	100	10000	100	10000	100

According to the evaluation made in Fakıuşağı neighbourhood, where the University was established in 2007, it has been determined that there has been an increase in settlement areas and other areas in 20 years, and a decrease in agricultural land and forest/pasture areas (Figure 4). While settlements in Fakıuşağı district had an area of 6% in 1999, it reached an area of 60% in 2019. Settlements have increased by 54%. Agricultural lands were 135 hectares in 1999, but decreased to 36 hectares in 2019. The bare surfaces class, expressed as the other, increased between 1999 and 2009, and a decrease occurred in the following years. While pasture and forest areas increased between 1999 and 2009, as in the province of Osmaniye, a decrease was observed between 2009 and 2019 (Table 2).

Table 2. Fakıuşağı neighborhood land use classes areas

Osmaniye of Province	**1999**		**2009**		**2019**	
Land use classes	**Area (Ha)**	**Percent (%)**	**Area (Ha)**	**Percent (%)**	**Area (Ha)**	**Percent (%)**
Agriculture Area	134.56	71	45.07	24	36.22	134.56
Residential Area	12.11	6	39.82	21	113.09	12.11
Pasture and Forest Areas	8.57	5	21.17	11	10.65	8.57
The Other Area	34.76	18	83.94	44	30.04	34.76
Total Area	190	100	190	100	190	190

The land use status of Fakıuşağı district by years is given in Figure 5.

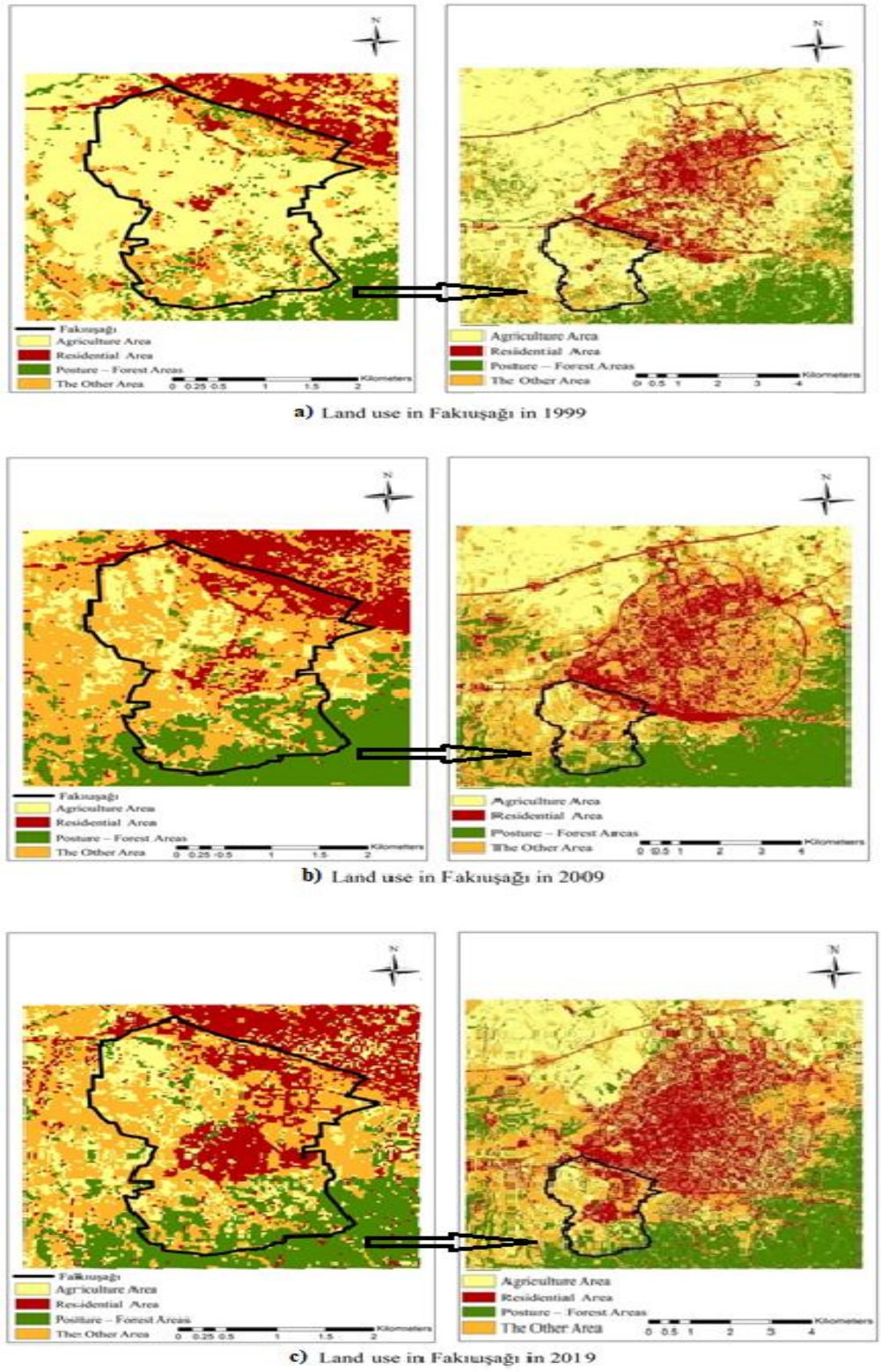

Figure 5. Fakıuşağı neighbourhood land use maps (a) 1999 year, (b) 2009 year, (c) 2019 year

When the change maps are examined by years, it is seen that there are important developments in Osmaniye between 1999-2009. It can be seen that there are important developments in almost the whole city. However, when the analysis of change for the years 2009-2019 is examined, it is determined that there is more movement towards the north of the city, and changes are experienced in the close locations of the university established in the north of the city. When the change maps are examined, in other words, it can be concluded that with the establishment of Korkut Ata University in 2007, the city shifted to the north direction in the next 10 years.

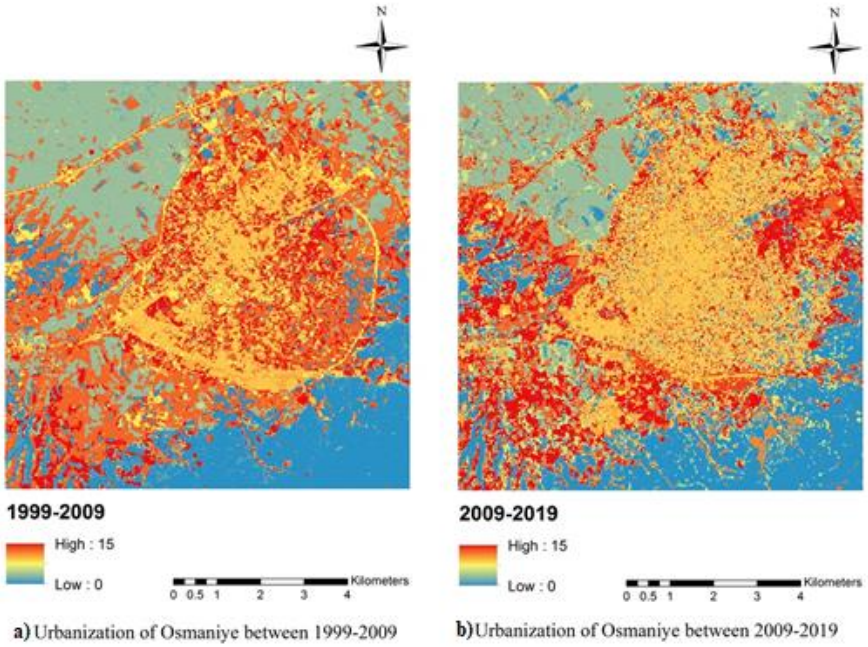

Figure 6. Map of Osmaniye land use change a) 1999-2009 years b) 2009-2019 years

4. DISCUSSION

In order to minimize the effects of agricultural, pasture and forest areas from rapid population growth, land use areas should be determined precisely and sustainable land use plans should be developed and implemented. It is very important to use the concept of land or soil, which is one of the limited resources, in a planned way. Geographical Information Technologies also makes it possible to plan land use, obtain, collect location-based data about setting/place and space, analyze and produce new solutions to problems with the obtained data. Studies in the literature on GIS and Remote Sensing Technologies, which are a part of it, were discussed under three headings as stated in the introduction. These studies consist of widely used topics that examine the misuse of agricultural lands, misuse of natural resources, and urbanization and the process of urbanization. When examining the studies dealing with urbanization and the dynamics that trigger the urbanization process, it was seen that the rapidly increasing human population and the rapid growth in the city were mostly due to migration due to industrialization. (Aydın, 2009; Çelikoyan & Şeker, 2005; Green, et al., 1994; Gülersoy, 2013; Kara & Karatepe, 2012; Özdemir & Bahadır, 2008; Weng, 2002). In the literature, there are also urbanization studies in which road services and tourism are effective as well as urban movements brought by industrialization (Başer, 2019; Özdemir & Bahadır, 2008; Treitz et al., 1992). However, when the studies are examined, no study has been found that examines the change in the land cover in the city caused by a dynamic as a university. The local economic impacts of universities are very effective in terms of both income and employment, knowledge production, investment increase, cultural and social standards established by universities to improve the social infrastructure, and the formation of subsectors. (Amstrong et al., 1994; Bleaney et al., 1992; Borland et al., 2000; Çayın & Özer 2015; Görkemli, 2009; Huggins & Cooke 1997; Öztürk et al., 2011; Pen State Extensionand & Penn College-MSETC, 2012; Serel, & Kaşlı, 2008; Tavoletti, 2007; Tösten et al., 2013; Tiuzbaian, 2003; Newland, 2003). It is stated that universities established in small and medium-sized cities in Turkey are more effective than big cities in the economic development of the city (Arslan, 2014; Ceyhan & Güney, 2011; Çayın & Özer, 2015; Demireli & Taşkın, 2013; Ergün, 2014; Erkekoğlu, 2000; Sönmez & Başkaya, 2013). With the existence of the university, educational opportunities increase, intellectual accumulation increases and new residential areas are created (Tösten, 2013). The difficulty of finding hundreds of acres of land in city centres and the high cost of land in city centers, even if found, cause universities to be established far from or outside the city centre (Öncel, 2019). In the province of Osmaniye, where this situation was experienced, the change in land use was determined within the scope of the study and the effect of the university, which is one of the biggest dynamics of the city, on the city was determined spatially. The change in land use in Osmaniye city centre and university region (Fakıuşağı district) was evaluated temporarily. In the 20-year period, the establishment process of Osmaniye Korkut Ata University, the opening of various trade centres and the changes in the administrative structure of the city in the process caused considerable changes in land use.

Despite the valuable insights provided by Keleş & Durduran in their 2019 study on the spatial changes in Osmaniye since its establishment as an administrative province in 1996. Nevertheless, it is

crucial to underscore that their research did not specifically delve into the influence of a key element within the city namely, the university on land use dynamics. Therefore, this study aims to fill this gap by examining the classification results of settlement areas for the years 1999, 2009, and 2019, which reveal a notable increase from 1083.20 ha to 2898.04 ha. The subsequent analysis will delve into the specific influence of the university on this observed spatial transformation. In this study, according to the classification results, the settlement area amounts for the years 1999, 2009 and 2019 are 1083.20 ha, 1466.42 ha and 2898.04 ha, respectively. The settlement area in Fakıuşağı district was 12 hectares in 1999. In 1999, the university was not established yet, and it was being educated as a vocational college on the university grounds. With the establishment of Osmaniye Korkut Ata University on 29 May 2007, the residential area in Fakıuşağı district increased to 40 hectares in 2009. In 2019, it was determined that the residential area increased rapidly and reached 113 hectares. In this neighborhood, it has been observed that there has been an increase of 54% in the residential areas within 20 years with the effect of the university. It has also been observed that this increase caused a significant decrease in agriculture and other land classes.

According to the land use maps made in the province of Osmaniye, it was observed that the agricultural areas, which were 5514.89 hectares in 1999, decreased to 3083.9 hectares in 2009 and 2533.65 hectares in 2019. Especially the agricultural areas in the Fakıuşağı neighborhood negatively affected the establishment of the university. The agricultural area, which was 145 hectares in 1999, decreased to 36 hectares in 2019 after the university was established. There was a decrease of about 21%. In the forest and pasture areas, the area in Osmaniye province, which was 1454.56 ha in 1999, increased to 2187.83 ha in 2009. This 7% increase is thought to be due to the inclusion of the province of Osmaniye in the "National Afforestation and Erosion Control Mobilization" afforestation works carried out in Turkey in 2007. However, this afforestation study was not sustainable, forest areas decreased by approximately 2% in 2019 compared to 1999 and decreased to 1987.35 hectares. The same situation was experienced in the forest and pasture areas in Fakıuşağı district. The forest and pasture areas, which were 9 hectares in 1999, increased by 21 hectares in 2009 and decreased to 11 hectares in 2019.

In the province of Osmaniye, areas in the other class increased from 19.47% to 25.81% in 20 years. In the Fakıuşağı district, the areas in this class were 18% in 1999 and increased to 44% in 2009. However, this area was determined to be 15% in 2019. The reason for the decrease in this class in 2019 is that between 2009-2019, the new settlements in the region were covered from these unproductive lands instead of agricultural lands. Because, in 2005, the Soil Protection and Land Use Law No. 5403, which aims to protect agricultural lands in Turkey, entered into force. With this law, the misuse of agricultural lands has started to be prevented.

5. CONCLUSION

Agricultural lands are often used without proper planning, leading to the occupation of fertile areas for settlements or trade centers. This haphazard approach can have negative consequences, impacting resource utilization and sustainable development. Therefore, a closer look at land-use patterns is essential for making informed decisions and developing effective policies that balance urban development with the preservation of agricultural productivity.

Agricultural lands, especially in developing countries, are under pressure due to reasons such as wrong and unplanned land use, high population growth, insufficient institutional support, or soil erosion. This pressure decreases the fertility value of the soil and shows how important planned land use is. This situation necessitates the creation of land use plans for sectors such as forestry, agriculture, and settlement, which are based on land, taking into account social, economic, and environmental variables.

This study examined the temporal change in the land use of Osmaniye province and revealed that a large dynamic such as a university affects a small or medium-sized city very much. According to the results, it has been observed that the need for new settlements caused by rapid population growth damages natural and agricultural areas. The agricultural land class experienced a 20 percent loss between 1999 and 2019, and was the most affected by population growth and urbanization pressure.

(Most affected by population growth and urbanization pressure, with a loss of 20% has been class.) The residential areas class shows a significant population increase in the region with an increase of approximately 2.5 times and the formation of new urban areas. Established in 2007, the university has become one of the most important reasons for the increase in settlements in this process. The establishment of the university caused the population of the city to increase and at the same time, this neighborhood, which was a village in the past, gradually to become more structured. In addition, it has also caused the destruction of natural habitats, agriculture, pasture and forest areas. Before the university was established in 2007, the neighborhood did not even have a settlement of 1000 people, while it reached a population of 2940 in 2009 and 11352 in 2019. This situation shows that the establishment and development of the university increases the residential areas of the city, as well as provides new job opportunities, meeting the needs of the society in both economic and social city studies. The establishment of universities in a city,

on the one hand, improves the social-economic infrastructure facilities in the region where the university is established, and on the other hand changes the land use in the region. Considering this situation in landscaping plans, effective policy arrangements should be made to protect the agriculture, pasture and forest areas around the university area.

GIS and Remote Sensing technologies should be widely used to detect changes in land use, to reduce the negative effects of newly established universities on urban growth, especially in small and medium-sized provinces, and to develop sustainable development strategies for the city.

Author contributions

C. Yağcı: Designed the research Investigation, Writing the manuscript–review and editing.
D. Erkek: Collected the datasets and analyzed the data, Methodology, Validation.

F. İşcan: Investigation, writing–review and editing, Commented on the manuscript.

Conflicts of Interest

The authors declare no conflict of interest

Research and publication ethics statement

In the study, the authors declare that there is no violation of research and publication ethics and that the study does not require ethics committee approval.

REFERENCES

Andersson, R., Quigley, J. M. & Wilhemsson, M. (2009). Urbanization, productivity, and innovation: Evidence from investment in higher education, *Journal Of Urban Economics,* 66(1), 2-15. https://doi.org/10.1016/j.jue.2009.02.004

Armstrong, W., Darrall, J. & Grove-Whıte, R. (1994). Building Lancester's Future: Economic and Environmental Implications of Lancester University's Expansion to 2001. University of Lancester. *Department of Economics and Center for the Study of Environmental Change*, U.K.

Arslan, H. (2014). The Economic Contribution of The Cankiri Karatekin University to City and The Analysis of Student' Expenditures in Terms of Different Variables. *Dicle University Social Sciences Institute Journal,* (12), 114-127.

Aydın, O. (2009). Analysis of physical urban development of Ankara city using by geographic information systems (GIS) and remote sensing (RS). *Master's Thesis*, Ankara University, 129p (in Turkish).

Aydın, T. K. & Durduran, S. S. (2021). Temporal Change of Land Use/Land Cover in Ereğli-Bor Sub-Watershed by Remote Sensing Methods. *Turkish Journal of Agricultural and Natural Sciences*, 8(3), 629-641. https://doi.org/10.30910/turkjans.936107

Başer, V. (2019). Analysis of Land Use Change of Highlands with Geographic Information System: The Case of Giresun. *BEU Journal of Science,* 8(1), 167-175. https://doi.org/10.17798/bitlisfen.446264

Bayar, R. (2018). In terms of land use change in agricultural areas in Turkey. *Turkish Journal of Geographical Sciences*, 16(2), 187-200. https://doi.org/10.1501/Cogbil_0000000197

Bleaney, F., Bınks, R., Greenaway, D., Reed, V. & Whynes, K. (1992). What does a University Add to Its Local Economy? *Applied Economics*, 24(3), 305-311. https://doi.org/10.1080/0003684920000013

Borland, J., Dawkins, P., Johnson, D. & Williams, R. (2000). Returns to Investment in Higher Education. *The Melbourne Economics of Higher Education Research Program Report.*

Breuste, H. J. (2004). Decision making, planning and design for the conservation of indigenous vegetation within urban development. *Landscape and Urban Planning,* 68(4), 439-452. https://doi.org/10.1016/S01692046(03)00150-6

Caniberk, M., Sesli F. A. & Bektaş S. (2015). Determining the temporal changes of land use by using orthophotos: The sample of Elmalı basin. *Acta Montanistica Slovaca*, 20(2), 86-97.

Çayın, M. & Özer, H. (2015 Contribution of Universities to The Economy of Provinces and Consumption Structure of Students: The Case of Muş Alparslan University. *Dokuz Eylül University Faculty of Economics and Administrative Sciences Journal*, 30(2), 131-147.

Çelikoyan, T. M. & Şeker, D. Z. (2005) Detection of Landuse Changes Between 1903-2003 By Using Different Types of Data-100 Years of Istanbul. *TMMOB Harita ve Kadastro Mühendisleri Odası 10. Türkiye Harita Bilimsel ve Teknik Kurultayı*, Ankara, Türkiye (in Turkish).

Ceyhan, S. & Güney, G. (2011). The Contribution Of Bartın University To Bartın States Economic Development With 20 Yearly Projection. *Fırat University Journal of Social Science,* 21(2), 183-207.

Çolak, H. E. & Memişoğlu, T. (2018). Determination of Temporal Change in Agricultural Land Use in Trabzon with GIS. *Afyon Kocatepe University Journal of Science and Engineering*, 18(3), 946-958. https://doi.org/10.5578/fmbd.67647

Dalğar, H., Tunç, H., & Kaya, M. (2009). The Role of University Institutions in Regional Development and Bucak Sample. *Mehmet Akif Ersoy University Journal of Social Sciences Institute*, (1), 39-50.

Demireli, C. & Taşkın, E. (2013). Economic Contributions of University Students to Their Education Locations: Sample of Kütahya City Cente. *Dumlupınar University, Journal of Social Sciences,* 37, 321-328.

Dengiz, O., & Turan, İ. D. (2014). Determination of Temporal Change Land Use / Land Cover Using

Remote Sensing and Geographic Information System Techniques the Central District of Samsun (1984-2011). *Turkish Journal of Agricultural Research*, 1(1), 78-90. https://doi.org/10.19159/tutad.45474

Dhanaraj, K. & Angadi, D. P. (2022). Land use land cover mapping and monitoring urban growth using remote sensing and GIS techniques in Mangaluru, India. *GeoJournal*, 87(2), 1133-1159.

Ergun, C. (2014). Evaluations on Town-Gown Relationship: İn Case of Mehmet Akif Ersoy University. *Mehmet Akif Ersoy University Journal of Education Faculty*, 1(31), 216-237.

Erkekoğlu, H. (2000). Bölge Üniversitelerinin Yerel Ekonomiye Katkıları: Sivas Cumhuriyet Üniversitesi Örneği (in Turkish). *Erciyes University Journal of Faculty of Economics and Administrative Sciences,* 16, 203-210.

Genç, L. & Bostancı, Y.B. (2007). Determination of Agriculture Land Use and Land Cover Change Using Remote Sensing and GIS in TROIA National Park. *Journal of Tekirdag Agricultural Faculty,* 4(1), 27-41.

Görkemli, H.N. (2009) Economical Impacts of Selcuk University to the City of Konya. *The Journal of Selcuk University Social Sciences Institute,* 22, 169-186.

Green, K., Kempka, D. & Lackey, L. (1994). Using Remote Sensing to detect and monitor land-cover and land-use change. *Photogrammetric Engineering and Remote Sensing,* 60, 331–337.

Gülersoy, A. E. (2014). Temporal Change of Land Use in Seferihisar (1984-2010) and Proposals for Optimal Land Use *SDU Faculty of Arts and Sciences Journal of Social Sciences*, 2014(31), 155-180.

Gürbüz, M., Denizdurduran, M., Karabulut, M. & Kızılelma, Y. (2012). Remote Sensing and GIS Land on the Elbistan Plain Using Usage/Occurring in Land Cover Analysis of Changes*. KSU Engineering Journal of Sciences,* Special Issue,30-37.

Hadeel, A. S., Jabbar, M. T. & Chen, X. (2011). Remote sensing and GIS application in the detection of environmental degradation indicators. *Geo-Spatial Information Science*, 14(1), 39–47. https://doi.org/10.1007/s11806-011-0441-z

Huggins, R. & Cooke, P. (1997). The Economic Impact of Cardiff University: Innovation, Learning and Job Generation. *GeoJournal*, 41(4), 325-337. https://doi.org/10.1023/A:1006863820399

Kara, F. & Karatepe, A. (2012) Land Use Change Analysis of Beykoz District (1986-2011) with Remote Sensing Technologies. *Marmara Geographical Review,* 25, 378 – 389.

Keleş, B. & Durduran, S. S. (2019). In Terms Of Land Use And Land Cover Change Using Remote Sensing Technique: Case Of Study in Osmaniye City. *Necmettin Erbakan University Journal of Science and Engineering,* 1(1), 32-52.

Köse, M. (2023). Sanayi Kuruluşlarının Mekânsal Değişim Üzerindeki Etkileri: Kozan Şehri Örneği. HUMANITAS-Uluslararası Sosyal Bilimler Dergisi, 11(22), 260-282.

Masser, I. (2001). Managing our urban future: the role of Remote Sensing and Geographic Information Systems, *Habitat International*, 25(4), 503-512. https://doi.org/10.1016/S0197-3975(01)00021-2

Newland, D. (2003). The Role of Universities in Learning Regions. *ERSA 2003 Congress*, 398, University of Jyvaskyla, Finland.

Özdemir, M. A. & Bahadır, M. (2008). Timely Change (1992-2007) of Land Use in Yalova Province. *İstanbul University Journal of Geography,* 17, 1-15.

Öztürk, S., Torun, İ., & Özkök, Y. (2011). Contributions Of Universities Established In Anatolia To The Socio-Economic Structure Of The Cities. *Mustafa Kemal University Journal of Social Sciences Institute*, 8(16), 145-158.

Penn State Extensıon & Penn College (MSETC) (2012). Economic Impacts of Marcellus Shale in Bradford County: Employment and Income in 2010. http://www.marcellus.pu.edu/resources/PDFs/EI_Bradford.pdf [Access Date: 28.11.2013].

Safari, A., Sohrabi, H., Powell, S. & Shataee, S. (2017). A comparative assessment of multi-temporal Landsat 8 and machine learning algorithms for estimating aboveground carbon stock in coppice oak forests. *International Journal of Remote Sensing,* 38(22), 6407–6432. https://doi.org/10.1080/01431161.2017.1356488

Serel, A. & Kaşlı, M. (2008). An Empirical Research for University Students' Expenses Impacts on Local Development. *Journal of Management and Economics,* 15, 2, 99-113.

Sönmez, M. E. & Başkaya, Z. (2013). Socio - Economic Impacts of Universities on the Cities: A Case Study from Kilis 7 Aralık University, Turkey. *3rd International Geography Symposium*, GEOMED 2013.

Sönmez, M.E. (2011). The Urban Expansion in Adana, Turkey, and Relationship between Land use Changes in its Surroundings. *Turkish Geographical Review,* (57), 55-69.

Tavoletti E. (2007). The Local and Regional Economic Role of Universities: The Case of the University of Cardiff. *University of Cardiff Working Paper,* W.P. No: 9; 1-46.

Tıuzbaıan, N. (2003). The Local Income Multiplier Model Oxford Brookes University. *Annals of the University PetroÇani-Economics,* 3; 212-220.

Tösten, R., Çenberlitaş, İ. & Gökoğlan, K. (2013). The Expenditure Analysis For The Students Of Dicle University And İts Contribution To The Economy Of Diyarbakir *Dicle University Social Sciences Institute Journal,* 5(10), 90-114.

Treitz, P., Howarth, P. & Gong, P. (1992). Application of satellite and GIS technologies for land-cover and land-use mapping at the rural-urban fringe: a case study. *Photogrammetric Engineering & Remote Sensing.*

Tucker, C. J., Townshend, J. R. G. & Goff, T. E. (1985). African land-cover classification using satellite data. *Science*, 227(4685), 369–375. https://doi.org/10.1126/science.227.4685.369

URL-1: https://www.usgs.gov/ [Access Date: 17.01.2022].

URL-2: https://on5yirmi5.com/dosya/turkiyenin-illeri/80-osmaniye-hakkinda-genel-bilgi/ [Access Date: 17.06.2023].

URL-3: https://biruni.tuik.gov.tr/ [Access Date: 09.08.2022].

Üzmez, U. (2012). Solution Seeking To Medium Sized Urban Areas Problem In The Turkey: Example Of Zonguldak. *Gazi University Journal of Faculty of Economics and Administrative Sciences,* 14/2, 127-158.

Weng, Q. (2002). Land use change analysis in the Zhujiang Delta of China using satellite Remote Sensing, GIS and stochastic modeling. *Journal of Environmental Management*, 64(3), 273–284. https://doi.org/10.1006/jema.2001.0509

Zhang, K. H. & Song, S. (2003). Rural–urban migration and urbanization in China: Evidence from time-series and cross-section analyses, China Economic Review, 14(4), 386-400. https://doi.org/10.1016/j.chieco.2003.09.018

Araştırma Makalesi/Research Article
https://doi.org/10.51489/tuzal.1395189

2024; 6(1); 12-25

Turkish Journal of Remote Sensing

https://dergipark.org.tr/en/pub/tuzal

e-ISSN 2687-4997

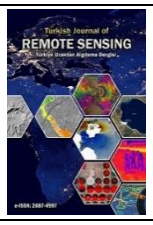

Determination of the Effects of Various Spectral Index Combinations on Seasonal Land Use and Land Cover (LULC) Changes Using Random Forest (RF) Classification Case Study: Southeast Marmara Region 2016-2020

Eda Aşci[1], Levent Genç[*2,3]

[1]*Çanakkale Onsekiz Mart University, Engineering Faculty, Geomatics Engineering, Çanakkale, Turkey*
[2]*Çanakkale Onsekiz Mart University, Faculty of Architecture and Design, Department of Urban and Regional Planning, Land Use and Climate Change Laboratory, Çanakkale, Turkey*
[3]*Canakkale Onsekiz Mart University, Computer-Agriculture-Planning (ComAgPlan) Study Group, Canakkale, Turkey*

Keywords
Remote Sensing
LULC
Vegetation Indices
South-Eastern Marmara Region

ABSTRACT

The effects of irregular population growth, migration mobility, and vegetation dynamics by humans can lead to changes in Land Use and Land Cover (LULC). Changes in LULC are particularly significant in coastal areas associated with industrial activities. The southeastern Marmara region, which is one of Turkey's industrial coastal areas, is also affected by the surrounding changes. The study area was selected to determine LULC change and classification accuracy using Sentinel-2 vegetation indices combinations. In the study area, the Gemlik-Bursa Northern Interchange Investments Area and TOGG (Turkey's Automobile Initiative Group) factory are located. The study area was determined by creating a 5-km buffer zone from the coast to the mainland covering Armutlu district of Yalova province and Osmangazi, Mudanya, and Gemlik districts of Bursa province. Random Forest (RF) classification technique was applied both to the original bands and to 21 new band combinations that are derived from Sentinel-2 multispectral satellite imagery for 3 seasons in 2016 and 2020. The new band combinations used for classification were created by adding the normalized vegetation indices, the original bands and the bands obtained from the simple ratio formula. In 2016, the highest accuracy results for the winter, spring, and summer seasons were observed for the OI12 (82.93%), ORF (84.44%), and ORF (84.67%) indices, while in 2020 were observed for the OI5 (85.89%), ORF (84.75%), and OI6 (84.63%) indices. In Southeast Marmara, investment decisions taken at national level have led to population growth in the region. Although it was observed that there was no significant change in classification accuracy with the addition of spectral features to the original bands such as NDVI and SR, we believe that future testing of the data with different statistical and machine learning methods provide higher accuracy.

Spektral İndeks Kombinasyonlarının Rastgele Orman (RO) Sınıflandırması Kullanarak Mevsimsel Arazi Kullanımı ve Bitki Örtüsü (AKBÖ) Değişiklikleri Üzerindeki Etkilerinin Belirlenmesi: Güneydoğu Marmara Bölgesi Örneği 2016-2020

Anahtar Kelimeler:
Uzaktan Algılama
AKBÖ
Vejetasyon İndeksler
Güney-Doğu Marmara Bölgesi

ÖZ

Düzensiz nüfus artışı, göç hareketliliği ve insanların vejetasyon dinamiklerine etkileri Arazi Kullanım ve Bitki Örtüsü (AKBÖ) değişimlerine yol açabilmektedir. AKBÖ değişiklikleri sanayi ile ilişkili kıyı bölgelerinde oldukça önemlidir. Türkiye'nin önemli kıyı alanlarından olan Güneydoğu Marmara alanı da çevredeki değişimlerden etkilenmektedir. Çalışma alanı, Sentinel-2 tabanlı bitki örtüsü indeksleri kombinasyonlarını kullanarak gerek AKBÖ değişimini gerekse sınıflandırmanın doğruluğunu belirlemek amacıyla seçilmiştir. Çalışma alanında Gemlik- Bursa Kuzey Kavşağı yatırım alanı ve yeni inşa edilen TOGG (Türkiye'nin Otomobili Girişim Grubu) fabrikası yer almaktadır. Çalışma alanı, Yalova ili Armutlu ilçesi ve Bursa ili Osmangazi, Mudanya ve Gemlik ilçelerini kapsayan alanda kıyıdan anakaraya 5 km'lik tampon bölge

Article Info

Received: 23/11/2023
Accepted: 21/01/2024
Published: 30/06/2024

Citation:

Aşci, E. & Genç, L. (2024). Determination of the Effects of Various Spectral Index Combinations on Seasonal Land Use and Land Cover (LuLc) Changes Using Random Forest (RF) Classification Case Study: Southeast Marmara Region 2016-2020. Turkish Journal of Remote Sensing, 6 (1), 12-25.

***Corresponding Author:** Levent Genc, leventgc@comu.edu.tr, +90 286 218 0018 (3032)

oluşturularak belirlenmiştir. Rastgele Orman (RO) sınıflandırma tekniği, 2016 ve 2020 yıllarında 3 sezon boyunca Sentinel-2 multispektral uydu görüntülerinden elde edilen indeksler kullanılarak orijinal bantlara ve 21 yeni bant kombinasyonuna uygulanmıştır. Sınıflandırma için kullanılan yeni bant kombinasyonları, normalize edilmiş bitki örtüsü indeksleri (NDVI), orijinal bantlar ve basit oran (SR) formülünden elde edilen bantlar eklenerek oluşturulmuştur. En yüksek doğruluk sonuçları 2016 yılı kış, ilkbahar ve yaz mevsimleri için OI12 (%82,93), ORF (%84,44) ve yine ORF (%84,67) indekslerinde gözlemlenirken, 2020 yılında OI5 (%85,89), ORF (%84,75) ve OI6 (%84,63) indekslerinde gözlemlenmiştir. Güneydoğu Marmara'da ulusal düzeyde alınan yatırım kararları bölgede nüfus artışına yol açmıştır. NDVI ve SR gibi orijinal bantlara spektral özelliklerin eklenmesiyle sınıflandırma doğruluğunda önemli bir değişiklik olmadığı gözlemlenmiş olsa da verilerin gelecekte farklı istatistiksel ve makine öğrenimi yöntemleriyle test edilmesinin sınıflama doğruluğunu daha fazla artırabilir.

1. INTRODUCTION

Land use and land cover (LULC) dynamics and understanding their relationship with the environment are important. It is known that LULC occur due to natural or human-induced events (Dewidar, 2010). Changes in LULC at regional and global level can be associated with irregular migration movements, population changes, industrial developments, agricultural activities, and forest fires. Therefore, understanding these changes is of great importance, especially in identifying the pressure caused by impervious surfaces. The investigation of land cover changes through quantitative data analysis and visual interpretation is possible through Remote Sensing (RS). Many researchers have preferred to use RS data to reveal the results of land cover change (El-naggar, 2018; Joshi et al., 2011; Sharma & Joshi, 2016). RS data is commonly used in geographic information production due to its ability to provide data at different resolutions according to land conditions, as well as its open-access and free availability. The Sentinel data, provided by the European Space Agency (ESA), are one of the sources contributing to the production of high-quality information since 2015 (Cavur et al., 2019; Myint Htun et al., 2023; Yulianti, 2019). RS data is widely used, especially in determining the reasons for changes in urban areas, studying spatial changes in vegetation classes, and investigating the impact of different resolution bands on the land, etc. It is known that the spatial changes in cities are associated with industrial investments and population changes, and this uncontrolled progression is thought to influence LULC and urban planning. Studies highlight the pressure on urban dynamics caused by development decisions, especially in industrial areas (Batunacun et al., 2018; Chandra Pandey et al., 2019). Additionally, it is observed that satellite data, with their band combinations, can be used to examine these changes and developments, yielding more realistic results in various land cover classes.

In this context, different methods and techniques that emerge for determining LULC changes are considered sustainable in terms of facilitating scientific research. When determining LULC change results, classification techniques and different band combinations suitable for the study areas are commonly used. Many researchers strive to achieve maximum accuracy in LULC classification through mathematical and statistical inferences. Machine Learning (ML) algorithm is one of them. An ML algorithm such as Random Forest (RF) is frequently used when monitoring LULC changes in urban land cover and vegetation classification (Asci et al., 2021; Breiman, 2001; Chehata et al., 2009; Scornet, 2015). The RF technique is used to separate pixels based on their spectral values. It involves assigning the training data's previously learned information to LULC classes. With its tree structure, it aims to minimize the error between pixels, thus enhancing accuracy in classification (Guan et al., 2012). Another method aimed at improving classification accuracy involves creating new band combinations (Genc, 2002). This allows for the identification of changes on the ground by understanding how pixels with dominant spectral reflectance values respond to new band combinations.

Learning the change dynamics of LULC classes through satellite data enables easier and more appropriate development of sustainable projects. RS has been used extensively to track developments, especially in industrial areas, to link local knowledge with global outcomes, and to explore new analyses and mathematical expressions for understanding the landscape. (Mukhawana et al., 2023; Sathian & Brema, 2023). It is important to calculate the accuracy of the classifications made in different ways as an indicator and learn about the feasibility of using this method (Kumar & Agrawal, 2019). We can use these results.

Bursa and Yalova provinces in Turkey are positioned within the category of developing and rapidly growing regions, often referred to as industrial cities. While the rapid developments in the industrial sector impact various aspects of life, their contributions to the country's Gross Domestic Product (GDP) may change. Factors such as significant investment decisions have led to an acceleration in migration activities and irregular population growth in industrial-focused regions.

In this context, Bursa, which is known as an industrial city in Turkey and where projects such as 'Turkey's Automobile Joint Venture Group' (TOGG) and Bursa-North Interchange are located, was

selected as the coastal study area together with Yalova province.

The aim of the study is to determine the accuracy performance of the images created with combinations of indices produced using Sentinel-2A satellite data. Secondary aims include examining the LULC changes that occurred during the construction of the government - supported TOGG factory in the area.

2. MATERIALS and METHOD

2.1. Study Area

The study area consists of the Gemlik district of Bursa, with 13 neighborhoods; the Mudanya district of Bursa with 17 neighborhoods; 2 neighborhoods in the Osmangazi district of Bursa; and 7 villages in the Armutlu district of Yalova province, covering a total area of 495,864 km^2 in the southeast of the Marmara region in Turkey (Figure 1). As the province of Yalova has a different form of administration, the term 'village' is used instead of 'neighborhood'.

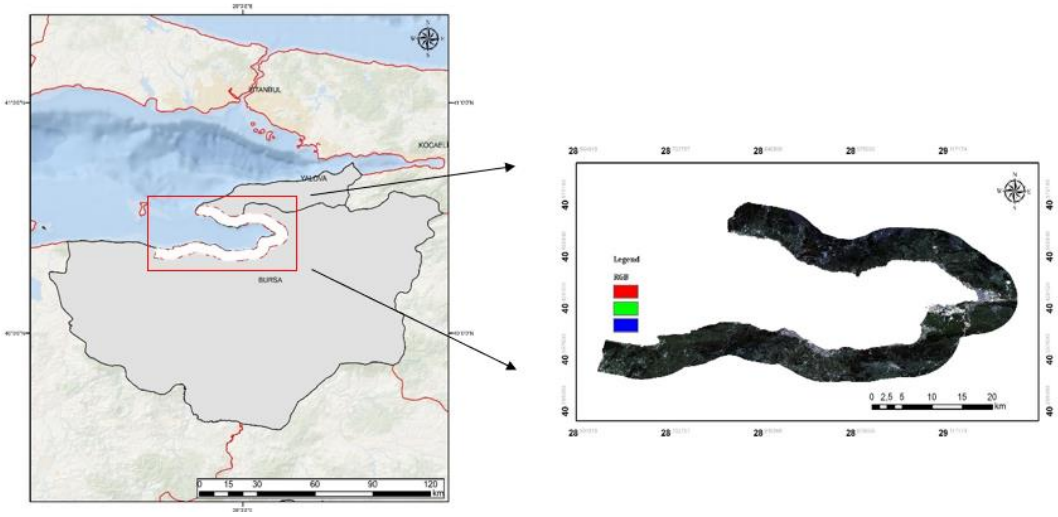

Figure 1. Study area

The study area has been defined by selecting a 5-km buffer zone from the coastline towards the mainland. The complete list of villages and neighborhoods in the area is given in Table 1.

Table 1. List of neighborhoods and villages in study area

City	District	Neighborhood Village
Bursa	Gemlik	Cihatlı Neighborhood Engurucuk Neighborhood Karacaali Neighborhood Kurtul Neighborhood Kucukkumla Neighborhood Narli Neighborhood Yenikoy Neighborhood Ata Neighborhood Buyukkumla Neighborhood Gencali Neighborhood Kumla Neighborhood Kursunlu Neighborhood Parsbey Neighborhood
Bursa	Osmangazi	Osmangazi Neighborhood Gundogdu Neighborhood
Bursa	Mudanya	Altintas Neighborhood Aydinpinar Neighborhood Burgaz Neighborhood Camlik Neighborhood Cepni Neighborhood Egerce Neighborhood Esence Neighborhood Goynuklu Neighborhood Haitpasa Neighborhood Isıklı Neighborhood Kumkaya Neighborhood Mesudiye Neighborhood Sogutpinar Neighborhood Tirilye Neighborhood

		Yali Neighborhood

Table 1. Cont.

City	District	Neighborhood Village
Bursa	Mudanya	Yaliciftlik Neighborhood Yaman Neighborhood Yorukali Neighborhood
Yalova	Armutlu	Hayriye Village Fistikli Village Kapakli Village Mecidiye Village Bayir Neighborhood Karsiyaka Neighborhood 50. Yil Neighborhood

2.2. Data Used

The Sentinel-2 mission is a terrain monitoring mission consisting of two satellites (Sentinel-2a and Sentinel-2b) providing optical imagery in 13 spectral bands. It has a spatial resolution ranging from 10 m to 60 m (Table 2).

The study obtained six Sentinel-2A satellite images for the years 2016 and 2020 from the European Space Agency Copernicus website (https://scihub.copernicus.eu/). Image processes were applied to the images taken on January 9, 2016, April 18, 2016, August 16, 2016, February 2, 2020, April 17, 2020, and August 15, 2020.

Table 2. Sentinel – 2 bands features

Sentinel-2 Bands	Central Wavelength(µm)	Resolution (m)
Band 1 – Coastal Aerosol	0.443	60 m
Band 2 – Blue	0.492	10 m
Band 3 – Green	0.560	10 m
Band 4 – Red	0.665	10 m
Band 5 – Vegetation Red Egde	0.704	20 m
Band 6 – Vegetation Red Egde	0.741	20 m
Band 7 – Vegetation Red Egde	0.783	20 m
Band 8 – NIR	0.833	10 m
Band 8a – Vegetation Red Egde	0.865	20 m
Band 9 – Water Vapour	0.945	60 m
Band 10 – SWIR – Cirrus	0.1374	60 m
Band 11 – SWIR	0.1614	20 m
Band 12 – SWIR	0.2202	20 m

2.3. Pre-Preprocessing and Classification

The satellite images to be used in the study may contain various errors. To make the images usable by rectifying errors, pre-processing has been applied to the images. The Sentinel-2A satellite data used in the study are Level 1 data, which have not undergone atmospheric correction. Therefore, an atmospheric correction process was applied to the images initially. Subsequently, a reprojection process was applied to bring the images into convenient projection. A resampling process was carried out to ensure that the bands with different resolutions in the satellite image have a consistent resolution (all at 10 m). All images were determined by considering a 5-km buffer zone and then clipped from the main image. All processing steps were carried out using the SNAP 7.0 program.

The preferred method in this research is shaped by extracting prominent features in images using spectral indices and then classifying all generated images with the RF classification technique to create LULC maps (Chan & Paelinckx, 2008; Ghimire et al., 2010; Pal, 2005).

The classification process has been created with six LULC classes: Agriculture (A), Forest (F), Olive (O), Pasture (P), Urban (U), and Water (W). In the selection of these classes, fieldwork was conducted to detect LULC types, and the classes were determined through visual interpretation. A total of 2050 training data were used for classification for the 6 LULC classes. For accuracy analysis, 410 ground control points were randomly selected for each classification to form homogeneous test data for the 6 LULC classes (training/test data: 2050/410). The process from acquiring the images to the accuracy analysis is shown in Figure 2.

Figure2. Flowchart of the study

Image classification is commonly used in RS to obtain quantitative data from satellite images (Baeza & Paruelo, 2020; Radhika & Varadar, 2016; Meinel & Neubert, 2004; Mendoza & Martins, 2006). In this study, a total of 2050 training vectors were defined for classification, with attention to the areas covered by the 6 LULC classes in the field. Information about the band combinations used in the classification process, as well as the names, formulas, and references to the resulting indices, can be found in Table 3. In the nomenclature of the combinations in Table 3, 'O' represents the original bands (10 bands) in the image, 'I' represents the new band created with the NDVI index (Table 3), and 'SR' represents the new band created with the simple ratios (Table 3).

Table 3. Indices and their features

Name	Bands	Formula	Classification Method	Algorithm	References
O_{RF}	B2, B3, B4, B5, B6, B7, B8, B8A, B11, B12	*B2+B3+B4+B5+ B6+B7+B8+B8A+B 11+B12*	Random Forest	Machine Learning	(Colkesen et al., 2021; Demarchi, et al., 2014; Goel & Abhilasha, 2017; Hütt et al., 2016; Jamali & Abdul Rahman, 2019a, 2019b; Kavzoglu et al., 2015; Phiri et al., 2020; Rodriguez-Galiano et al., 2012; Wu et al., 2021)
OI_5	B2, B3, B4, B6, B7, B8, B8A, B11, B12	$B2+B3+B4+B6+ B7+B8+B8A+B11+ B12+(\frac{B5-B4}{B5+B4})$	Random Forest	Machine Learning	(Ahamed et al., 2011; Gitelson et al., 2002)
OI_6	B2, B3, B4, B5, B7, B8, B8A, B11, B12	$B2+B3+B4+B5+ B7+B8+B8A+B11+ B12+(\frac{B6-B4}{B6+B4})$	Random Forest	Machine Learning	(Xianju et al., 2017)
OI_7	B2, B3, B4, B5, B6, B8, B8A, B11, B12	$B2+B3+B4+B5+ B6+B8+B8A+B11+ B12+(\frac{B7-B4}{B7+B4})$	Random Forest	Machine Learning	(Zarco-Tejada et al., 2001)
OI_8	B2, B3, B4, B5, B6, B7, B8A, B11, B12	$B2+B3+B4+B5+ B6+B7+B8A+B11+ B12+(\frac{B8-B4}{B8+B4})$	Random Forest	Machine Learning	(Barnes et al., 2000; Herrmann et al., 2011; Le Maire et al.,2004; Main et al., 2011; Penuelas et al., 1997; Wu et al., 2008)
OI_{8a}	B2, B3, B4, B5, B6, B7, B8, B11, B12	$B2+B3+B4+B5+ B6+B7+B8+B11+B 12+(\frac{B8A-B4}{B8A+B4})$	Random Forest	Machine Learning	(Tesfaye et al., 2021 Tucker, 1980; Zhang et al., 2017)
OI_{11}	B2, B3, B4, B5, B6, B7, B8, B8A, B12	$B2+B3+B4+B5+ B6+B7+B8+B8A+B 12+(\frac{B11-B4}{B11+B4})$	Random Forest	Machine Learning	Panigrahy et al., 2009; Tucker, 1979)
OI_{12}	B2, B3, B4, B5, B6, B7, B8, B8A, B11	$B2+B3+B4+B5+ B6+B7+B8+B8A+B 11+.(\frac{B12-B4}{B12+B4})$	Random Forest	Machine Learning	-
OI_5SR_6	B2, B3, B4, B7, B8, B8A, B11, B12	$B2+B3+B4+B7+ B8+B8A+ B11+B12+ (\frac{B5-B4}{B5+B4})+(\frac{B6}{B5})$	Random Forest	Machine Learning	-
OI_5SR_7	B2, B3, B4, B6, B8, B8A, B11, B12	$B2+B3+B4+B6+ B8+B8A+ B11+B12+ (\frac{B5-B4}{B5+B4})+(\frac{B7}{B5})$	Random Forest	Machine Learning	-

Table 3. Cont.

Name	Bands	Formula	Classification Method	Algorithm	References
OI_6SR_6	B2, B3, B4, B7, B8, B8A, B11, B12	B2+B3+B4+B7+ B8+B8A+ B11+B12+ $(\frac{B6-B4}{B6+B4})+(\frac{B6}{B5})$	Random Forest	Machine Learning	-
OI_6SR_7	B2, B3, B4, B8, B8A, B11, B12	B2+B3+B4+ B8+B8A+ B11+B12+ $(\frac{B6-B4}{B6+B4})+(\frac{B7}{B5})$	Random Forest	Machine Learning	-
OI_7SR_6	B2, B3, B4, B8, B8A, B11, B12	B2+B3+B4+ B8+B8A+ B11+B12+ $(\frac{B7-B4}{B7+B4})+(\frac{B6}{B5})$	Random Forest	Machine Learning	-
OI_7SR_7	B2, B3, B4, B6, B8, B8A, B11, B12	B2+B3+B4+ B6+B8+B8A+ B11+B12+ $(\frac{B7-B4}{B7+B4})+(\frac{B7}{B5})$	Random Forest	Machine Learning	-
OI_8SR_6	B2, B3, B4, B7, B8A, B11, B12	B2+B3+B4+ B7+ B8A+ B11+B12+ $(\frac{B8-B4}{B8+B4})+(\frac{B6}{B5})$	Random Forest	Machine Learning	-
OI_8SR_7	B2, B3, B4, B6, B8A, B11, B12	B2+B3+B4+ B6+ B8+B8A+ B11+B12+ $(\frac{B8-B4}{B8+B4})+(\frac{B7}{B5})$	Random Forest	Machine Learning	-
$OI_{8a}SR_6$	B2, B3, B4, B7, B8, B11, B12	B2+B3+B4+ B7+ B8+ B11+B12+ $(\frac{B8A-B4}{B8A+B4})+(\frac{B6}{B5})$	Random Forest	Machine Learning	-
$OI_{8a}SR_7$	B2, B3, B4, B6, B8, B11, B12	B2+B3+B4+ B6+ B8+ B11+B12+ $(\frac{B8A-B4}{B8A+B4})+(\frac{B7}{B5})$	Random Forest	Machine Learning	-
$OI_{11}SR_7$	B2, B3, B4, B6, B8, B8A, B12	B2+B3+B4+ B6+ B8+B8A+ B12+ $(\frac{B11-B4}{B11+B4})+(\frac{B7}{B5})$	Random Forest	Machine Learning	-
$OI_{12}SR_6$	B2, B3, B4, B7, B8, B8A, B11	B2+B3+B4+ B7+ B8+B8A+ B11+ $(\frac{B12-B4}{B12+B4})+(\frac{B6}{B5})$	Random Forest	Machine Learning	-
$OI_{12}SR_7$	B2, B3, B4, B6, B8, B8A, B11	B2+B3+B4+ B6+ B8+B8A+ B11 + $(\frac{B12-B4}{B12+B4})+(\frac{B7}{B5})$	Random Forest	Machine Learning	-

2.4. Classification

Indices are a mathematical set of operations frequently used in RS that enable the extraction of dominant features by utilizing spectral bands to understand the state of the terrain. The goal is to determine changes in LULC by examining the responses provided by the values in the bands for specific information extraction over an area. Various combinations are created to obtain the desired geographic information, resulting in the generation of indices.

A total of 21 indices have been created in the study. Seven of these indices contain only the bands formed in the 'I' shape, while the remaining 14 include bands formed in both 'I' and 'SR' shapes. The bands referred to as 'I' use NDVI mathematics, while the bands referred to as 'SR' use simple ratio mathematics. When creating these indices, all bands used in the new bands (except the red band - B4) have been subtracted from the original band content.

In this way, the subtracted original bands and the newly created index bands have been combined.

The RF classification technique involves constructing patterns by forming multiple decision trees with random input data, including a structural classification process (Perumal & Bhaskaran, 2010). Decision trees are created by branching test data in the training process (Goel & Abhilasha, 2017).

In this context, each tree is determined by combinations arising from the data in the field and the vectors affected by independent variables. Each input vector data contains pixel values within its content (Breiman, 2001; Phiri et al., 2020). When compared to other machine learning techniques, the reason for preferring RF is its ability to make pixel values meaningful with a small amount of training data and its high capability for fast processing.

RF classification technique uses the Gini index as a criterion in the machine learning algorithm. The equation for the Gini index is given in Equation 1 below. It is used as an attribute selection criterion to measure the impurity of a feature with respect to classes (Pal, 2005).

$$\sum\sum(fC_i,T)/(|T|)\ (fC_J,T)/(|T| \quad (1)$$

The Gini index branches the test data into a tree structure based on classes. Here, T represents the training dataset, and performs random pixel assignment is performed to the representative of class C_i (Pal, 2005).

2.5. Accuracy Assessment

Accuracy analysis is crucial in UA (Akturk & Altunel, 2019; Whiteside et al., 2011) for quantifying the accuracy of classification outputs on a class-by-class basis. It is important for investigating discrepancies between satellite data and actual terrain and examining user errors. In the verification process, the comparison between each pixel in the field and ground control points is used to understand the quality of the generated data.

In the study, control points were randomly selected homogeneously from different pixels considering the areas of LULC classes. Accuracy analysis conducted total 410 ground control points were created in the Google Earth Pro program for the 6 main LULC classes in each classification. According to the equation found in Guan et al. (2012), ground control points were selected beyond the maximum number for each class for the verification process (Equations 2). For the accuracy analysis of the classification, ground sample points were obtained separately for each classification, with a total of 410 homogenous points for each classification. The created ground control points were processed on Sentinel-2 satellite imagery with 10 m resolution. The indices that yielded the highest and lowest accuracy as a result of the combinations were determined separately for each of the three seasons. The equations used to create the error matrix in the study are provided in Equations 3 and 4 (Zaidi et al., 2017). Accuracy assessment results in the classified images were obtained for the RF classification technique using SNAP 7.0 software.

$$N = \frac{Z^2 * p(100-q)}{E^2} \quad (2)$$

N = number of points to be selected
Z = two-sided confidence level (from normal standard deviation)
p = expected percentage accuracy
q = logic operator
E= allowable error

$$Overall\ Accuracy = \frac{Sum\ of\ true\ random\ points}{Cumulative\ sum\ of\ all\ random\ points} \quad (3)$$

$$k_c = \frac{Observed - Expected}{1 - Expected} \quad (4)$$

3. RESULTS

In this study, which explored new created index combinations, the aim was to find the combination that provides the highest accuracy in classification.

3.1. Results of the Accuracy Analysis of the LULC Classification

In all accuracy analysis results, the highest and lowest accuracy rates for the years 2016 and 2020 are as follows for different seasons.

For the 2016-winter season (OI_8SR_7- overall accuracy: 76.04%, kappa: 0.73, OI_{12}- 82.93%, 0. 79), for the 2016-spring season ($OI_{11}SR_7$- 76.16%, 0.71, O_{RF}-84.44%, 0.82), 2016-summer season (OI_{8a}- 76.64%, 0.71, O_{RF}- 84.67%, 0. 83%) and respectively, 2020-winter season ($OI_{11}SR_7$- overall accuracy: 75.12%, kappa: 0.70, O_{RF}- 82.72%, 0.79), 2020-spring season ($OI_{12}SR_7$- 75. 12, 0.70%, O_{RF}- 84.75%, 0.82), for 2020-summer season ($OI_{11}SR_7$- 78.05%, 0.73, O_{I6}- 84.63%, 0.81) (Table 4-Table 5).

The results of the accuracy analysis conducted for RF classification using original satellite image bands and classification with a combination of 21 indices, in terms of the reasons for the highest and lowest accuracy, are as follows:

- For the winter season of 2016, classification results have been obtained for OI_{12} (high) and OI_8SR_7 (low) (Table 4). OI_{12} yielded a high classification result because, during the period when Band 12 had an impact, there was a high moisture content in the early growth stage of crops in the study area. Additionally, the specific characteristics of the index used in its mathematics, such as B12 measuring moisture content (for both soil and vegetation) and B8 being used for vegetation detection, contributed to the high result. In the classification of OI_8SR_7, it was observed that on the specified date, the mathematical expression did not capture the

vegetation pixels with Band 8 (B8). Band 7 (B7) did not have an impact on pixel visibility because it was subtracted from the original bands.

- For the spring season of 2016 (Table 4), the O_{RF} classification provided better discrimination for both urban and agricultural areas. This was attributed to the fact that the original content and combination of the ten bands remained unchanged. At the examined date, the land surface was covered with vegetation up to 70-80%, facilitating the distinction between urban and agricultural areas. Similarly, in the $OI_{11}SR_7$ classification for the same season, the low accuracy rate was exclusion of Band 5 (B5) and B7 from the original band combination. Attributed to the weakening of detection due to the vegetation at the date (mostly in the early growth stage). This was also due to the challenge of detection caused by Band 11 (B11)'s wide band range.
- In the summer season of 2016 (Table 4), once again, the O_{RO} classification provided higher accuracy results for the same reasons as the spring season. However, it was believed that the low accuracy of the OI_{8a} index might have been due to the agricultural areas not being selected in the classification process because the vegetation cover in the study area was less extensive.

Table 4. Results of the Accuracy Analysis in 2016(light blue: low accuracy, pink: high accuracy

Bands	9.01.2016				18.04.2016				16.08.2016			
	Producer	User	Overall	Kappa	Producer	User	Overall	Kappa	Producer	User	Overall	Kappa
O_{RF}	0.839	0.788	81.220	0.769	0.800	0.711	84.436	0.815	0.619	0.963	84.670	0.826
OI_5	0.926	0.806	79.756	0.773	0.895	0.773	79.512	0.723	0.944	0.791	81.265	0.741
OI_5SR_6	0.740	0.673	76.832	0.721	0.840	0.778	78.537	0.744	0.760	0.844	78.586	0.744
OI_5SR_7	0.780	0.639	77.750	0.744	0.700	0.745	79.268	0.723	0.780	0.830	78.345	0.747
OI_6	0.854	0.854	82.439	0.734	0.880	0.786	77.995	0.688	0.833	0.811	79.756	0.769
OI_6SR_6	0.780	0.661	77.017	0.717	0.820	0.774	78.832	0.743	0.760	0.826	78.832	0.738
OI_6SR_7	0.780	0.661	78.780	0.720	0.680	0.756	77.129	0.717	0.740	0.822	78.838	0.735
OI_7	0.743	0.788	78.293	0.718	0.955	0.824	80.456	0.728	0.774	0.828	81.707	0.752
OI_7SR_6	0.780	0.672	76.585	0.721	0.860	0.782	78.780	0.739	0.800	0.833	78.345	0.741
OI_7SR_7	0.740	0.627	76.829	0.709	0.860	0.768	76.642	0.739	0.800	0.833	78.102	0.738
OI_8	0.737	0.737	77.317	0.748	0.974	0.804	77.805	0.740	0.875	0.718	79.512	0.764
OI_8SR_6	0.780	0.661	76.830	0.720	0.820	0.745	78.431	0.741	0.800	0.833	78.589	0.740
OI_8SR_7	0.820	0.661	76.039	0.731	0.860	0.768	78.378	0.749	0.780	0.830	78.398	0.738
OI_{8a}	0.828	0.857	76.755	0.708	0.750	0.818	76.341	0.710	0.862	0.543	76.642	0.710
$OI_{8a}SR_6$	0.780	0.672	77.017	0.722	0.840	0.750	78.780	0.744	0.780	0.830	78.208	0.736
$OI_{8a}SR_7$	0.780	0.672	76.773	0.719	0.880	0.786	79.024	0.746	0.860	0.827	79.707	0.755
OI_{11}	0.895	0.895	80.813	0.758	0.923	0.750	78.166	0.721	0.862	0.862	80.976	0.761
$OI_{11}SR_6$	0.780	0.661	76.284	0.714	0.760	0.679	76.341	0.714	0.800	0.816	78.832	0.744
$OI_{11}SR_7$	0.800	0.690	78.240	0.737	0.800	0.667	76.156	0.712	0.860	0.827	79.319	0.750
OI_{12}	0.931	0.844	82.927	0.791	0.766	0.818	76.341	0.708	0.750	0.871	80.244	0.755
$OI_{12}SR_6$	0.820	0.683	77.017	0.722	0.740	0.822	77.073	0.722	0.860	0.827	79.218	0.749
$OI_{12}SR_7$	0.828	0.857	76.286	0.716	0.860	0.811	78.398	0.739	0.840	0.824	79.075	0.747

- For the winter season of 2020, the OI_5 classification provided higher accuracy results (Table 5) because agricultural areas did not exhibit significant features at the examined date, while urban and other areas did. Furthermore, the absence of mathematical operations on the original ten bands contributed to the higher accuracy. In contrast, the $OI_{11}SR_7$ index was found to not match agricultural areas due to the bands included in its content, which did not allow for the measurement of moisture content and vegetation content.
- For the spring season of 2020 (Table 5), the significant effect of the O_{RF} index, like the spring season of 2016, was understood to be due to the same influencing factors. The low results of the $OI_{12}SR_7$ index can be attributed to the exclusion of B5 and B7 from the original bands, crucial for vegetation analysis. Additionally, along with the detection weakness in the combination formed with Band 12 (B12), provides an explanation for the observed low values.
- For the summer season of 2020 (Table 5), OI6 index was identified as more suitable for classification. This suitability stems from its interaction with the red-edge band in the original bands, thereby enhancing its discriminative power for vegetation separation, especially during the targeted season. On the other hand, for $OI_{11}SR_7$, it was understood that there were no products in the field where the moisture content in vegetation would have an effect, and the removal of B5 and B7 from the original bands had a negative impact.

Table 5. Results of the Accuracy Analysis in 2020 (light blue: low accuracy, pink: high accuracy)

Bands	2.02.2020				17.04.2020				15.08.2020			
	Producer	User	Overall	Kappa	Producer	User	Overall	Kappa	Producer	User	Overall	Kappa
O_{RF}	0.925	0.803	82.716	0.788	0.828	0.649	84.748	0.817	0.926	0.806	82.439	0.785
OI_5	0.838	0.775	85.885	0.790	0.920	0.742	83.659	0.798	0.864	0.905	81.944	0.813
OI_5SR_6	0.821	0.657	79.756	0.756	0.844	0.864	78.802	0.795	0.700	0.972	81.220	0.792
OI_5SR_7	0.893	0.610	78.293	0.761	0.857	0.706	75.610	0.739	0.780	0.800	80.244	0.808
OI_6	0.829	0.850	82.683	0.701	0.935	0.906	84.185	0.783	0.743	0.788	84.634	0.770
OI_6SR_6	0.700	0.778	79.756	0.720	0.844	0.809	82.927	0.757	0.829	0.806	82.809	0.744
OI_6SR_7	0.720	0.766	80.244	0.732	0.778	0.833	78.537	0.728	0.786	0.733	84.146	0.763
OI_7	0.870	0.930	76.039	0.739	0.853	0.906	82.816	0.741	0.710	0.815	81.573	0.746
OI_7SR_6	0.700	0.745	76.829	0.711	0.857	0.706	79.756	0.749	0.600	0.844	78.922	0.768
OI_7SR_7	0.821	0.657	77.805	0.743	0.857	0.667	77.317	0.748	0.867	0.765	80.488	0.783
OI_8	0.957	0.898	79.024	0.748	0.813	0.830	79.951	0.800	0.750	0.828	79.024	0.779
OI_8SR_6	0.683	0.778	76.098	0.757	0.800	0.783	79.024	0.749	0.800	0.833	80.779	0.772
OI_8SR_7	0.683	0.757	78.780	0.739	0.711	0.762	78.810	0.708	0.780	0.848	81.951	0.760
OI_{8a}	0.773	0.895	76.098	0.706	0.964	0.871	79.661	0.739	0.778	0.778	81.220	0.768
$OI_{8a}SR_6$	0.700	0.778	78.049	0.734	0.667	0.833	79.024	0.747	0.756	0.861	83.659	0.803
$OI_{8a}SR_7$	0.700	0.745	76.341	0.714	0.857	0.615	78.537	0.740	0.720	0.837	79.692	0.758
OI_{11}	0.879	0.967	76.456	0.698	0.882	0.833	77.805	0.714	0.829	0.853	82.022	0.774
$OI_{11}SR_6$	0.720	0.783	78.537	0.741	0.893	0.595	78.049	0.738	0.740	0.822	78.729	0.743
$OI_{11}SR_7$	0.700	0.700	75.122	0.700	0.756	0.756	75.610	0.708	0.740	0.787	78.049	0.734
OI_{12}	0.828	0.857	78.049	0.729	0.867	0.963	80.244	0.748	0.771	0.659	79.775	0.746
$OI_{12}SR_6$	0.740	0.771	76.585	0.717	0.857	0.686	79.268	0.750	0.740	0.804	78.832	0.744
$OI_{12}SR_7$	0.740	0.771	76.575	0.716	0.733	0.767	75.122	0.702	0.680	0.773	78.537	0.740

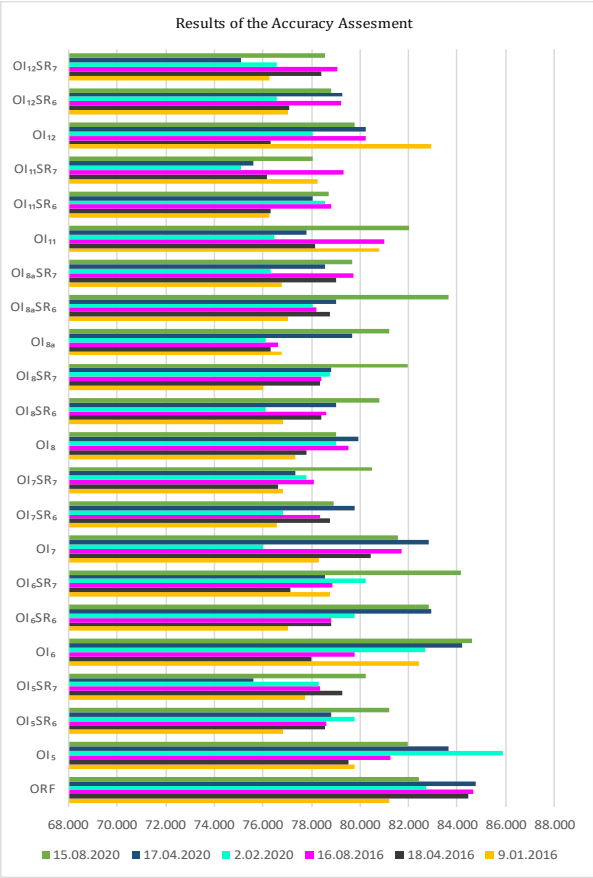

Figure 3. Accuracy Analysis Results

-In the changes obtained according to the combinations with the highest accuracy in 2016 and 2020 in the winter images (Figure 4 – Figure 5), it was observed that artificial green areas were formed because of the expropriation of the olive areas on the roadside. Therefore, it is understood that there has been a transformation from class O to class A. Technical errors in the classification of satellite data due to the ongoing construction of the Gemlik-Bursa North Interchange showed that U areas were confused with P class.

- Looking at the observations obtained from the spring images (Figure 6 – Figure 7), it is thought that there is a transformation from F areas to A areas, and that U and O classes have increased with the formation of rural settlements next to agricultural areas. It was also observed that the Gemlik-Bursa North Interchange, which was put into service on March 12, 2017, also affected the change of U areas.

- On the basis of the summer season (Figure 8 – Figure 9), it was concluded that the vegetation in the P class was mixed with the F class with the growing plant size.

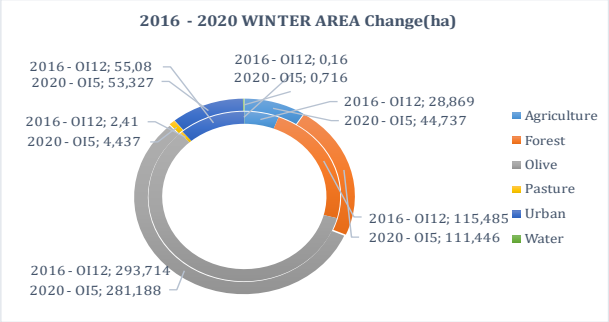

Figure 4. 2016 – 2020 the area changes in classes (Winter)

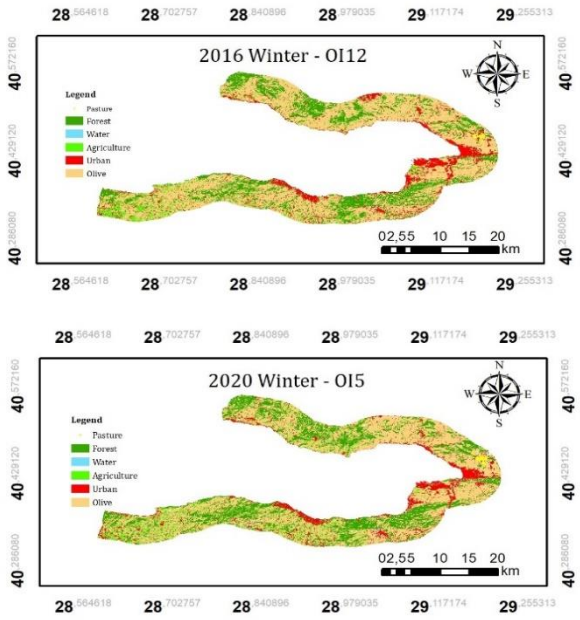

Figure 5. 2016 – 2020 the area changes in classes - map display (Winter)

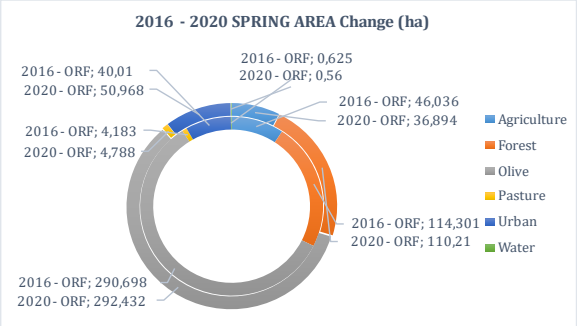

Figure 6. 2016 – 2020 the area changes in classes (Spring)

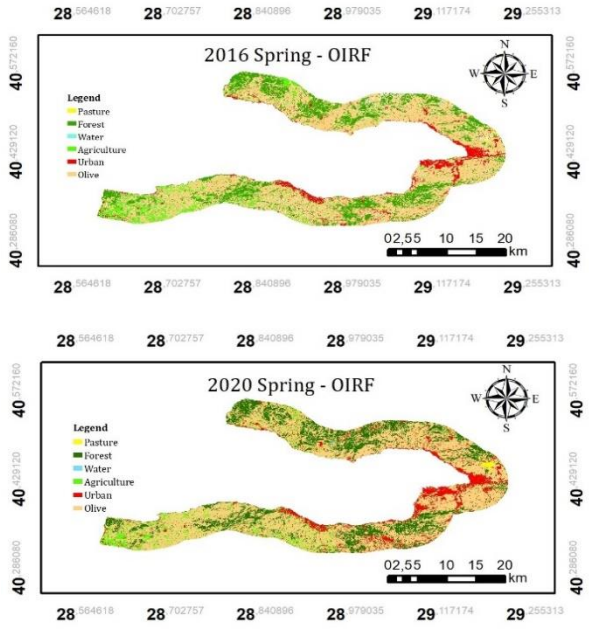

Figure 7. 2016 – 2020 the area changes in classes – map display (Spring)

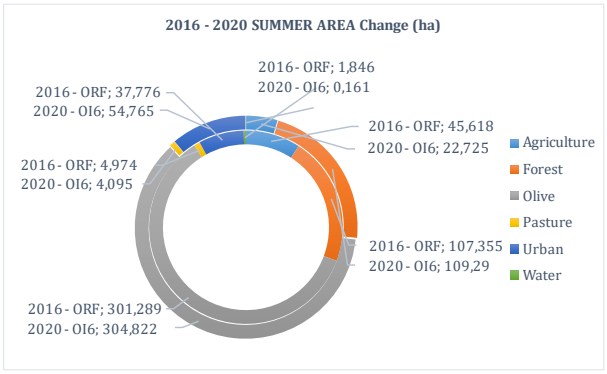

Figure 8. 2016 – 2020 the area changes in classes (Summer)

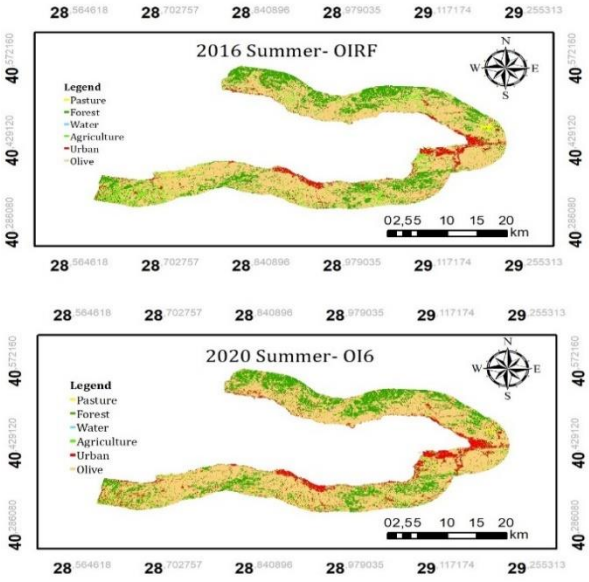

Figure 9. 2016 – 2020 the area changes in classes - map display (Summer)

4. DISCUSSION and CONCLUSION

4.1. Discussion

This study aimed to map LULC classes for three seasons using satellite imagery from 2016 and 2020 in order to observe the temporal effects of various state-funded investment decisions in Southeast Marmara region. It was found that the classification, using new indices, yielded accuracy results similar to those obtained from the original images. The construction of the TOGG factory and the decisions related to the Gemlik-Bursa Northern Interchange were observed to increase urbanization and consequently lead to population growth in the area. Additionally, it is believed that the COVID-19 pandemic, which occurred during the study period, led to an increase in the construction and real estate sectors, especially due to migrations to rural coastal areas such as Mudanya and Armutlu.

When examining the accuracy analysis results of the performed classifications, it was observed that the classification results from the original bands showed high accuracy. Additionally, the indices created using B6, B12, and B5 (indices without a simple ratio) also yielded favorable accuracy outcomes.

In this study, the combination that yielded the highest accuracy among index classifications was identified. The observed changes between 2016 and 2020 are believed to have resulted from various socioeconomic and technical reasons.

Accordingly, the dynamics of transformation from class O to class A in winter images are thought to be related to the expropriation of olive groves near the main road, leading to the creation of artificial green areas. Changes in classes U and P, on the other hand, were understood to be caused by technical errors in classification due to the continuation of the Gemlik-Bursa Northern Interchange project. In the spring season, there was a transformation from class F to class A due to the need for fertile soil. Consequently, the emergence of rural-urban areas, near agricultural areas led to an increase in classes U and O. Additionally, it was observed that the Gemlik-Bursa Northern Interchange, which became operational on March 12, 2017, impacted class U during the season. During the summer season, it was concluded that the growing vegetation height in class P often led to confusion with class F during the classification process. This study, conducted at the coastal scale, can be extended to examine other vegetation types in the region, and more detailed analyses can be applied.

The research emphasizes the importance of exploring the dynamics of land cover changes using new derived indices. In a study by Gitelson et al. (2002), various indices such as NDVI, ARVI, Soil Adjusted Vegetation Index (SAVI), and the red edge (700 nm) vegetation index were used for classification to measure sensitivity to atmospheric effects. It was found that NDVI yielded higher results. This study is in line with the aim of finding an index suitable for the purpose, but using existing indices may not provide a sufficient foundation for future modelling based on the accuracy assessment results which do not significantly differ from what expected.

A similar study conducted in the Western Ghats of South India addressed the effects of the pandemic through LULC classes and applied classification processes to Sentinel-2A satellite imagery using the NDVI index between 2018 and 2021. The study concluded that the dynamics of vegetation and urbanization changed due to the pandemic (Sathian & Brema, 2023). The outputs of this study, suggesting that changes in vegetation were based on urbanization, align with the findings of our study.

This study aimed to contribute to the literature by addressing the existing issues and providing an original perspective through the creation of LULC class results using classified images based on indices. In this context, our classifications and results have shown that investments in industrial zones near coastal areas are likely to have various effects, including population growth, migration movements, and changes in vegetation dynamics. It was determined that the increase in urban areas due to population growth had significant effects on LULC classes. The use of remote sensing data, different classification techniques, and various specific band combinations is expected to give more accurate results for future studies determining LULC dynamics.

4.2. Conclusion

The study was conducted to investigate LULC and vegetation dynamics along the coastal area of Southeastern Marmara Region with band combinations created using new vegetation indices. The combination that gives the best classification accuracy according to the seasons was determined and the accuracy analysis was used as a classification success scale. it was identified that how investment decisions taken by the government have led to an increase in impervious surfaces and how this has led to a change in other LULC classes The RF classification technique was applied to indices obtained from Sentinel-2A satellite images in three different seasons in 2016 and 2020. Subsequently, accuracy analysis was performed on classified images using ground control points obtained through Google Earth Pro. The study shows that the coastal area of Southeastern Marmara has been examined in detail with respect to LULC classes affected by various decisions using indices obtained from open-access and medium-resolution satellites. The study concludes that government investments in coastlines have caused significant LULC changes in the region and that these changes will be the beginning of other changes in the region. It is also concluded that the detailed LULC change detection can be further improved with the help of remote sensing and advance machine learning techniques.

In future studies, the use of machine learning methods, high-resolution images, more complex indices, and different classification techniques will facilitate a faster understanding of LULC dynamics and the investigation of future predictions.

Acknowledment

This study is part of the Eda ASCI's Master Thesis on Graduate School of Çanakkale Onsekiz Mart University, School of Graduate Studies, Department of Geographical Information Technology, Turkey.

Author contributions

E. Asci: Collected the datasets and analyzed the data, Classification, Validation.
L. Genc: Designed the research, Investigation, Writing the manuscript–review and editing.

Conflicts of Interest

The authors declare no conflict of interest.

Research and publication ethics statement

In the study, the authors declare that there is no violation of research and publication ethics and that the study does not require ethics committee approval.

REFERENCES

Ahamed, T., Tian, L., Zhang, Y. & Ting, K. C. (2011). A Review of Remote Sensing Methods for Biomass Feedstock Production. Biomass and Bioenergy, 35. https://doi.org/10.1016/j.biombioe.2011.02.028

Akturk, E. & Altunel, A. O. (2019). Accuracy Assesment of a Low-Cost UAV Derived Digital Elevation Model (DEM) in a Highly Broken and Vegetated Terrain. *Measurement,* 136, 382-386. https://doi.org/10.1016/j.measurement.2018.12.101

Asci, E., Inalpulat, M. & Genc, L. (2021). Identification of Residential Development Impacts on Agrıcultural Lands Using Landsat Imageries: Case Study of Bursa, Nilufer (1990-2020). *III. Balkan Agricultural Congress (AGRIBALKAN),* Edirne, Turkey.

Baeza, S. & Paruelo, J. M. (2020). Land Use/Land Cover Change (2000-2014) in The Rio De La Plata Grasslands: An Analysis Based on MODIS NDVI Time Series. *Remote Sensing*, 12(3). https://doi.org/10.3390/rs12030381

Barnes, E. M., Clarke, T. R., Richards, S. E., Colaizzi, P. D., Haberland, J., Kostrzewski, M., Waller , P., Choi, C., Rilye, E., Thomson, T., Lascano, R. J., Li, H. & Moran, M. S. (2000). Coincident Detection of Crop Water Stress, Nitrogen Status and Canopy Density Using Ground Based Multispectral Data. Proc. *5th Int. Conf. Precis Agric*, 1619(6).

Batunacun, Nendel, C., Hu, Y. & Lakes, T. (2018). Land-Use Changea and Land Degradation on The Mongolian Plateau from 1975 To 2015—A Case Study From Xilingol, China. *Land Degradation and Development,* 29(6), 1595–1606. https://doi.org/10.1002/LDR.2948

Breiman, L. (2001). Random Forests. *Machine Learning*, 45, 5-32. https://doi.org/10.1023/A:1010933404324

Cavur, M., Duzgun, H. S., Kemec, S. & Demirkan, D. C. (2019). Land Use and Land Cover Classification of Sentinel-2A: St.Petersburg Case Study. *International Archives of the Photogrammetry, Remote Sensing and Spatial Information Sciences - ISPRS Archives*, 42(1/W2). https://doi.org/10.5194/isprs-archives-XLII-1-W2-13-2019

Chan, J. C. W. & Paelinckx, D. (2008). Evaluation of Random Forest and Adaboost Tree-Based Ensemble Classification and Spectral Band Selection for Ecotope Mapping Using Airborne Hyperspectral Imagery. *Remote Sensing of Environment,* 112(6), 2999–3011. https://doi.org/10.1016/J.RSE.2008.02.011

Chandra Pandey, P., Koutsias, N., Petropoulos, G. P., Srivastava, P. K., & Ben Dor, E. (2019). Land Use/Land Cover in View of Earth Observation: Data Sources, Input Dimensions, and Classifiers-A Review of The State of The Art. *Geocarto International,* 36, 957–988. https://doi.org/10.1080/10106049.2019.1629647

Chehata, N., Guo, L. & Forests, R. (2009). Airborne Lidar Feature Selection for Urban Classification Using Random Forests. *Laser Scanning*, XXXVIII(3/W8), Paris, France.

Colkesen, I., Ozturk, M. Y., Kavzoglu, T. & Sefercik, U. G. (2021). Determination of sea surface mucilage formations using multitemporal Sentinel-2 imagery. *In Proceedings of the the 42nd Asian Conference on Remote Sensing (ACRS2021),* Can Tho City, Vietnam, 22-24.

Demarchi, L., Canters, F., Cariou, C., Licciardi, G. & Chan, J. C. W. (2014). Assessing The Performance of Two Unsupervised Dimensionality Reduction Techniques on Hyperspectral APEX Data for High Resolution Urban Land-Cover Mapping. *ISPRS Journal of Photogrammetry and Remote Sensing,* 87. https://doi.org/10.1016/j.isprsjprs.2013.10.012

Dewidar, K. M. (2010). Detection of Land Use/Land Cover Changes for the Northern Part of The Nile Delta (Burullus Region), Egypt. *International Journal of Remote Sensing,* 25(20), 4079–4089. https://doi.org/10.1080/01431160410001688312

El-naggar, A. M. (2018). Determination of optimum segmentation parameter values for extracting building from remote sensing images. *Alexandria engineering journal*, 57(4), 3089-

3097. https://doi.org/10.1016/j.aej.2018.10.001

Genc, L. (2002). Comparison of Landsat MSS and TM imagery for long term forest land cover change assessment. *Doctoral Thesis*, University of Florida, USA, 177p (in English).

Ghimire, B., Rogan, J., & Miller, J. (2010). Contextual Land-Cover Classification: Incorporating Spatial Dependence in Land-Cover Classification Models Using Random Forests and The Getis Statistic. *Remote Sensing Letters*, 1(1), 45–54. https://doi.org/10.1080/01431160903252327

Gitelson, A. A., Kaufman, Y. J., Stark, R. & Rundquist, D. (2002). Novel Algorithms for Remote Estimation of Vegetation Fraction. *Remote Sensing of Environment,* 80(1). https://doi.org/10.1016/S0034-4257(01)00289-9

Goel, E. & Abhilasha, E. (2017). Random Forest: A Review. *International Journal of Advanced Research in Computer Science and Software Engineering.* https://doi.org/10.23956/ijarcsse/v7i1/01113

Guan, H., Yu, J., Li, J. & Luo, L. (2012). Random Forests-Based Feature Selection For Land-Use Classification Using Lidar Data and Orthoimagery. *The International Archives of the Photogrammetry, Remote Sensing and Spatial Information Sciences,* XXXIX-B7. https://doi.org/10.5194/isprsarchives-xxxix-b7-203-2012

Herrmann, I., Pimstein, A., Karnieli, A., Cohen, Y., Alchanatis, V. & Bonfil, D. J. (2011). LAI Assessment of Wheat and Potato Crops by Venμs and Sentinel-2 Bands. *Remote Sensing of Environment,* 115(8). https://doi.org/10.1016/j.rse.2011.04.018

Hütt, C., Koppe, W., Miao, Y. & Bareth, G. (2016). Best Accuracy Land Use/Land Cover (LULC) Classification To Derive Crop Types Using Multitemporal, Multisensor, and Multi-Polarization SAR Satellite Images. *Remote Sensing.* https://doi.org/10.3390/rs8080684

Jamali, A. & Abdul Rahman, A. (2019a). Evaluation of Advanced Data Mining Algorithms in Land Use/Land Cover Mapping. *International Archives of the Photogrammetry, Remote Sensing and Spatial Information Sciences - ISPRS Archives,* 42(4/W16). https://doi.org/10.5194/isprs-archives-XLII-4-W16-283-2019

Jamali, A. & Abdul Rahman, A. (2019b). Sentinel-1 Image Classification For City Extraction Based on The Support Vector Machine and Random Forest Algorithms. *International Archives of the Photogrammetry, Remote Sensing and Spatial Information Sciences - ISPRS Archives*, 42(4/W16). https://doi.org/10.5194/isprs-archives-XLII-4-W16-297-2019

Joshi, R. R., Warthe, M., Dwivedi, S., Vijay, R. & Chakrabarti, T. (2011). Monitoring Changes in Land Use Land Cover of Yamuna Riverbed in Delhi: A Multi-Temporal Analysis. *International Journal of Remote Sensing*, 32(24), 9547–9558. https://doi.org/10.1080/01431161.2011.565377

Radhika, K. & Varadar, S. (2016). A Tutorial on Classification of Remote Sensing Data. *International Research Journal of Engineering and Technology (IRJET),* 3(8), 881-885.

Kavzoglu, T., Colkesen, I. & Yomralioglu, T. (2015). Object-Based Classification with Rotation Forest Ensemble Learning Algorithm Using Very-High-Resolution Worldview-2 Image. *Remote Sensing Letters,* 6(11). https://doi.org/10.1080/2150704X.2015.1084550

Kumar, V. & Agrawal, S. (2019). Agricultural Land Use Change Analysis Using Remote Sensing And GIS: A Case Study of Allahabad, India. *International Archives of the Photogrammetry, Remote Sensing and Spatial Information Sciences - ISPRS Archives*, 42(3/W6), 397–402. https://doi.org/10.5194/ISPRS-ARCHIVES-XLII-3-W6-397-2019

Le Maire, G., François, C. & Dufrêne, E. (2004). Towards Universal Broad Leaf Chlorophyll Indices Using PROSPECT Simulated Database and Hyperspectral Reflectance Measurements. *Remote Sensing of Environment,* 89(1). https://doi.org/10.1016/j.rse.2003.09.004

Main, R., Cho, M. A., Mathieu, R., O'Kennedy, M. M., Ramoelo, A. & Koch, S. (2011). An Investigation Into Robust Spectral Indices for Leaf Chlorophyll Estimation. *ISPRS Journal of Photogrammetry and Remote Sensing,* 66(6). https://doi.org/10.1016/j.isprsjprs.2011.08.001

Meinel, G. & Neubert, M. (2004). A Comparison of Segmentation Programs for High Resolution Remote Sensing Data*. International Archives of Photogrammetry and Remote Sensing,* 35(Part B), 1097-1105.

Mendoza, G. A. & Martins, H. (2006). Multi-Criteria Decision Analysis in Natural Resource Management: A Critical Review of Methods and New Modelling Paradigms. *Forest Ecology and Management,* 230, 1–22. https://doi.org/10.1016/j.foreco.2006.03.023

Mukhawana, M. B., Kanyerere, T. & Kahler, D. (2023). Review of In-Situ and Remote Sensing-Based Indices and Their Applicability for Integrated Drought Monitoring in South Africa. *Water*, 15. https://doi.org/10.3390/w15020240

Myint Htun, A., Shamsuzzoha, M. & Ahamed, T. (2023). Rice Yield Prediction Model Using Normalized Vegetation and Water Indices from Sentinel-2A Satellite Imagery Datasets. *Asia-Pacific Journal of Regional Science*, 7, 491–519. https://doi.org/10.1007/s41685-023-00299-2

Pal, M. (2005). Random Forest Classifier for Remote Sensing Classification. *International Journal of Remote Sensing,* 26(1), 217–222. https://doi.org/10.1080/01431160412331269698

Panigrahy, R. K., Ray, S. S. & Panigrahy, S. (2009). Study on the utility of IRS-P6 AWIFS SWIR band for crop discrimination and classification. *Journal of the Indian Society of Remote Sensing*, 37, 325-333. https://doi.org/10.1007/s12524-009-0026-6

Penuelas, J., Pinol, J., Ogaya, R., Filella, I., Pen Ä Uelas, J., Pin, J. & Ol, Ä. (1997). Estimation of Plant Water Concentration By The Reflectance Water Index WI (R900/R970). *International Journal of Remote Sensing,* 18(13), 2869–2875. https://doi.org/10.1080/014311697217396

Perumal, K. & Bhaskaran, R. (2010). Supervised Classification Performance of Multispectral Images. *Journal of Computing*, 2(2), 124-129.

Phiri, D., Simwanda, M., Salekin, S., Nyirenda, V. R., Murayama, Y. & Ranagalage, M. (2020). Sentinel-2 Data for Land Cover/Use Mapping: A Review. *Remote Sensing,* 12(14). https://doi.org/10.3390/rs12142291

Rodriguez-Galiano, V. F., Ghimire, B., Rogan, J., Chica-Olmo, M. & Rigol-Sanchez, J. P. (2012). An Assessment Of The Effectiveness Of A Random Forest Classifier For Land-Cover Classification. *ISPRS Journal of Photogrammetry and Remote Sensing,* 67(1), 93–104. https://doi.org/10.1016/J.ISPRSJPRS.2011.11.002

Sathian, S. & Brema, J. (2023). Assessment of Vegetative Cover Dynamics During Pre and Post Covid-19 Period Using Sentinel-2A Imageries in the Western Ghats, South India. *Journal of Metrology Society of India*, 14. https://doi.org/10.1007/s12647-023-00683-5

Scornet, E. (2015). Random Forests and Kernel Methods. *IEEE Transactions on Information Theory,* 62(3), 1485-1500. https://doi.org/10.1109/TIT.2016.2514489

Sharma, R. & Joshi, P. K. (2016). Mapping Environmental Impacts Of Rapid Urbanization in The National Capital Region of India Using Remote Sensing Inputs. *Urban Climate*, 15(2016), 70-82. https://doi.org/10.1016/j.uclim.2016.01.004

Tesfaye, A. A. & Gessesse Awoke, B. (2021). Evaluation of The Saturation Property of Vegetation Indices Derived from Sentinel-2 in Mixed Crop-Forest Ecosystem. Spatial Information Research, 29, 109-121. https://doi.org/10.1007/s41324-020-00339-5

Tucker, C. J. (1979). Red and Photographic Infrared Linear Combinations for Monitoring Vegetation. *Remote Sensıng of Environment*, 8, 127–150. https://doi.org/10.1016/0034-4257(79)90013-0

Tucker, C. J. (1980). Remote Sensing of Leaf Water Content in the Near İnfrared. *Remote Sensing of Environment,* 10(1), 23–32. https://doi.org/10.1016/0034-4257(80)90096-6

Whiteside, T. G., Boggs, G. S. & Maier, S. W. (2011). Comparing Object-Based and Pixel-Based Classifications for Mapping Savannas. *International Journal of Applied Earth Observation and Geoinformation*, 13(6), 884–893. https://doi.org/10.1016/j.jag.2011.06.008

Wu, C., Niu, Z., Tang, Q. & Huang, W. (2008). Estimating Chlorophyll Content from Hyperspectral Vegetation Indices: Modeling and Validation. *Agricultural and Forest Meteorology,* 148(8–9). https://doi.org/10.1016/j.agrformet.2008.03.005

Wu, T., Luo, J., Gao, L., Sun, Y., Dong, W., Zhou, N., Liu, W., Hu, X., Xi, J., Wang, C. & Yang, Y. (2021). Geo-Object-Based Vegetation Mapping via Machine Learning Methods with an Intelligent Sample Collection Scheme: A Case Study of Taibai Mountain, China. *Remote Sensing.* https://doi.org/10.3390/rs13020249

Xianju, L., Gang, C., Jingyi, L., Weitao, C., Xinwen, C. & Yiwei, L. (2017). Effects of RapidEye Imagery's Red-edge Band and Vegetation Indices on Land Cover Classification in an Arid Region. *Chinese Geographical Science,* 27(5), 827–835. https://doi.org/10.1007/s11769-017-0894-6

Yulianti, E. (2019). Multi-Temporal Sentinel-2 Images for Classification Accuracy. *Journal of Computer Science,* 15, 258–268. https://doi.org/10.3844/jcssp.2019.258.268

Zaidi, S. M., Akbari, A., Abu Samah, A., Kong, N. S. Gisen, J. I. A. (2017). Landsat-5 Time Series Analysis for Land Use/Land Cover Change Detection Using NDVI and Semi-Supervised Classification Techniques. *Polish Journal of Environmental Studies,* 26(6), 2833-2840. https://doi.org/10.15244/pjoes/68878

Zarco-Tejada, P. J., Miller, J. R., Noland, T. L., Mohammed, G. H. & Sampson, P. H. (2001). Scaling-Up and Model Inversion Methods with Narrowband Optical Indices for Chlorophyll Content Estimation in Closed Forest Canopies with Hyperspectral Data. *IEEE Transactions on Geoscience and Remote Sensing*, 39(7). https://doi.org/10.1109/36.934080

Zhang, T., Su, J., Liu, C., Chen, W. H., Liu, H., & Liu, G. (2017). Band selection in sentinel-2 satellite for agriculture applications. *In 2017 23rd international conference on automation and computing (ICAC)*, Huddersfield, UK, 1-6.

Araştırma Makalesi/Research Article
https://doi.org/10.51489/tuzal.1400620

2024; 6(1); 26-34

Turkish Journal of Remote Sensing

https://dergipark.org.tr/en/pub/tuzal

e-ISSN 2687-4997

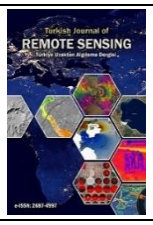

Determination of Potential Geothermal Areas in Konya Seydişehir District Using GIS-based Multi-Criteria Decision Analysis

Münevver Gizem Gümüş*[1], Süleyman Savaş Durduran[2]

[1]Niğde University, Engineering Faculty, Geomatics Engineering, Niğde, Turkey
[2]Necmettin Erbakan University, Engineering Faculty, Geomatics Engineering, Konya, Turkey

Keywords
Analytical Hierarchy Method
Geographic Information System
Multi-Criteria Decision Making
Geothermal Energy
Spatial Analysis

ABSTRACT

Today, one of the main challenges that countries face in their economic and social development efforts is to ensure access to cheap, clean and reliable energy resources. Especially the damages caused by fossil fuels and major environmental problems such as global warming increase the need for renewable energy sources. Turkey is among the richest countries in the world in terms of geothermal energy potential. Our country has great geothermal potential, ranking first in Europe and seventh in the world. Seydişehir district of Konya province is a residential area that has attracted attention in recent years with its geothermal energy potential and developments in the field of thermal tourism and the process of exploring geothermal areas is ongoing. In this study, the Analytic Hierarchy Process (AHP) method, which is a GIS-based Multi-Criteria Decision Analysis method (MCDA), was used to identify potential geothermal areas. All criteria used for the AHP method were determined by taking expert opinion and literature research. The potential geothermal map of the region was produced by combining the weighted layers of the standardized data according to AHP. With such a study, it is foreseen that the geothermal potential areas identified in the region will constitute an important infrastructure inventory for local governments and decision-makers in terms of evaluating and developing geothermal resources and providing suggestions for investments to be made in order to bring the maximum capacity to the national economy.

Konya Seydişehir İlçesinde CBS Tabanlı Potansiyel Jeotermal Alanların Belirlenmesi için Çok Ölçütlü Karar Analizi Kullanımı

Anahtar Kelimeler:
Analitik Hiyerarşi Yöntemi
Coğrafi Bilgi Sistemi
Çok Ölçütlü Karar Verme
Jeotermal Enerji
Mekânsal Analiz

ÖZ

Günümüzde, ülkelerin ekonomik ve sosyal kalkınma çabalarında karşılaştıkları temel sorunlardan biri, ucuz, temiz ve güvenilir enerji kaynaklarına erişimi sağlamaktır. Özellikle fosil yakıtların yaydığı zararlar ve küresel ısınma gibi büyük çevresel sorunlar, yenilenebilir enerji kaynaklarına olan ihtiyacı artırmaktadır. Türkiye, jeotermal enerji potansiyeli bakımından dünya genelinde zengin ülkeler arasında yer almaktadır. Ülkemiz, Avrupa'da birinci, dünyada ise yedinci sırada yer alarak büyük bir jeotermal potansiyele sahiptir. Konya ili Seydişehir ilçesi, son yıllarda jeotermal enerji potansiyeli ve termal turizm alanındaki gelişimleriyle dikkat çeken ve jeotermal alanları araştırma süreci devam eden bir yerleşim bölgesidir. Bu çalışmada, potansiyel jeotermal alanların tespiti için CBS tabanlı Çok Kriterli Karar Analiz yöntemi olan Analitik Hiyerarşi Süreci (AHP) yöntemi kullanılmıştır. AHP yöntemi için kullanılan tüm ölçütler uzman görüşü alınarak ve literatür araştırmaları sonucu oluşturulmuştur. Belirlenen kriterler AHP'ye göre standartlaştırılmış verilerin ağırlıklı katmanları birleştirilerek bölgenin potansiyel jeotermal haritası üretilmiştir. Böyle bir çalışma ile bölgedeki belirlenen jeotermal potansiyel alanların ülke ekonomisine maksimum kapasite ile kazandırılması amacıyla jeotermal kaynakların değerlendirilmesi, geliştirilmesi ve yapılacak yatırımlar için öneriler sunulması noktasında yerel yönetimler ve karar vericiler için önemli bir altlık envanter oluşturacağı öngörülmektedir.

Article Info

Received: 05/12/2023
Accepted: 01/01/2024
Published: 30/06/2024

Citation:

Gümüş, M. G. & Durduran, S. S. (2024). Determination of Potential Geothermal Areas in Konya Seydişehir District Using GIS-based Multi-Criteria Decision Analysis. Turkish Journal of Remote Sensing, 6 (1), 26-34.

***Corresponding Author:** Münevver Gizem Gümüş, gizemkisaaga@ohu.edu.tr, +90 388 225 4643

1. INTRODUCTION

Today, the continuous increase in energy consumption and the deepening of environmental problems have led people to more sustainable energy sources. Renewable energy sources are resources that can be continuously regenerated by natural processes and can be used indefinitely. These resources contribute to environmentally friendly, sustainable, and clean energy production compared to fossil fuels. Geothermal energy, which is one of these energy sources, is obtained by extracting the energy in the form of vapor or hot water from the thermal energy of the earth. Geothermal energy sources offer low carbon emissions and a continuous energy source (Bulut & Filiz, 2005). The exploration and development of geothermal resources is a very interesting research topic today. The identification of geopotential areas is a complex process integrating Geographic Information System (GIS) and remote sensing technologies. Geoprocessing analyzes the natural resources, climate, topography, topography, and other factors in a region to identify potential risks and opportunities. These areas play a fundamental role in strategic decision-making in many areas such as planning, natural resource management, environmental sustainability, and disaster risk reduction. Different studies have been conducted in the literature to identify potential geothermal areas. Yousefi et al. (2007) created a model using GIS as a decision-making tool for targeting potential geothermal resources in Iran. Noorollahi et al. (2015) developed the GIS Model for Geothermal Resource Exploration (GM-GRE) tool, a toolbox that uses GIS as a decision-making tool to locate potential geothermal areas. Nwaiwu et al. (2023) utilized Multi-Criteria Decision-Making (MCDA) techniques for a GIS-based geothermal site selection study in Nigeria. Noorollahi et al. (2007) conducted a study to determine the geothermal potential in Akita and Iwate regions. In this research, they developed a GIS model using a weighted overlay selection query to identify priority areas for geothermal exploration by considering geological, thermal, and geochemical factors. Yalcin & Gul (2017), in the study conducted in Akarçay Basin, geothermal potential areas were identified using GIS-based MCDA. Analytic Hierarchy Process (AHP) method was used in the decision analysis phase and the geothermal potential map of the region was created by synthesizing the weights of standardized data layers.

Abuzied et al. (2020) performed a GIS-based analysis utilizing a Multi-Criteria Decision-Making approach. The study focused on geothermal resource exploration in the coastal region of the Gulf of Suez, Egypt, employing data derived from remote sensing and geophysical techniques. Yalcin et al. (2023) used the machine learning method Maximum Entropy (Maxent) Method and MCDA to identify potential geothermal areas in their study. The results of the two methods were compared and the potential status of the region was revealed.

Turkey is among the richest countries in the world in terms of geothermal energy potential (Figure 1). Our country has great geothermal potential, ranking first among European countries and seventh in the world (Kilic, 2016; Serpen et al., 2009; Kömürcü & Akpınar, 2009).

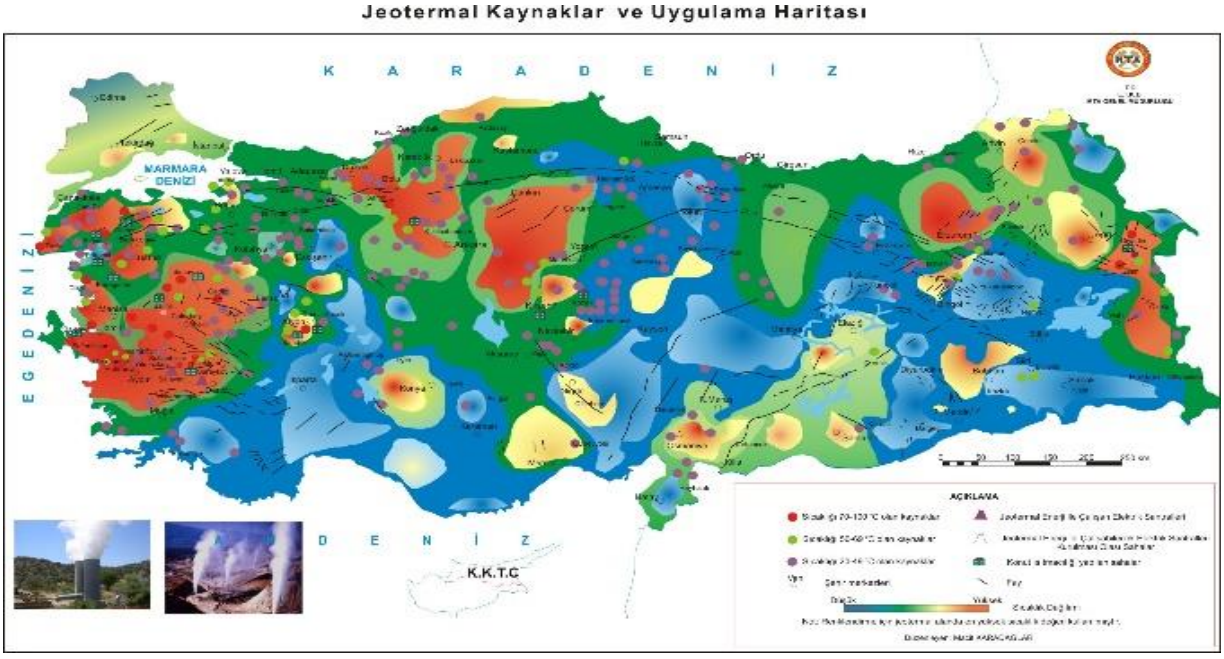

Figure 1. Türkiye geothermal resources and application map (URL-2)

The biggest advantage of geothermal energy is that it can be used in many different areas such as home heating, greenhouse cultivation, tourism, industry, and medicine as well as electricity generation. In our country, greenhouse activities are carried out on 1200 acres with geothermal energy,

and 100,000 acres of residential area is heated in 15 different settlements. Konya province is a very important potential area in terms of geothermal energy resources, and almost all of the fields in the region can be used as hot springs and drinking water. The temperatures of the existing resources in the area vary between 250-45°C (URL-1). The distribution of geothermal fields in Konya is concentrated around Beyşehir, Seydişehir, Ilgın, Tuzlukçu, Hüyük, Cihanbeyli, Ereğli, Karapınar, and Doğanhisar, especially in the western region where fracture zones are known to be intense (Figure 2).

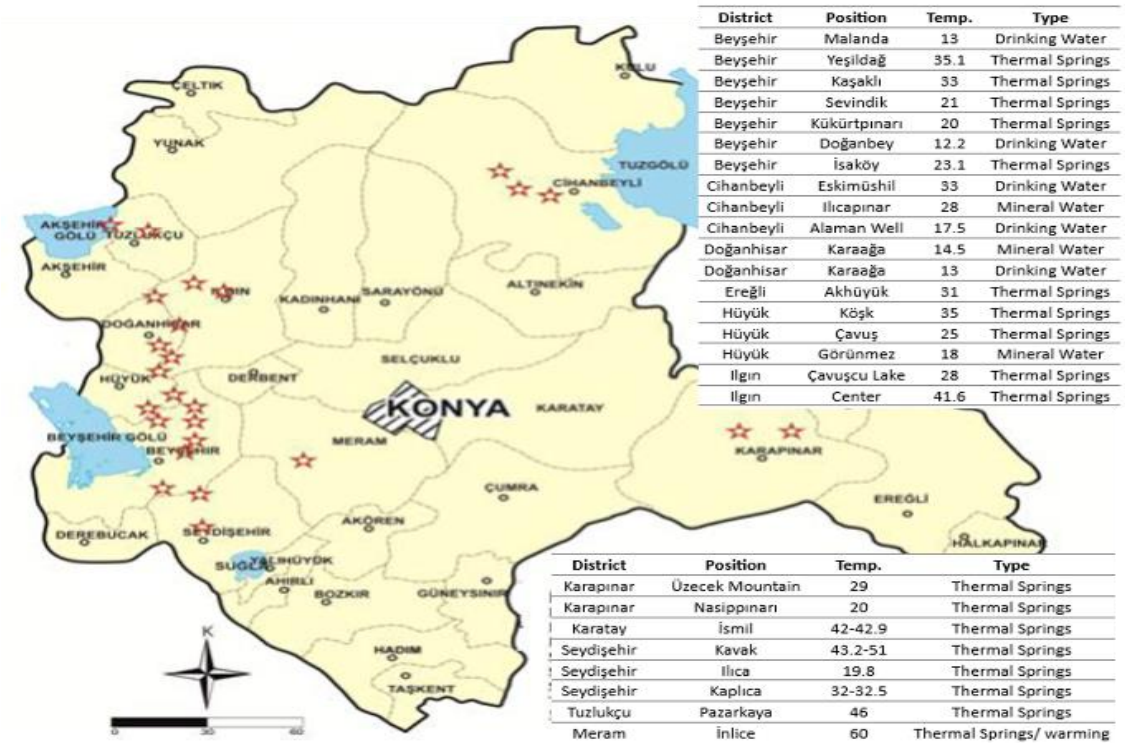

District	Position	Temp.	Type
Beyşehir	Malanda	13	Drinking Water
Beyşehir	Yeşildağ	35.1	Thermal Springs
Beyşehir	Kaşaklı	33	Thermal Springs
Beyşehir	Sevindik	21	Thermal Springs
Beyşehir	Kükürtpınarı	20	Thermal Springs
Beyşehir	Doğanbey	12.2	Drinking Water
Beyşehir	İsaköy	23.1	Thermal Springs
Cihanbeyli	Eskimüshil	33	Drinking Water
Cihanbeyli	Ilıcapınar	28	Mineral Water
Cihanbeyli	Alaman Well	17.5	Drinking Water
Doğanhisar	Karaağa	14.5	Mineral Water
Doğanhisar	Karaağa	13	Drinking Water
Ereğli	Akhüyük	31	Thermal Springs
Hüyük	Köşk	35	Thermal Springs
Hüyük	Çavuş	25	Thermal Springs
Hüyük	Görünmez	18	Mineral Water
Ilgın	Çavuşcu Lake	28	Thermal Springs
Ilgın	Center	41.6	Thermal Springs

District	Position	Temp.	Type
Karapınar	Üzecek Mountain	29	Thermal Springs
Karapınar	Nasippınarı	20	Thermal Springs
Karatay	İsmil	42-42.9	Thermal Springs
Seydişehir	Kavak	43.2-51	Thermal Springs
Seydişehir	Ilıca	19.8	Thermal Springs
Seydişehir	Kaplıca	32-32.5	Thermal Springs
Tuzlukçu	Pazarkaya	46	Thermal Springs
Meram	İnlice	60	Thermal Springs/ warming

Figure 2. Distribution of Geothermal Areas in Konya (Arık, 2011)

In this study, it is aimed to identify the potential geothermal areas of Seydişehir district of Konya province, which has attracted attention in recent years with its geothermal energy potential and developments in the field of thermal tourism, and which is a settlement region whose geothermal areas research process is ongoing. In this context, AHP method, which is a GIS-based MCDA method, was used to identify potential geothermal areas. All criteria used for the AHP method were created by taking expert opinions and as a result of literature research. The data sets used in the analysis consist of geological, hydrogeological, topographic, and geophysical information. The potential geothermal map of the region was produced by combining the weighted layers of the standardized data according to AHP. The workflow diagram of the study is as shown in the figure 3.

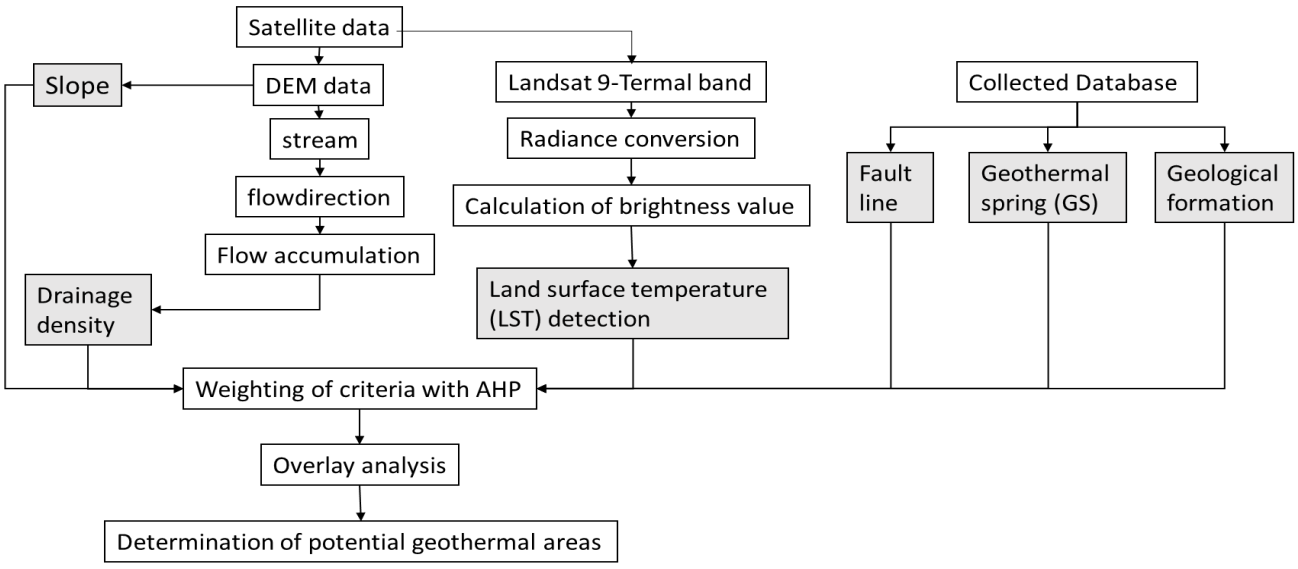

Figure 3. Workflow diagram

2. METHOD

2.1. Study Area

Seydişehir district is a region located 107 km from Konya city center. The average height above sea level is 1,123 meters. The district borders Beyşehir in the north, Yalıhüyük, Ahırlı, and Akseki districts of Antalya province in the south, Derebucak in the west and Akören district in the east. Located on the northern foothills of the Taurus Mountains, the district lies in a fertile valley called Suğla Plain. Mount Küpe Mountain extends from the west to the south, while Mount Gidengelmez is home to rich bauxite deposits in the south. There are many springs and springs on the slopes of Mount Küpe. There are also natural beauties such as Pınarbaşı, Kuğulu, and Beldibi Ponds, which are located in Seydişehir and fed by the springs on Mount Küpe (URL-3). Beyşehir Lake lies to the northwest of the district and Suğla Lake to the southeast. Seydişehir district is a region that attracts attention with its impressive geographical features and natural richness (Figure 4).

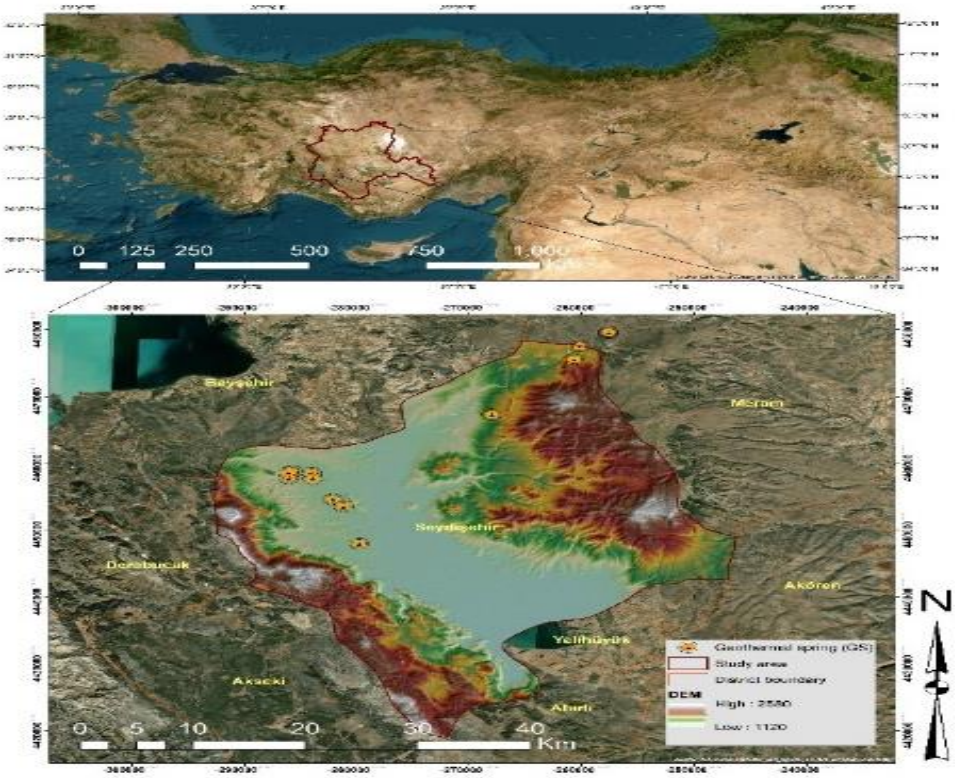

Figure 4. Seydisehir district boundary (study area) representation

Survey studies have been carried out by the General Directorate of Mineral Research and Exploration (MTA) since 1998 to determine the geothermal energy potential of Konya-Seydişehir district and its surroundings. There are wells and springs in Seydişehir-Center, İnlice, Bükçe, Kavak and Yenice villages (URL-1). In 2006, 2 geothermal exploration drillings were carried out at these points (Figure 5).

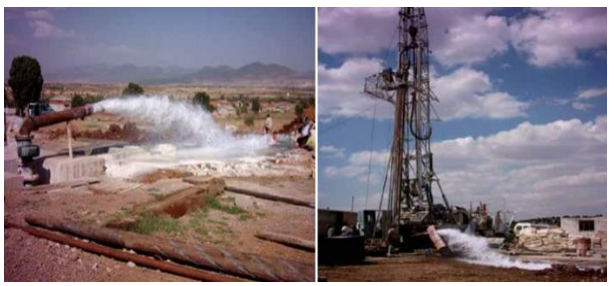

Figure 5. Konya Seydişehir KSK-1 well production image (URL-2)

In the first well of the drilling works, a temperature of 38.3°C and in the other well, a temperature of 43.2°C and a total flow rate of 130 l/s were reached (URL-2) (Table 1).

Table 1. Well Data in Seydişehir Geothermal Area (URL-1)

Location	Well name	Temperature (°C)	Flow (l/sec)	Depth (m)	Company	Opening year
Center	Ilıcatepe, IT-1	32	1.42		Seydişehir Municipality	
	Ilıca hot spring ITky-2	32.1	0.2		Seydişehir Municipality	
	Ketirlik hill, JT-1	43	8	118	Seydişehir Municipality	
	OSBky					
Kavak Village	KSK-1	38.6	100	182	Wells have been vandalized	2006
	KSK-2	43.3	40	317	Wells have been vandalized	2006
	KSK-3					2006
İnlice	İK-1	54.5	30	751	AGN. PET. CONST. MAD.	2010
	BK-1 well					
Yenice	SK-1	37	2.5	348	Seydişehir Thermal Facilities	2008
	SK-2	38.6	110	411		2016

2.2. Criteria Selection and Data Used

In the criterion selection stage, the criteria that affect the decision problem should be identified. The criteria should reflect the objectives in the decision-making process and include factors that are important for the decision to be taken correctly. Criteria selection is a stage of high importance in the finalization of the study. In the study, the criteria were determined by literature research and expert opinions in the field. The criteria determined are "Drainage density, Distance to the fault line, Slope, Land Surface Temperature, Distance to existing resources, Geological formation".

ALOS PALSAR DEM images were used for drainage data and slope data among the data belonging to the criteria. ALOS PALSAR contains data provided by a synthetic aperture radar (SAR) satellite developed by Japan's Remote Sensing and Space Exploration Agency (JAXA). ALOS PALSAR's data resolution generally comes in two main modes: Fine (F) mode with a resolution of 1 to 3 meters and ScanSAR (Scan Synthetic Aperture Radar) mode with a resolution of 10 to 100 meters (URL-4). It was used in this study due to its high resolution and open access (URL-5).

Fault line and geological formation data were provided by the General Directorate of Mineral Research and Exploration (URL-2). The existing geothermal resource data was created based on the locations identified in the Konya province report of the Geothermal Resources Assessment Project (URL-1).

Landsat 9 TIRS image was used for land surface temperature data. The thermal satellite data was obtained from the open access source of the US Geological Survey (USGS) (URL-6, 2023). Landsat 9's Thermal Infrared Sensor 2 (TIRS-2) is a sensor designed to measure thermal radiation emitted from the land surface. TIRS-2 operates in two thermal infrared bands. These bands generally cover wavelengths between 10.60-11.19 micrometers and 11.50-12.51 micrometers. The resolution of the thermal bands for Landsat 9's Thermal Infrared Sensor 2 (TIRS-2) is 100 meters. This refers to the unit of distance used by the sensor when measuring the area of a pixel on the surface. Thus, each pixel represents an area of 100 square meters on the land surface (URL-6). These thermal bands help determine the temperature characteristics of objects by measuring the thermal energy emitted from the earth's surface. Landsat 9's thermal bands are used in applications such as agriculture, water management, natural resources monitoring and tracking environmental changes. All the criteria used in the study are presented in Figure 6.

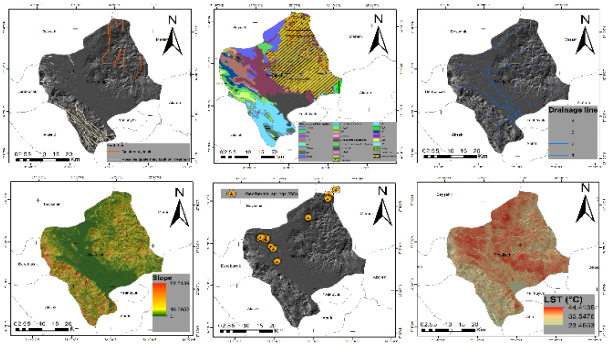

Figure 6. Criteria used to identify potential geothermal fields

2.3. Calculation of Land Surface Temperature

Land Surface Temperature (LST) is an important remote sensing parameter that represents the temperature of an earth point (Brunsell & Gillies, 2003; Solanky et al., 2018). The definition of LST refers to the actual temperature of the object, net of atmospheric effects (Deo & Şahin, 2017). In geothermal research, the measurement of LST plays an important role in identifying heating or cooling events in the subsurface. This provides critical information for the exploration and evaluation of geothermal energy resources.

Landsat TIR receives thermal temperature data and stores this information as a DN between 0 and 255. The first step in the calculation of LST values is radiometric correction. The aim here is to convert the DN values obtained from the satellite data into spectral radiance values. Equation (1) used for this process is as follows:

$$L\lambda = [(LMAX\lambda - LMIN\lambda)/(QCALMAX - QCALMIN)] * [QCAL - QCALMIN] + LMIN\lambda \quad (1)$$

Lλ: Spectral radiance at the sensor (W/m2sr µm), LMAXλ: Spectral radiance scaled relative to QCALMAX, LMINλ: Spectral radiance scaled by QCALMIN, QCAL: Luminance values, QCALMAX: Maximum brightness value, QCALMIN: Refers to the minimum brightness value.

To convert the spectral radiance values obtained by applying this mathematical model into real LST values, the following equation is used (2):

$$Tb = K2 /(\ln(((K1 /l\lambda) + 1)) \quad (2)$$

K1= Calibration constant, K2 = Calibration constant, Tb = Surface Temperature Finally, the LST values are obtained by converting the obtained surface temperature into degrees (Equation 3).

$$LST = Tb - 273 \text{ (Kelvin to Degree conversion)} \quad (3)$$

2.4. Analytic Hierarchy Method (AHP)

The AHP method is a mathematical model used in the multi-criteria decision-making process developed by Saaty (1994). This method is used to determine the importance of different criteria and alternatives in the decision-making process (Saaty,1980; Saaty, 2004). The process steps of the AHP method in identifying potential geothermal areas can be listed as follows: First, the criteria to be used in the decision-making process are determined. Then, the importance levels of the criteria are determined. Then, the alternatives, if any, in the decision-making process are evaluated according to the determined criteria. Weighted scores are calculated by multiplying the importance scores obtained by weighting the criteria by the scores obtained by evaluating the alternatives. Finally, the results obtained are evaluated and the potential geothermal map of the region is produced by combining the weighted layers of the standardized data according to AHP.

3. RESULTS

In the study, criteria were first established to identify potential geothermal areas. Six basic indicators were determined in line with literature studies (Şener & Şener, 2021; Li et al., 2023; Tinti et al. ,2018; Kiavarz & Jelokhani-Niaraki, 2017; Xu et al., 2021; Meng et al., 2021) and expert opinions. These criteria are; "Proximity to fault line, Drainage density, Proximity to existing resources, Land surface temperature, Slope and Geological formation". Priority values were determined by 12 different experts by making pairwise comparisons between the hierarchically ranked subjective criteria. All data were analyzed in the Expert Choice v.11 program and normalization was performed by dividing each column value separately by the total of the relevant column. These values obtained through the normalization process constitute the weight of each criterion (Figure 7).

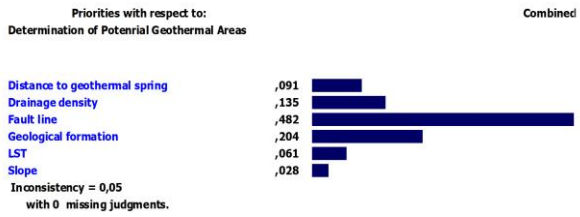

Figure 7. Potential site selection criteria and weights –Expert Choice program output

When the graphs created as a result of the study are examined, it is seen that the criterion with the highest degree of importance in the comparison of the six main criteria is the proximity to the fault line (0.482). The next ranking was determined as Geological formation (0.204), Drainage density (0.135), Distance to geothermal springs (0.091), Land surface temperature (0.061) and Slope criterion (0.028).

The findings found in the AHP method were mapped in order to be integrated into GIS and to visualize the data obtained by concretizing them. The data collected according to the priority values created by AHP were processed in ArcGIS 10.8 software and potential geothermal field analysis for Seydişehir district of Konya province was carried out. In the spatial analysis dimension, the district center boundary layer was created first. Then, the relevant criteria data were digitized and a separate vector data layer was created for each criterion. For the drainage density criterion, it was produced over DEM data using the hydrology analysis module in ArcGIS toolbox. The density map was created using the Euclidean Distance Method. The distance of each pixel in the raster generated by Euclidean Distance to the nearest drainage line was calculated. Similarly, slope analysis was performed on DEM data using the surface analysis module in ArcGIS toolbox. Euclidean distance method was also used for distance analysis of geological formation and proximity to existing resources. For the last criterion, land surface temperature, thermal bands were utilized and mapped by applying the process steps specified in the methodology (Figure 8).

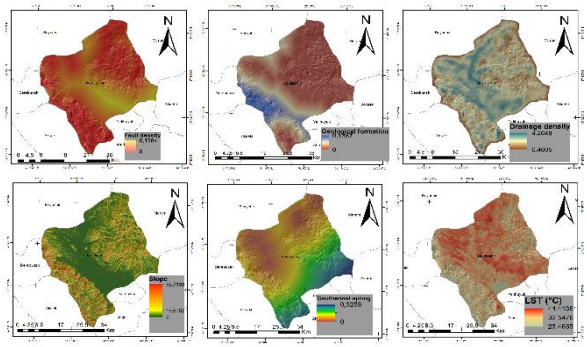

Figure 8. Mapping of criteria densities

The class ranges for the relevant criteria were then normalized and mapped (Figure 9).

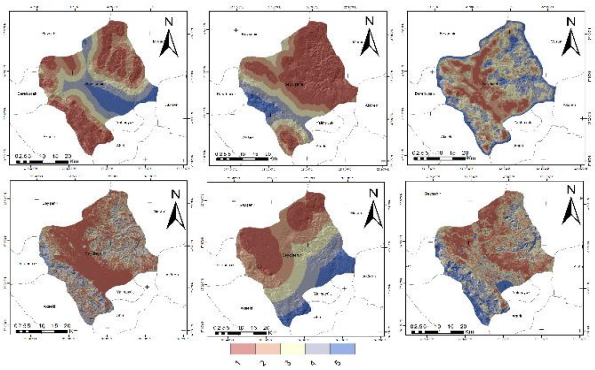

Figure 9. Normalized criteria layers; a. fault line proximity criterion, b. Geological formation criterion, c. Drainage density criterion, d. Slope criterion, e. Geothermal spring proximity criterion, f. LST criterion

Normalization is the process of bringing data into a specific range or distribution. In this process, data is usually standardized using a specific formula or method. The standardization method, which is an AHP stage, is used to standardize the values of the criteria layers between 0 and 1. This standardization process makes data at different scales comparable. Especially in the study where the geothermal potential area was examined, the maximum and minimum value range method was used. This method shows the positive and negative impacts of the geothermal potential area by standardizing according to the lowest and highest values of each criteria layer. In this context, using the normalization method, the new values close to 0 indicate a low geothermal area potential and close to 1 indicates a high potential.

In the synthesis section, which is the last stage of the study, a model was created by weighted registration with all normalised data layers. Modelling was performed using the Modelbuilder module in ArcGIS software. Modelling the synthesis stage of AHP using ArcGIS software provides an effective way to perform complex site selection analyses and integrate geographic elements. The synthesis process using the model was preferred because it allows the users to bring together a set of tools and processes to create and manage complex workflows without writing software code. The model design visualisation is presented in Figure 10.

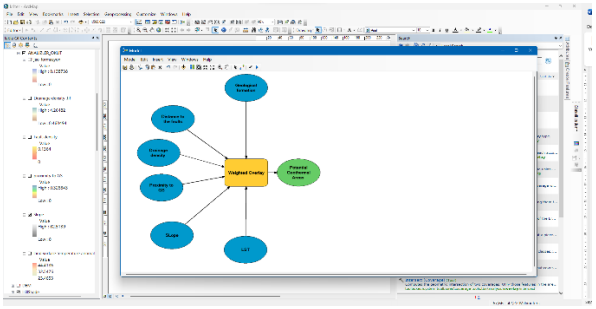

Figure 10. Analysis model created in ArcGIS Model Builder

This model was run to create a potential geothermal map of the region in 5 classes. The resulting map was classified from blue to red, from unsuitable to suitable areas (Figure 11)

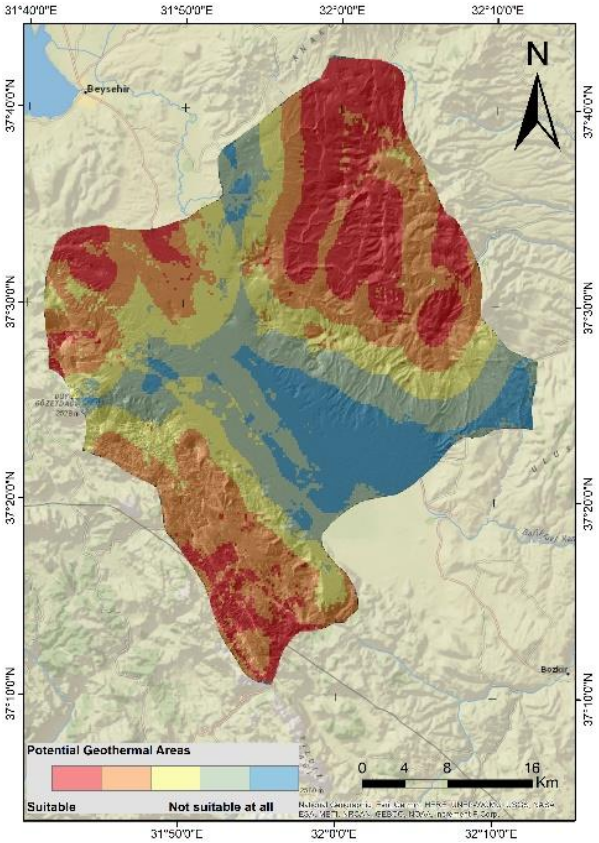

Figure 11. Map of the potential geothermal area in Seydişehir district

4. CONCLUSION

In this study, it is aimed to identify the potential geothermal areas of Seydişehir district of Konya province, which has attracted attention with its geothermal energy potential and developments in the field of thermal tourism in recent years and which is a residential area with ongoing geothermal areas research process. In this context, AHP method, which is a GIS-based MCDA method, was used to identify potential geothermal areas. All criteria used for the AHP method were created by taking expert opinions and as a result of literature research. The data sets used in the analysis consist of geological, hydrogeological, topographic, and geophysical information. The potential geothermal map of the region was produced by combining the weighted layers of the standardized data according to AHP. As a result of the analysis, the potential suitability of the region was classified in five basic classes from unsuitable to suitable areas. According to the potential suitability map produced in the study, 297.38 km^2 (22%) of the total area of 1362.5 km^2 of Seydişehir district is highly suitable for geothermal potential, 395.88 km^2 (29%) is moderately suitable, 265.02 km^2 (19 %) of the area is low suitable, 236.22 km^2 (17 %) of the area is not suitable for geothermal potential and 167.99 km^2 (12 %) of the area is completely unsuitable.

Determination of geothermal energy potential is an important issue in many aspects. Determining this potential is of great importance for energy planning and resource management. It also provides great benefits in issues such as minimizing environmental impacts, sustainable energy production and the use of alternative energy sources. Geothermal energy has many advantages over fossil fuels. The first of these is that geothermal energy is an environmentally friendly energy source. Unlike fossil fuels, greenhouse gas emissions in geothermal energy production are very low and its environmental impacts are minimal. In addition, geothermal energy is a continuous and unlimited resource, which provides a great advantage in terms of continuity of energy supply.

Identification of geothermal potential areas in an integrated manner with GIS and remote sensing makes many contributions to the literature. By using these methods, geothermal energy potential areas can be identified more quickly, economically and in detail. In addition, this integration provides important data for more efficient utilization of geothermal resources and energy planning. Determination of geothermal energy potential supports the use of an environmentally friendly, sustainable, continuous, and economical energy source compared to fossil fuels. Determination studies integrated with GIS and remote sensing contribute to the creation of more effective and efficient energy policies by providing important data to the energy sector and academic literature. Therefore, the determination of geothermal energy potential is of great importance for the energy sector and the environment.

As a result, the use of additional energy sources offers significant advantages not only in the energy sector, but also in the areas of environmental protection and sustainability. These resources can play a critical role for energy efficiency, economic growth and environmental health at the global level. Investments in renewable energy are an important step towards leaving a clean environment for future generations and meeting energy needs in a sustainable way.

Acknowledgment

We thank the United States Geological Survey and Alaska Satellite Facility for providing open access data.

Author contributions

M. G. Gümüş: Data analysis, Research, Modeling, Visualization, Manuscript writing.
S.S. Durduran: Idea/Concept development, Data acquisition, Manuscript writing, Manuscript editing, Critical review.

Conflicts of Interest

The authors declare no conflict of interest.

Research and publication ethics statement

In the study, the authors declare that there is no violation of research and publication ethics and that the study does not require ethics committee approval.

REFERENCES

Abuzied, S. M., Kaiser, M. F., Shendi, E. A. H. & Abdel-Fattah, M. I. (2020). Multi-criteria decision support for geothermal resources exploration based on remote sensing, GIS and geophysical techniques along the Gulf of Suez coastal area, Egypt. *Geothermics,* 88, 101893. https://doi.org/10.1016/j.geothermics.2020.101893

Arık, F. (2011). Konya'da Bulunan Enerji Kaynakları ve Potansiyeli (in Turkish). *1. Konya Kent Sempozyumu*, Konya, Turkey, 26-27.

Brunsell N. A. & Gillies, R.R. (2003). Length scale analysis of surface energy fluxes derived from remote sensing, *Journal of Hydrometeorology,* 4(6), 1212–1219. https://doi.org/10.1175/1525-7541(2003)004<1212:LSAOSE>2.0.CO;2

Bulut, M. & Filiz, Ş. (2005). Bayındır jeotermal sahasının hidrojeolojisi, hidrokimyası ve izotopik özellikleri (İzmir, Batı Anadolu, Türkiye) (in Turkish). *Maden Tetkik ve Arama Dergisi*, (131), 63-78.

Deo, R. C. & Şahin, M. (2017). Forecasting long-term global solar radiation with an ANN algorithm coupled with satellite-derived (MODIS) land surface temperature (LST) for regional locations in Queensland. *Renewable and*

Sustainable Energy Reviews, 72, 828-848. https://doi.org/10.1016/j.rser.2017.01.114

Kiavarz, M. & Jelokhani-Niaraki, M. (2017). Geothermal prospectivity mapping using GIS-based Ordered Weighted Averaging approach: A case study in Japan's Akita and Iwate provinces. Geothermics, 70, 295-304. https://doi.org/10.1016/j.geothermics.2017.06.015

Kilic, F. C. (2016). Geothermal energy in Turkey. *Energy & Environment*, 27(3-4), 360-376. https://www.jstor.org/stable/90006618

Kömürcü, M. İ. & Akpınar, A. (2009). Importance of geothermal energy and its environmental effects in Turkey. *Renewable energy*, 34(6), 1611-1615. https://doi.org/10.1016/j.renene.2008.11.012

Li, X., Huang, C., Chen, W., Li, Y., Han, J., Wang, X., Bai, X., Yin, Z., Li, X., Hou, P. & Tong, J. (2023). GIS model for geothermal advantageous target selection. *Scientific Reports,* 13(1), 6024. https://doi.org/10.1038/ s41598-023-32785-0

Meng, F., Liang, X., Xiao, C. & Wang, G. (2021). Geothermal resource potential assessment utilizing GIS-based multi criteria decision analysis method. *Geothermics*, 89, 101969. https://doi.org/10.1016/j.geothermics.2020.101960196

Noorollahi, Y., Ghasempour, R. & Jalilinasrabady, S. (2015). A GIS based integration method for geothermal resources exploration and site selection. *Energy Exploration & Exploitation*, 33(2), 243-257. https://doi.org/10.1260/0144-5987.33.2.243

Noorollahi, Y., Itoi, R., Fujii, H. & Tanaka, T. (2007). GIS model for geothermal resource exploration in Akita and Iwate prefectures, northern Japan. Computers & geosciences, 33(8), 1008-1021. https://doi.org/10.1016/j.cageo.2006.11.006

Nwaiwu, U., Leach, M. & Liu, L. (2023). Development of an Improved Decision Support Tool for Geothermal Site Selection in Nigeria Based on Comprehensive Criteria. *Energies,* 16(22), 7602. https://doi.org/10.3390/en16227602

Saaty, T. L. (1990). How to make a decision: the analytic hierarchy process. *European journal of operational research,* 48(1), 9-26. https://doi.org/10.1016/0377-2217(90)90057-I

Saaty, T. L. (2004). Decision Making - The Analytic Hierarchy and Network Processes (AHP/ANP). *Journal of Systems Science and Systems Engineering*, 13(1), 1-35. https://doi.org/10.1007/s11518-006-0151-5

Saaty, T. L., 1980, Saaty, T. L. (1980). The analytic hierarchy process: planning, priority setting, resource allocation. *Journal of Mathematical Psychology*, 24(3), 287-234.

Şener, E. & Şener, Ş. (2021). Exploration of geothermal potential using integrated fuzzy logic and analytic hierarchy process (AHP) in Ağrı, Eastern Turkey. *Turkish Journal of Earth Sciences,* 30(9), 1134-1150. https://doi.org/10.3906/yer-2105-18

Serpen, U., Aksoy, N., Öngür, T. & Korkmaz, E. D. (2009). Geothermal energy in Turkey: 2008 update. *Geothermics*, 38(2), 227-237. https://doi.org/10.1016/j.geothermics.2009.01.002

Solanky, V., Singh, S. & Katiyar, S. K. (2018) Land Surface Temperature Estimation Using Remote Sensing Data, *In Hydrologic Modeling: Select Proceedings of ICWEES-2016*, Singapore, 343-351.

Tinti, F., Kasmaee, S., Elkarmoty, M., Bonduà, S. & Bortolotti, V. (2018). Suitability evaluation of specific shallow geothermal technologies using a GIS-Based multi criteria decision analysis implementing the analytic hierarchic process. *Energies*, 11(2), 457. https://doi.org/10.3390/en11020457

URL-1: http://www.kop.gov.tr/sayfalar/raporlar/77 [Access Date: 01.10.2023]

URL-2: https://www.mta.gov.tr/ 7 [Access Date: 09.10.2023]

URL-3: https://tr.wikipedia.org/wiki/Seydi%C5%9Fehir [Access Date: 21.11.2023]

URL-4: https://www.nik.com.tr/[Access Date: 11.10.2023]

URL-5: https://search.asf.alaska.edu/#/ [Access Date: 11.10.2023]

URL-6:https://www.usgs.gov/landsat-missions/landsat-9 [Access Date: 21.11.2023]

Xu, L., Wu, W., Qian, J., Huang, S., Xie, B., Hu, T., Lang, X., He, B. & Hu, C. (2023). Analysis of geothermal potential in Hangjiahu area based on remote sensing and geographic information system. *Frontiers in Earth Science*, 10, 1031665. https://doi.org/10.3389/feart.2022.1031665

Yalcin, M., & Gul, F. K. (2017). A GIS-based multi criteria decision analysis approach for exploring geothermal resources: Akarcay basin (Afyonkarahisar). *Geothermics,* 67, 18-28. https://doi.org/10.1016/j.geothermics.2017.01.002

Yalcin, M., Sari, F. & Yildiz, A. (2023). Exploration of potential geothermal fields using MAXENT and AHP: A case study of the Büyük Menderes Graben. *Geothermics*, 114, 102792. https://doi.org/10.1016/j.geothermics.2023.102792

Yousefi, H., Ehara, S. & Noorollahi, Y. (2007). Geothermal potential site selection using GIS in Iran. *In Proceedings of the 32nd workshop on geothermal reservoir engineering*, Stanford University, Stanford, California, 174-182.

Araştırma Makalesi/Research Article
https://doi.org/10.51489/tuzal.1443490

2024; 6(1); 35-56

Turkish Journal of Remote Sensing

https://dergipark.org.tr/en/pub/tuzal

e-ISSN 2687-4997

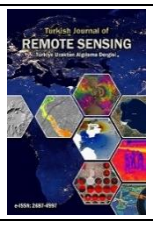

Analysis of Manyas Lake Surface Area and Shoreline Change Over Various Periods with DSAS Tool

Murat Uzun[*1]

[1]*Marmara University Department of Geography, İstanbul, Turkey*

Keywords
DSAS
Manyas Lake
Shoreline Change
Remote Sensing
GIS

ABSTRACT

In this study, the shoreline and lake surface area changes of Lake Manyas were analysed by using Geographical Information Systems (GIS) and Remote Sensing (RS) techniques for long term (1980-2020) and annual (2022) with DSAS tool. In the study, a formula was created using NDWI, MDWI, WRI water indices and NDVI, RVI, NDMI, GCI vegetation indices over Landsat satellite images of 1980, 1985, 1990, 1995, 2000, 2000, 2005, 2005, 2010, 2015, 2020 and all months of 2022, and shoreline extraction was performed. Then, shoreline and lake surface area change were analysed over different periods with NSM, EPR, SCE, LRR statistics in DSAS tool. According to the results of the analyses, the average shoreline changes between 1980 and 2020 was 139 m according to NSM statistics, 3,5 m/year according to EPR, 243.1 m according to SCE and 3.4 m/year according to LRR. While the shoreline extended a maximum of 1599 m, the minimum value was -403 m. From 1980 to 2020, 5.85 km^2 coastal accumulation, 1.03 km^2 coastal erosion and 146.5 km^2 permanent lake surface area data were determined on the surface area and shores of Lake Manyas. According to the monthly data of Lake Manyas for 2022, the shoreline is advancing by 18 m on average. Due to the natural dynamic process and the productive structure of the wetland system, the lake surface area reaches its widest size in April with 149.01 km^2 and its narrowest area is 146.05 km^2 in August. On the southern shores of Lake Manyas, reedbed development and coastal accumulation are intensely experienced with the progression of the Manyas Stream delta, while coastal erosion is observed on the northern shores.

Manyas Gölü Yüzey Alanı ve Kıyı Çizgisi Değişiminin Çeşitli Periyotlar Üzerinden DSAS Aracı ile Analizi

Anahtar Kelimeler:
DSAS
Manyas Gölü
Kıyı Çizgisi Değişimi
Uzaktan Algılama
CBS

ÖZ

Bu çalışmada Manyas Gölü'nün kıyı çizgisi ve göl yüzey alanı değişimi, Coğrafi Bilgi Sistemleri (CBS) ve Uzaktan Algılama (UA) teknikleri kullanılarak, uzun dönemli (1980-2020) ve yıllık (2022) olarak DSAS aracı ile analiz edilmiştir. Çalışmada 1980, 1985, 1990, 1995, 2000, 2005, 2010, 2015, 2020 yıllarına ait ve 2022 yılının bütün aylarına ait Landsat uydu görüntüleri üzerinden NDWI, MDWI, WRI su indeksleri ve NDVI, RVI, NDMI, GCI bitki indeksleri kullanılarak formül oluşturulmuş, kıyı çizgisi çıkarımı yapılmıştır. Daha sonra DSAS aracındaki NSM, EPR, SCE, LRR istatistikleri ile kıyı çizgisi ve göl yüzey alanı değişimi farklı periyotlar üzerinden analiz edilmiştir. Analiz bulgularına göre 1980-2020 yılları arasında ortalama kıyı çizgisi değişimi NSM istatistiğinde 139 m, EPR'ye göre 3,5 m/yıl, SCE'ye göre 243,1 m ve LRR'ye göre 3,4 m/yıl olarak saptanmıştır. Kıyı çizgisi maksimum 1599 m ilerken minimum değer olarak -403 m gerilemiştir. Manyas Gölü yüzey alanı ve kıyılarında 1980'den 2020 yılına kadar 5,85 km^2 kıyı birikimi, 1,03 km^2 kıyı erozyonu ve 146,5 km^2 daimî göl yüzey alanı verisi tespit edilmiştir. Manyas Gölü 2022 yılı aylık verilerine göre kıyı çizgisi ortalama 18 m ilerlemektedir. Doğal dinamik süreç ve sulak alan sisteminin üretken yapısı nedeniyle göl yüzey alanı en geniş boyutuna nisan ayında 149,01 km^2 ile ulaşmakta, ağustos ayında ise en dar alanı 146,05 km^2 olarak görülmektedir. Manyas Gölü güney kıyılarında sazlık alan gelişimi ve Manyas Çayı deltasının ilerlemesi ile kıyı birikimi yoğun şekilde yaşanırken, kuzey kıyılarda kıyı aşınımı gözlemlenmiştir.

Article Info

Received: 27/02/2024
Accepted: 28/04/2024
Published: 30/06/2024

Citation:

Uzun, M. (2024). Analysis of Manyas Lake Surface Area and Shoreline Change Over Various Periods with DSAS Tool. Turkish Journal of Remote Sensing, 6 (1), 35-56.

***Corresponding Author:** Murat Uzun, murat_uzun53@hotmail.com

1. INTRODUCTION

Coasts are geomorphological units that form the transition area between water bodies and land, develop and change with dynamic processes of different origin, and intersect various ecosystems (Erinç, 1986; Turoğlu, 2017). The boundary between land and water mass is formed by coastlines. Coastlines undergo changes in long and short periods under the influence of tectonic and eustatic movements, wave and sea currents, materials transported by fluvial processes and anthropogenic activities (Erol, 1989; Tian et al., 2020; Pouye et al., 2023). Temporal and spatial detection of the changes that occur and modelling with quantitative data play a very important role in the planning and management of coastal change and in determining the extent of change and risk of ecological conditions (Davidson-Arnott, 2010; Grottolli et al., 2023). In this respect, shoreline change in Turkey and the world is analysed by applying various techniques in many different areas (Tağıl & Cürebal 2005; Darwish et al., 2017; Ataol et al., 2019; Topuz, 2018; Kılar & Çiçek, 2018; Çoban, 2020; Song et al., 2021; Uzun, 2021; Yasir et al., 2021; Bombino et al., 2022; Gómez-Pazo et al., 2022; Kazı & Karabulut, 2023; Murray et al., 2023).

Detection of shoreline changes is carried out using Geographic Information Systems (GIS) and Remote Sensing (RS) techniques through maps, satellite images, LIDAR and UAV images (Hu & Wang, 2020). In analysing the data, access to images at the desired date, the width of the study area, resolution and cost are very important (Paz-Delgado et al., 2022). In this respect, Landsat satellite imagery, which is free of charge, provides many temporal data and provides medium resolution, is more preferred in many studies. In shoreline analyses based on satellite images, different techniques that provide quantitative data temporally and spatially can be used. One of these techniques is the Digital Shoreline Analysis System (DSAS) tool. DSAS reveals the distance, annual erosion and deposition amount and the spatial distribution of these quantitative data over shorelines of different time periods (Himmelstoss et al., 2018). The DSAS tool and its statistical analyses are widely used in shoreline change research (Kuleli, 2010; Hakkou et al., 2023; Kale et al., 2019; Nassar et al., 2019; Dereli & Tercan, 2020; Samra & Ali, 2021; Lazuardi et al., 2022; Siyal et al., 2022; Akdeniz & İnam, 2023; Dinç, 2023; Kaya et al., 2023; Kılar, 2023; Şenol et al., 2023; Uzun, 2023).

The advancement and retreat of the shoreline with different origins leads to coastal erosion and coastal accretion (Bird, 2008; Turoğlu, 2009; Pouye, et al., 2023). This situation can affect many natural and human elements on the coast and cause the emergence of different risks (Wu et al., 2022). In this respect, it is very important to examine coastal changes not only through the sea-land system but also as the intersection area of various hydrographic elements with terrestrial elements and to analyses the changes from different perspectives in terms of future planning. This situation reveals the necessity of analysing the coastal changes of many hydrographic and morphological elements such as lake coasts, river coasts, dam-pond coasts, marsh areas.

Lakes are very important natural resources in terms of geomorphological, hydrographic, climatological and floristic aspects. These natural environment conditions offer diversity in terms of different morphological, biological and chemical properties (Sikder et al., 2023). Some of the lakes also contain wetlands due to their depth of less than 6 meters, ecosystem structures, limnological units, terrestrial and aquatic floristic features (Davidson, & Finlayson, 2018; Ataol & Onmuş, 2021). Changes in lacustrine wetlands, which have a productive ecosystem structure, can occur due to natural and anthropogenic processes (Davidson & Finlayson, 2018; Woolway et al., 2020). In the last 100 years, surface and coastal changes have been experienced in many lake wetlands due to increasing anthropogenic demands, misuse and planning (Ataol & Onmuş, 2021). As a result of the accumulation of materials carried by the hydrographic elements that feed the lake, morphological changes may occur in the lake surface area and shoreline along with delta, reedbed, swamp and peatland areas (Zuzek et al., 2003; Hoşgören, 1994; Turoğlu, 2017). Anthropogenic factors such as basin-based use of lake wetland resources, eutrophication of different origins, direct and indirect water withdrawal for agricultural purposes, use as a freshwater source, wetland drying and agricultural land opening can also cause major changes in lake surface area and shoreline (Maltby & Barker, 2009; Ataol & Onmuş, 2021). These changes cause temporal and spatial changes in the lake surface area and shoreline, and the emergence of coastal accumulation and erosion areas (Duru, 2017). Temporal and spatial determination of changes can reveal very important data in terms of understanding natural dynamic processes, producing models for the future, revealing threats in the lake wetland and hydrographic structure and taking measures.

The aim of this study is to quantitatively analyse the changes in the surface area and shoreline of Manyas Lake, which is covered by the Ramsar Convention wetland, over different periods (long and short term) with DSAS tool and to determine the temporal and spatial dimensions of the changes.

The research area is located in the southern part of the Marmara Sea in northwestern Turkey. Located in the tectonic depression in the southern part of the Marmara Region, the lake forms the western part of the Karacabey depression. Manyas Lake surface area is administratively within the borders of Balıkesir province. According to the geographical coordinate system, Lake Manyas is located between 40˚8'-

40°15' north latitude and 27°50' – 28°4' east longitude (Figure 1).

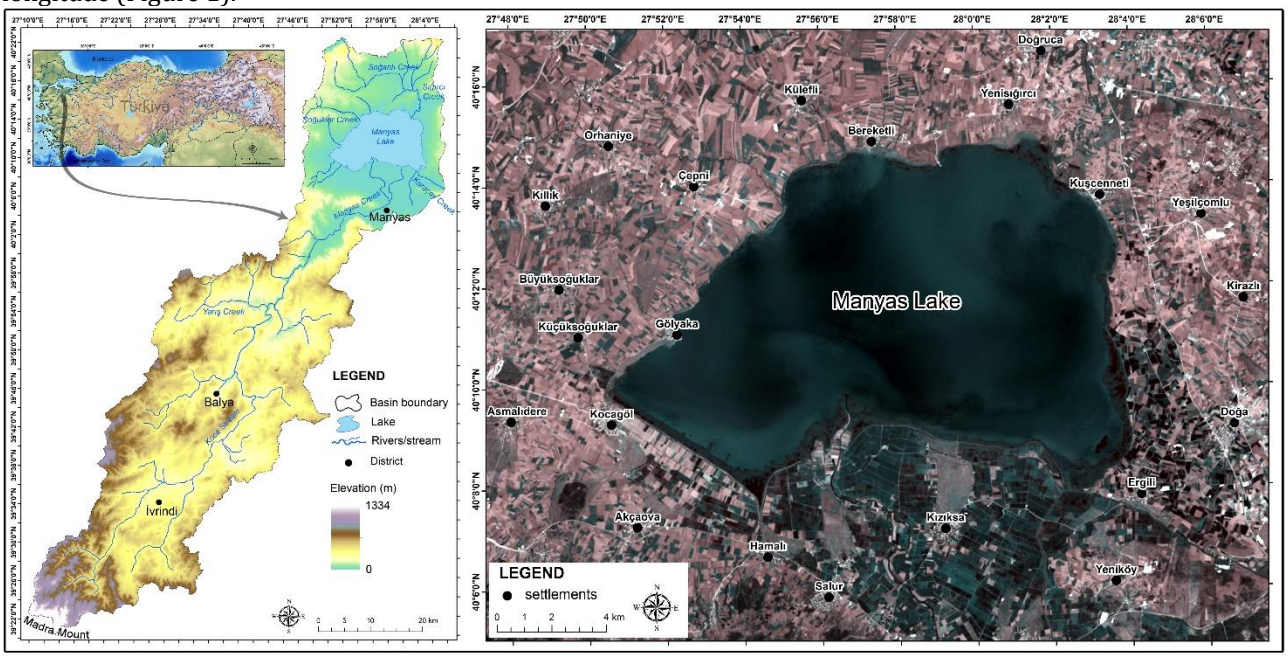

Figure 1. Location of the study area and Landsat satellite image of Manyas Lake in 2022

The average depth of the lake varies between 150-200 cm. The lake area, which is 14 m above sea level, varies seasonally, but is 146 km^2 on average. The main river source feeding the lake is Kocaçay Stream (Manyas Stream), which flows from the south to the north. The other main water source of the lake is the Sığırcı Stream flowing into the lake from the north. The outflow of the lake is Karaçay, which discharges from the southeastern part of the lake. The lake has been declared a Class A bird sanctuary due to its natural conditions, especially its ecosystem characteristics. In 1994, it constitutes Turkey's first five wetland lakes to be included in the scope of protection.

2. MATERIAL and METHOD

In the study, 1:25.000 scale topography sheets from HGM and Landsat satellite images from United States Geological Survey (USGS), written and printed sources of previous studies were used as materials. Firstly, the boundaries of Manyas Lake Basin were determined and a Digital Elevation Model (DEM) was created. Then, satellite images of 1980, 1985, 1990, 1995, 2000, 2005, 2010, 2015 and 2020 were obtained from Landsat (Table 1). In order to determine the monthly lake surface area and shoreline change, satellite images of each month of 2022 were also obtained from Landsat (Table 1). Atmospheric and radiometric adjustments of all satellite images were made in ArcGIS 10.8 software. In the long-term data to be analysed, a multispectral image was obtained by making a composite band without using the panchromatic band. In 2022, panchromatic band was used to capture the detail in the satellite images to be examined monthly and the bands were combined in this way. Then, the water surface band combination was applied to all satellite images and made suitable for examination before and after index analyses (Figure 3 and 12)

Before the analyses in the research, a systematic process of determining the shoreline in the most accurate way was established. Due to the presence of reeds on the shores of wetland lakes such as Lake Manyas, it is more difficult to determine the shoreline compared to other shores (Gao, 1996; Khorshiddoust et al., 2022; Şenol et al., 2023). For this reason, both water indices and green area and vegetation indices were used for shoreline determination (Table 2). In this respect, a study-specific formula was created using Normalized Difference Water Index (NDWI), Modified Normalized Difference Water Index (MDWI), Water Ratio Index (WRI) water indices and Normalized Difference Vegetation Index (NDVI), Ratio of Vegetation Index (RVI), Normalized Difference Moisture Index (NDMI), Green Chlorophyll Index (GCI) vegetation indices (Richardson & Wiegand, 1977; Myneni et al., 1995; McFeeters, 1996; Mcdonald et al., 1998; Xu, 2006; Shen & Li 2010; Janki et al., 2015) (Table 2). In the formula, vegetation index values were subtracted from water index values (Figure 2). The result obtained being greater than 0 indicates water surfaces. In this respect, the distribution of the formula result was reclassified. Shorelines were produced using the Threshold technique based on the binary classification (Pardo-Pascual et al., 2012; Hossain et al., 2021).

In the Threshold technique used in shoreline extraction, minimum and maximum threshold values in pixels are defined. In this respect, pixels

smaller than the minimum threshold are excluded, pixels larger than the maximum threshold are considered strong and the water area is accepted (Hossain et al., 2021). The analysis was performed by assuming that the low-value pixels at the boundary between the land and water surface exceeded the threshold value in the neighbourhood of the high-value pixel. In the study, the lake surface area and shorelines of Manyas Lake were determined in the 5-year period between 1980-2020 and in all months in 2022 with the specified shoreline determination stages and finally the Threshold method.

In the study, Digital Shoreline Analysis System (DSAS) was used for spatial and statistical value analysis of shoreline changes. End Point Rate (EPR), Net Shoreline Movement (NSM), Shoreline Change Envelope (SCE) and Linear Regression Rate (LRR) statistics within the DSAS system were used in the study.

Table 1. Characteristics of the satellite images used in the study

5-year period from 1980 to 2020				Months in 2022			
Date	**Satellite and Sensor ID**	**Resolution (DPI)**	**Cloud Cover (%)**	**Date**	**Satellite and Sensor ID**	**Resolution (DPI)**	**Cloud Cover (%)**
07.09.1980	Landsat 2-MSS	60	0	07.01.2022	Landsat 9-OLI-TIRS	30	12,94
01.07.1985	Landsat 5-TM	30	0	05.02.2022	Landsat 9-OLI-TIRS	30	3,71
31.07.1990	Landsat 5-TM	30	0	25.03.2022	Landsat 9-OLI-TIRS	30	9,29
26.05.1995	Landsat 5-TM	30	0	10.04.2022	Landsat 9-OLI-TIRS	30	3,45
02.07.2000	Landsat 7-ETM	30	0	12.05.2022	Landsat 9-OLI-TIRS	30	0,24
08.07.2005	Landsat 7-ETM	30	1	05.06.2022	Landsat 8-OLI-TIRS	30	0,58
23.08.2010	Landsat 7-ETM	30	4	23.07.2022	Landsat 8-OLI-TIRS	30	0,17
17.05.2015	Landsat 8 OLI-TIRS	30	0,29	16.08.2022	Landsat 9-OLI-TIRS	30	0,95
01.07.2020	Landsat 8 OLI-TIRS	30	0,07	09.09.2022	Landsat 8-OLI-TIRS	30	0,12
				03.10.2022	Landsat 9-OLI-TIRS	30	3,57
				11.11.2022	Landsat 9-OLI-TIRS	30	1,77
				22.12.2022	Landsat 9-OLI-TIRS	30	0,85

Table 2. Water and vegetation indices used in the study

Index Name		Formula	Reference
Normalized Difference Water Index	**NDWI**	$NDWI = \frac{(P_{NIR} - P_{SWIR2})}{(P_{NIR} + P_{SWIR2})}$	(Tucker, 1979; McFeeters, 1996)
Modified Normalized Difference Water Index	**MNDWI**	$MNDWI = \frac{(P_{greem} - P_{SWIR2})}{(P_{green} + P_{SWIR2})}$	(Xu, 2006; Singh et al., 2015)
Water Ratio Index	**WRI**	$WRI = \frac{(P_{green} + P_{red})}{(P_{NIR} + P_{SWIR2})}$	(Shen & Li, 2010)
Normalized Difference Vegetation Index	**NDVI**	$NDVI = \frac{(P_{NIR} - P_{red})}{(P_{NIR} + P_{red})}$	(Myneni et al., 1995)
Ratio of Vegetation Index	**RVI**	$RVI = \frac{P_{red}}{P_{NIR}}$	(Richardson & Wiegand, 1977)
Normalized Difference Moisture Index	**NDMI**	$NDMI = \frac{(P_{NIR} - P_{SWIR1})}{(P_{NIR} + P_{SWIR1})}$	(Mcdonald et al., 1998)
Green Chlorophyll Index	**GCI**	$GCI = \frac{P_{NIR}}{P_{green}} - 1$	(Janki et al., 2015)

After the determination of the shoreline in the study, firstly, DSAS analyses were performed for 5-year periods between 1980-2020, and the changes in lake surface area and shoreline were examined. In 8 different periods between 1980-2020, analyses were made using DSAS tool and NSM and EPR statistics. Then, the lake surface area and shoreline changes in the 40-year period between 1980-2020 were analysed with NSM, EPR, SCE and LRR statistics.

Due to the hydrographic structure of Manyas Lake, the effect of climatological conditions and the presence of wetlands, it is known that the lake surface area and shoreline change seasonally and monthly. For this reason, satellite images of Lake Manyas for all months in 2022 were obtained. However, shoreline and lake surface analyses were performed in February, April, June, August, August, October and December due to cloudiness rates. The shoreline over the specified months was subjected to NSM, EPR, SCE and LRR statistics and analysed with the DSAS tool.

With all the findings obtained, Manyas Lake surface area and shoreline change were analysed with different statistics for short and long periods.

The amount of shore change, accumulation and erosion areas were determined and the annual lake surface area was modelled.

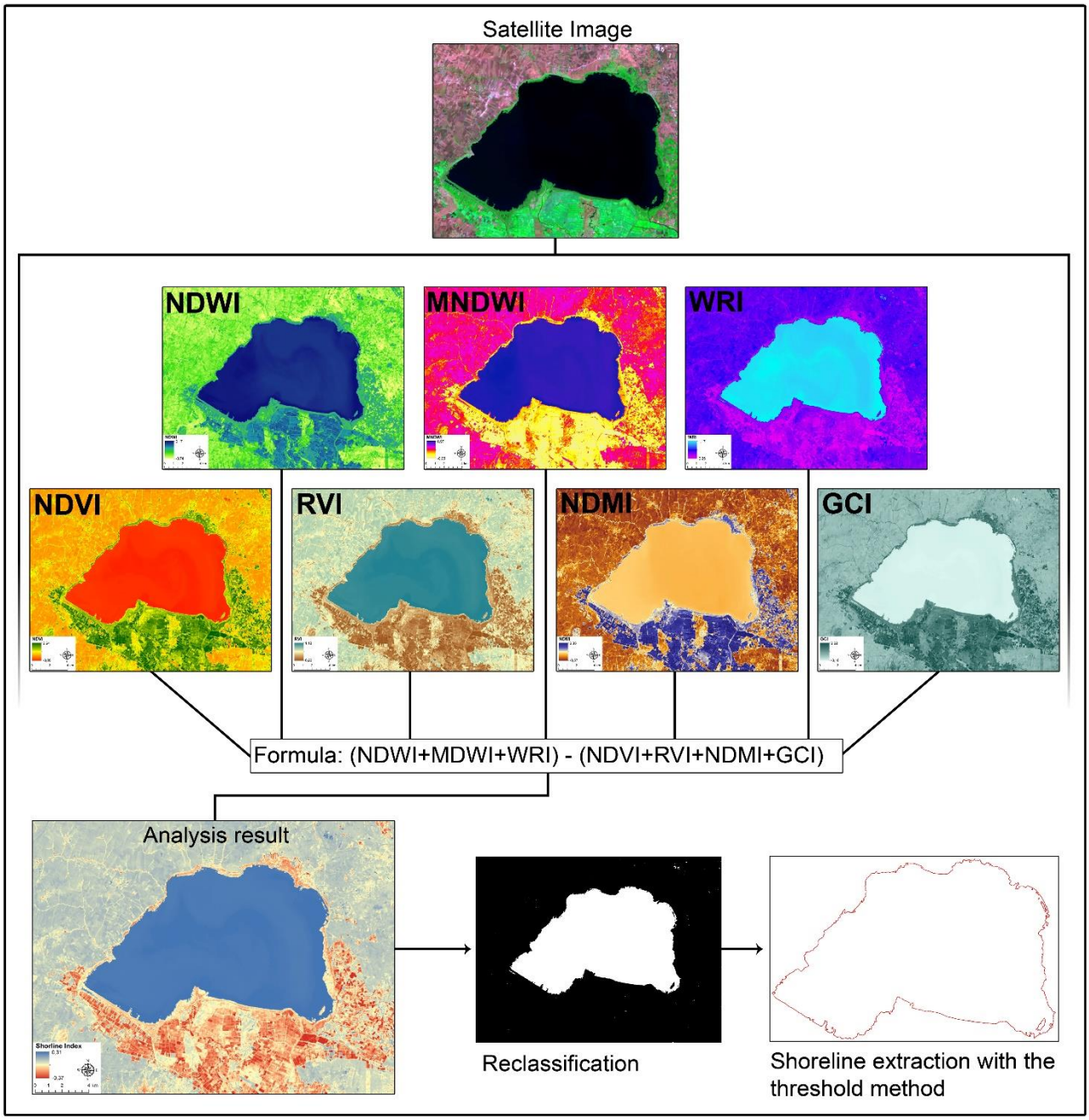

Figure 2. Work-flow diagram of the study and the method used to determine the shoreline

2.1. Analyses Used in Shoreline Change with DSAS Tool

The Digital Shoreline Analysis System (DSAS) enables statistical analysis of shorelines determined over different time periods uniformly and provides quantitative and distributional data (Himmelstoss et al., 2018). The basic working mechanism in the DSAS tool is based on drawing shorelines, drawing fixed baseline data, and assigning site- and width-specific transects. The shorelines analysed with DSAS also provide many quantitative data with statistical tests involving different algorithms. Net Shoreline Movement (NSM), End Point Rate (EPR), Shoreline Change Envelope (SCE) and Linear Regression Rate (LRR) statistics were utilized in the study.

The NSM statistic reveals the distance between the old and new shorelines during the periods analysed (Himmelstoss et al., 2018). With the NSM statistic, the average, maximum and minimum amount of the change value of the shorelines in the determined periods can be determined. The EPR statistic is calculated by dividing the old and new shoreline change distance in the determined period by time (Kılar & Çiçek, 2018). EPR results are used to explain the amount of annual coastal erosion and deposition (Song et al., 2021). SCE represents the greatest distance between all shorelines temporally

over a given transect. Since there is no sign of the total distance between two shorelines temporally, the SCE value is always positive and expressed in meters. LRR is calculated by dividing all shorelines in the determined profile by time. LRR analysis allows calculations to be made by minimizing the error in shoreline change (Himmelstoss et al., 2018).

In the study, the baseline was first drawn to determine the shoreline change of Manyas Lake in the DSAS V5.0 tool installed as an ArcGIS plug-in, and then the shoreline dates and uncertainty value were entered (Himmelstoss et al., 2018). The transect (profile) interval determined for shoreline change is 50 meters in long and short-term analyses. NSM and EPR statistics were used for the 5-year periods between 1980-2020, NSM, EPR, SCE and LRR statistics were used for the long-term analysis including all shorelines 1980-2020 and for the monthly analyses in 2022.

Each period data analysed from the lake surface area and shoreline change analyses were then converted to polygon in ArcGIS software. Using ArcGIS-geoprocessing-union feature, coastal erosion and coastal accretion areas and quantitative values were determined between the past and present periods.

3. FINDINGS

3.1. Analysis of Manyas Lake Surface Area and Shoreline Change over Short Periods between 1980-2020

Landsat satellite images of 1980, 1985, 1990, 2000, 2005, 2010, 2015 and 2020 were analysed for the surface area and shoreline change of Manyas Lake (Figure 3). The shorelines of each year were determined based on the water band combination of satellite images and the index formula. From the analyses, it was determined that the shoreline and lake surface area of Manyas Lake were changed by deposition and erosion in certain areas.

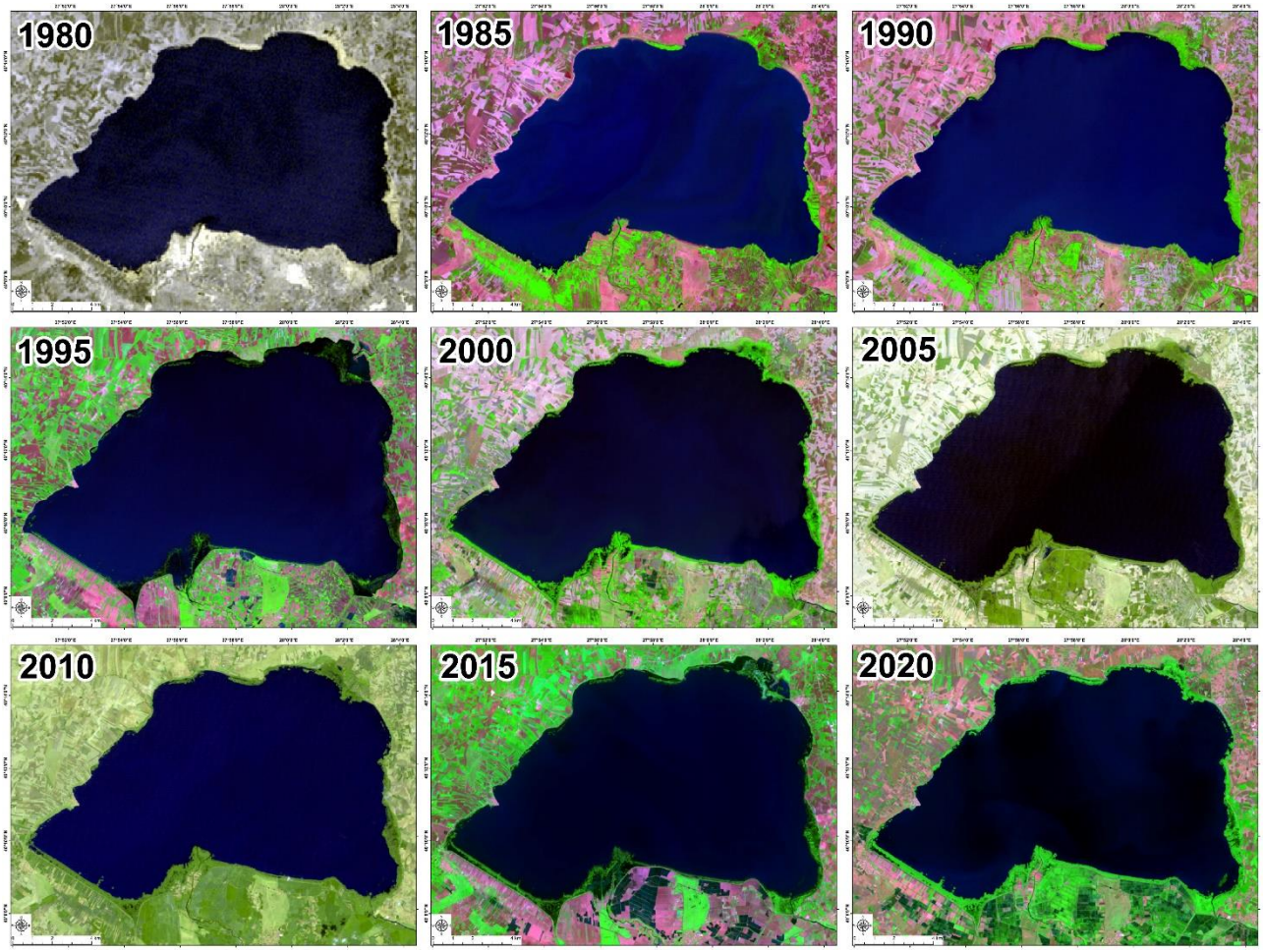

Figure 3. Five-year satellite images of Manyas Lake used in the study (1980-2020)

The shoreline length of Manyas Lake was calculated as 63.1 km in 1980, 64.6 km in 1985, 67.9 km in 1990, 81.1 km in 1995, 71.6 km in 2000, 68.7 km in 2005, 74.6 km in 2010, 69.7 km in 2015 and 73.5 km in 2020 (Figure 4). Natural dynamic processes, materials transported to the shore, seasonal and periodic climatological conditions, productive ecosystem structure of wetlands and vegetation factors have been effective in the variation of shoreline lengths. In this respect, the increase in the length of the shoreline in 1995 is related to the increase in the lake surface area due to

seasonal precipitation according to the satellite image date (May) (Figures 3 and 4). Other temporal changes were due to the expanding delta area in the south of the lake, small islets emerging due to reed areas and the increase in the indentation and protrusion structure in the lagoonal environment. This change in the shoreline length of Manyas Lake indicates that the ecosystem structure of the lake is variable and affected by geomorphological processes and climatological conditions.

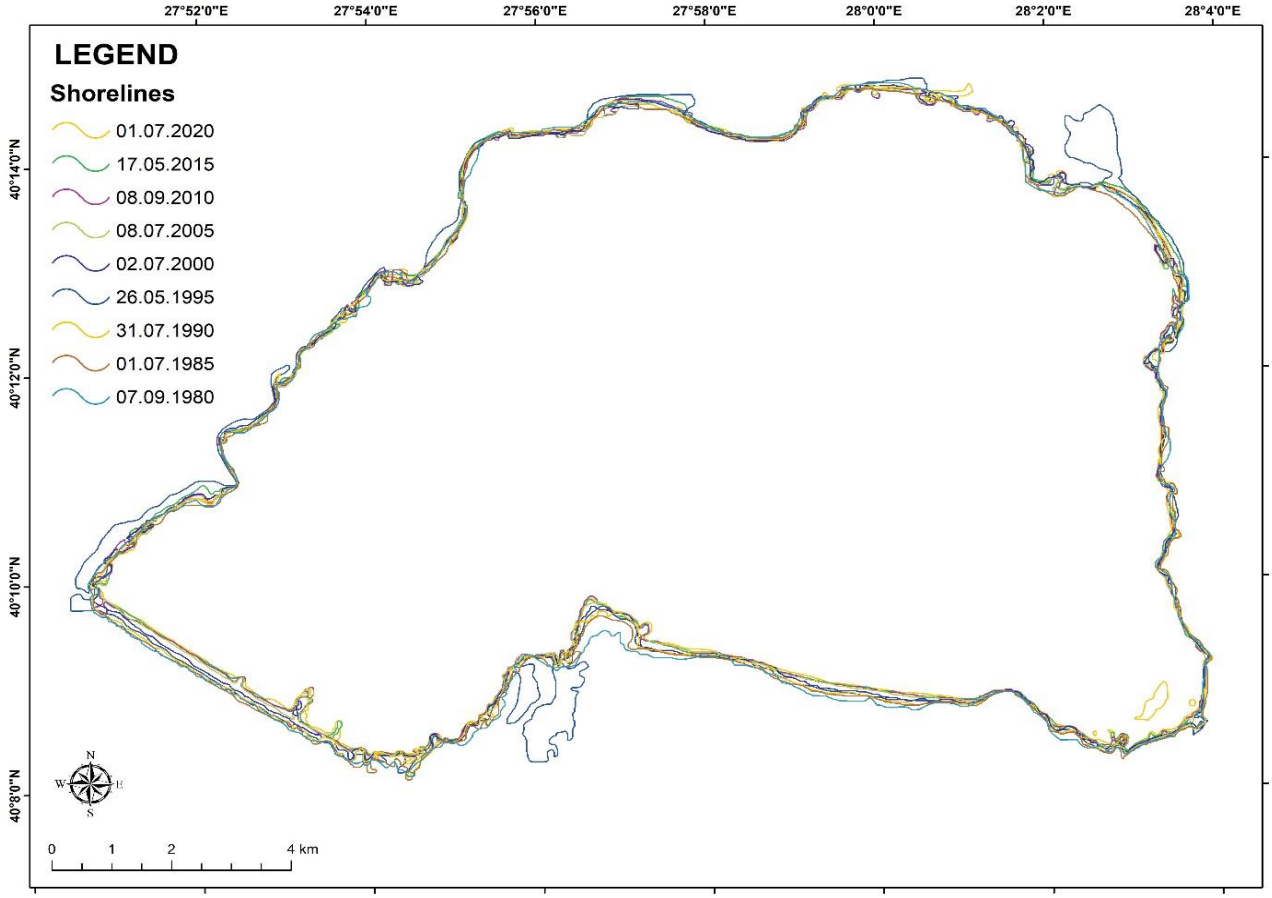

Figure 4. Shoreline of Manyas Lake in 5-year periods between 1980-2020

From the shoreline change analysis, it was determined that there is coastal accumulation in the southern part of Manyas Lake and the shoreline is advancing. In addition, the dynamic process formed by the rivers carrying material to the lake shores caused the shore progression to be observed in the Manyas Creek delta in the south of the shore and the expansion of reed beds and small islets. However, it was determined that coastal erosion occurred and coastal stretching occurred in the delta areas formed by short streams in the west and north of the lake. From the findings obtained, it was determined that different changes occurred in both shorelines and lake surface area in terms of quantitative and spatial distribution between 5-year periods. The change in the shorelines of Manyas Lake was analysed with NSM and EPR statistics in 5-year periods between 1980-2020 (Figures 5 and 6).

According to the results of NSM statistics, the maximum distance change of 796.9 m, minimum distance change of -213.8 m and average distance change of 28.5 m were determined in the shoreline of Manyas Lake during the 1980-1985 period (Table 3). In this period, coastal accumulation was observed in Manyas Stream (Kocaçay) delta and on the northern shores of the lake, while coastal erosion was observed on the eastern and western shores of the lake (Figure 5). According to NSM statistics, maximum 374 m, minimum -132.8 m and average 8.1 m distance change was observed in the shoreline during 1985-1990 period (Table 3). In this period, the positive shore change area is in the form of coastal accumulation in the southern part of the lake and especially in the delta area. Coastal erosions are concentrated in the reeds and delta areas in the western part of the lake (Figure 5). According to the NSM analysis in the 1990-1995 period, the maximum shoreline change was 208.1 m, the minimum was -567.6 m and the average was -37.2 m (Table 3). 1995 satellite image is taken from the seasonally wetter period and due to the climatological conditions, it is observed that the negative coastal progression peaks in the change data. Especially in the deltas of Sığırcı Creek in the north and Manyas Creek in the south, it was determined that the lagoonal environments expanded and the lake surface area moved into the land area (Figure 5). In the 1995-2000 period, according to the NSM statistics, a maximum distance of 600.8 m, a minimum distance of 173.8 m and an average shoreline change distance of 64 meters were

determined (Table 3). Contrary to the previous period, in the 1995-2000 period, coastal erosion areas increased especially on the southern shores due to the shrinkage of the lake area (Figure 5).

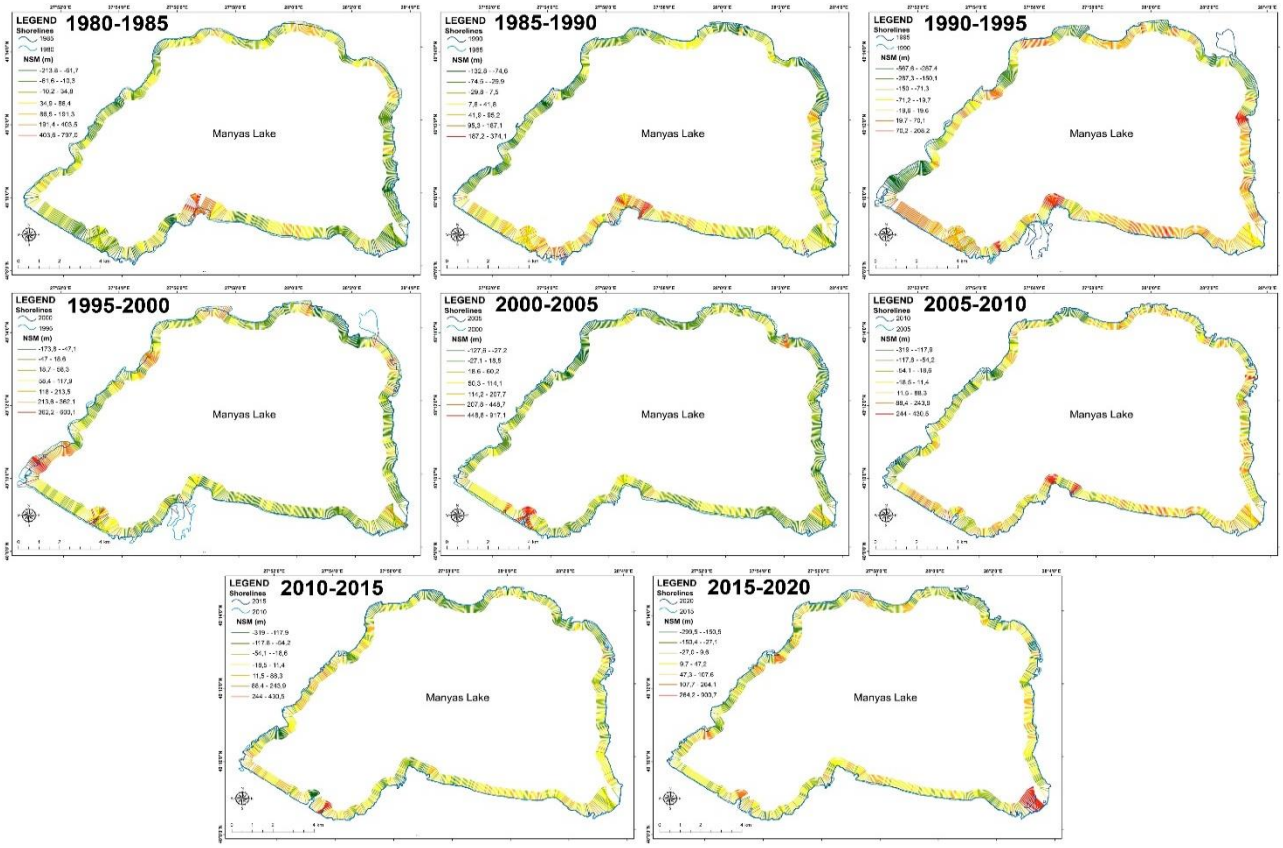

Figure 5. The result of NSM statistical analysis of the shoreline change of Manyas Lake in 5-year periods between 1980-2020

According to the NSM analysis between 2000-2005, a maximum of 917.1 m, a minimum of -127.6 m and an average shoreline change of 46.3 meters were determined (Table 3). Especially the plant development in the reed areas in the southwest of the lake caused the shoreline progression to reach its maximum extent. Coastal erosion areas are observed on the eastern and western shores of the lake (Figure 5). In the period between 2005-2010, according to the NSM analysis, a maximum distance change of 212.5 m, a minimum distance change of -215.3 m and an average distance change of 4.4 meters were determined (Table 3). In this period, as in the other periods, it is observed that there is coastal accumulation in the reeds and delta area in the south of the lake, and coastal erosion on the western and northern shores (Figure 5). According to the results of NSM statistics in the period between 2010-2015, the maximum distance change of 430.4 m, minimum distance change of -319 m and average distance change of -15.7 m were analysed (Table 3). During this period, shore accumulation is observed in the reed areas in the southwest of the lake, and shore erosion is observed on the western and northern shores (Figure 5). In the period between 2015 and 2020, a maximum distance change of 900.6 m, a minimum distance change of -359 m and an average distance change of 62.9 meters were recorded (Table 3). As in other periods, the accumulation areas on the southern shores of the lake attract attention in this period. Coastal erosion is observed in some reed areas on the northern and western shores of the lake (Figure 5).

Table 3. NSM and EPR statistical results of Lake Manyas shoreline in the determined periods

	NSM (m)			EPR (m/year)		
Period	**Mean**	**Maximum**	**Minimum**	**Mean**	**Maximum**	**Minimum**
1980-1985	28,5	796,9	-213,8	5,9	165,6	-44,4
1985-1990	8,1	374	-132,8	1,6	73,6	-26,1
1990-1995	-37,2	208,1	-567,6	-7,7	43,1	-117,7
1995-2000	64	600,8	-173,8	12,5	117,7	-34,1
2000-2005	46,3	917,1	-127,6	9,2	182,9	-25,4
2005-2010	4,4	212,5	-215,3	0,8	41,1	-41,6
2010-2015	-15,7	430,4	-319	-3,3	91,8	-68
2015-2020	32,7	900,6	-299,5	6,3	175,7	-58,4

When the average values of the NSM data analysed in 5-year periods of the shoreline change of Lake Manyas are examined, the maximum shoreline change distance of 555 m, minimum -256.1 and average 16.3 m were calculated. This situation shows that the lake surface area is shrinking and coastal accumulation is increasing, although there are different change sizes on the shores. Especially the reeds on the southern shores of the lake and the coastal accumulation areas in Manyas Creek delta attract attention.

According to the results of the EPR statistics of the shoreline change of Manyas Lake for the period between 1980-1985, the maximum shoreline change value of 165.6 m/year, minimum shoreline changes value of -44.4 m/year and average shoreline change value of 5.9 m/year were calculated (Table 3). During this period, positive changes were found in Manyas Creek delta and other deltas with various small areas, and negative changes were found in the east and west of the lake (Figure 6). In the period between 1985-1990, according to the results of EPR statistics, maximum 73.6 m/year, minimum -26.1 m/year and average 1.6 m/year changes in the shoreline were calculated (Table 3). During this period, coastal accretion occurred on the southern shores of the lake, while coastal erosion was observed on the northern and western shores (Figure 6). According to the EPR result between 1990-1995, the maximum change of 43.1 m/year, minimum change of -117.7 m/year and average change of -7.7 m/year were calculated (Table 3). It is seen from the findings that the lake surface area expansion in the 1995 satellite image is reflected in the data in the EPR analysis as in the NSM statistics (Figure 6). According to the results of the EPR statistics between 1995 and 2000, a maximum change of 117.7 m/year, a minimum change of -34.1 m/year and an average change of 12.5 m/year were determined (Table 3). Contrary to the previous period, it is seen that the positive values are more in this period and the coastal accumulation is concentrated on the lake shores (Figure 6).

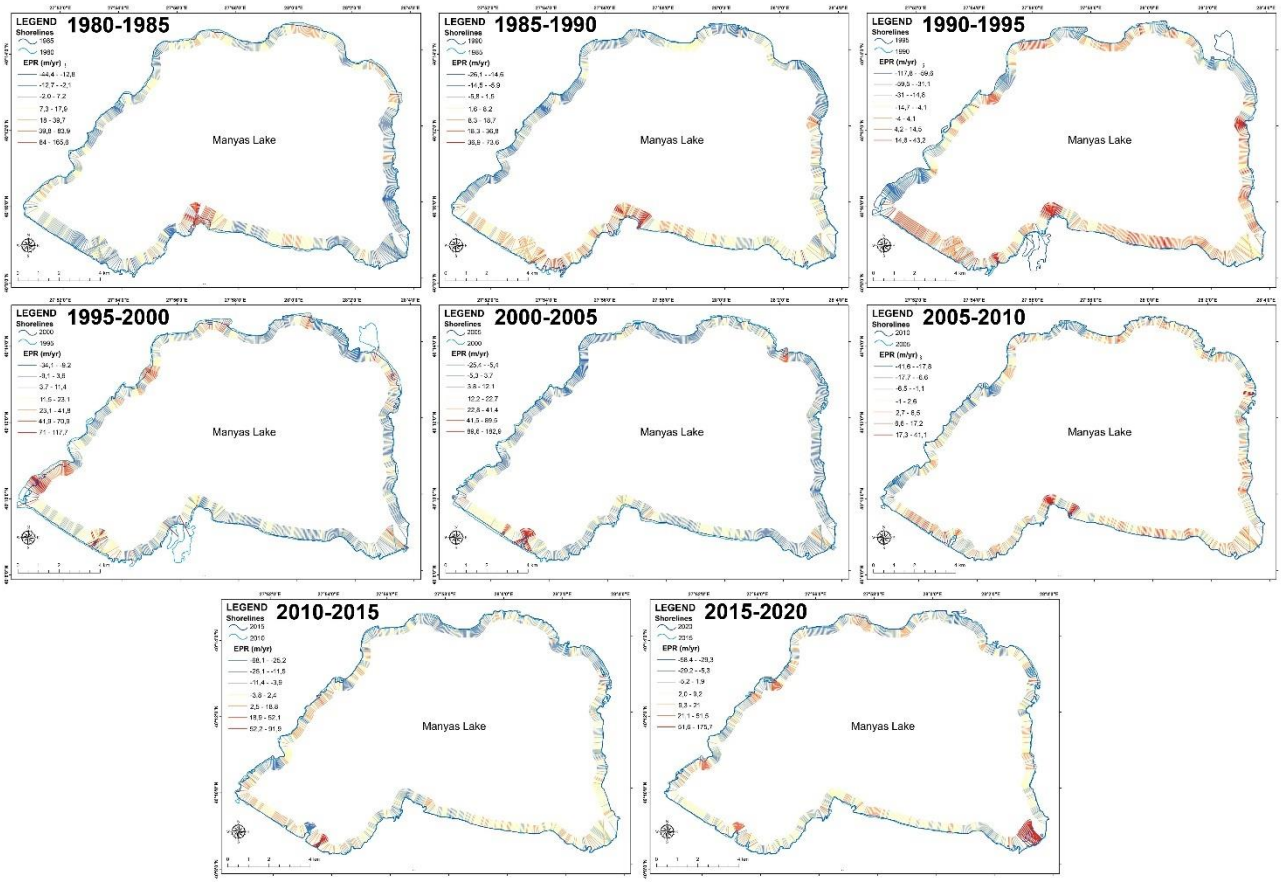

Figure 6. EPR statistical analysis results of the shoreline change of Manyas Lake in 5-year periods between 1980-2020

According to the EPR statistic data, maximum 182.9 m/year, minimum -25.4 m/year and average 9.2 m/year changes were recorded between 2000-2005 (Table 3). During this period, positive changes (coastal accumulation) on the southern shores of the lake and negative changes on the western shores are noteworthy (Figure 6). In the period between 2005-2010, according to the EPR analysis, a maximum change value of 41.1 m/year, a minimum change value of -41.6 m/year and an average change value of 0.8 m/year were obtained (Table 3). In this period, it was determined that the shoreline change was in the reed marsh areas in the west and southwest, while the extent of change in other areas showed very low values (Figure 6). In the period between 2010-215, according to EPR statistics, maximum

91.8 m/year, minimum -68 m/year and average -3.3 m/year changes in the shoreline were determined (Table 3). In this period, coastal advancement in the reeded area in the southwest of the lake and coastal stretching on the eastern and northern shores constitute the dominant processes (Figure 6). In the period between 2015 and 2020, according to the EPR statistics, a maximum change distance of 175.7 m/year, a minimum change distance of -58.4 m/year and an average change distance of 6.3 m/year were calculated (Table 3). During this period, shore advancement is observed in the reed areas and delta area on the southern shores of the lake, and shore retreat is observed in various parts of the northern shores (Figure 6).

When the average values of the EPR data analysed in 5-year periods of the shoreline change of Manyas Lake were examined, it was found that the maximum shoreline change was 111.4 m/year, the minimum was -51.9 m/year and the average was 3.1 m/year. Although there are different areas and sizes of change between the periods, it was determined that coastal accumulation occurred on the southern shores of Manyas Lake and coastal erosion occurred in certain areas of the western and northern shores. From the analyses, it is seen that the changes in NSM and EPR statistics are spatially similar. Since Manyas Lake is fed by short streams with low flow rates from the north and west, it was determined that coastal erosion occurs on these shores, while in the south, coastal accumulation is high due to the delta progression with the material carried by Manyas Creek, which is the continuation of Kocaçay, and the expansion of the reed area in the southwest.

With the change in the shoreline of Manyas Lake, changes also occur in the surface area of the lake over the years (Figures 7 and 8). The surface area of Lake Manyas was 152.4 km^2 in 1980, 151.1 km^2 in 1985, 150.8 km^2 in 1990, 155.1 km^2 in 1995, 149.7 km^2 in 2000, 147.8 km^2 in 2005, 147.8 km^2 in 2010, 148.6 km^2 in 2015 and 147.5 km^2 in 2020 (Figure 8). Although increasing and decreasing trends are observed in the lake surface area in certain periods, it was determined that the surface area of Manyas Lake was in a decreasing trend between 1980-2020. This situation reveals that the accumulation and erosion areas on the lake shore vary between the periods, but the coastal accumulation is more in the long term.

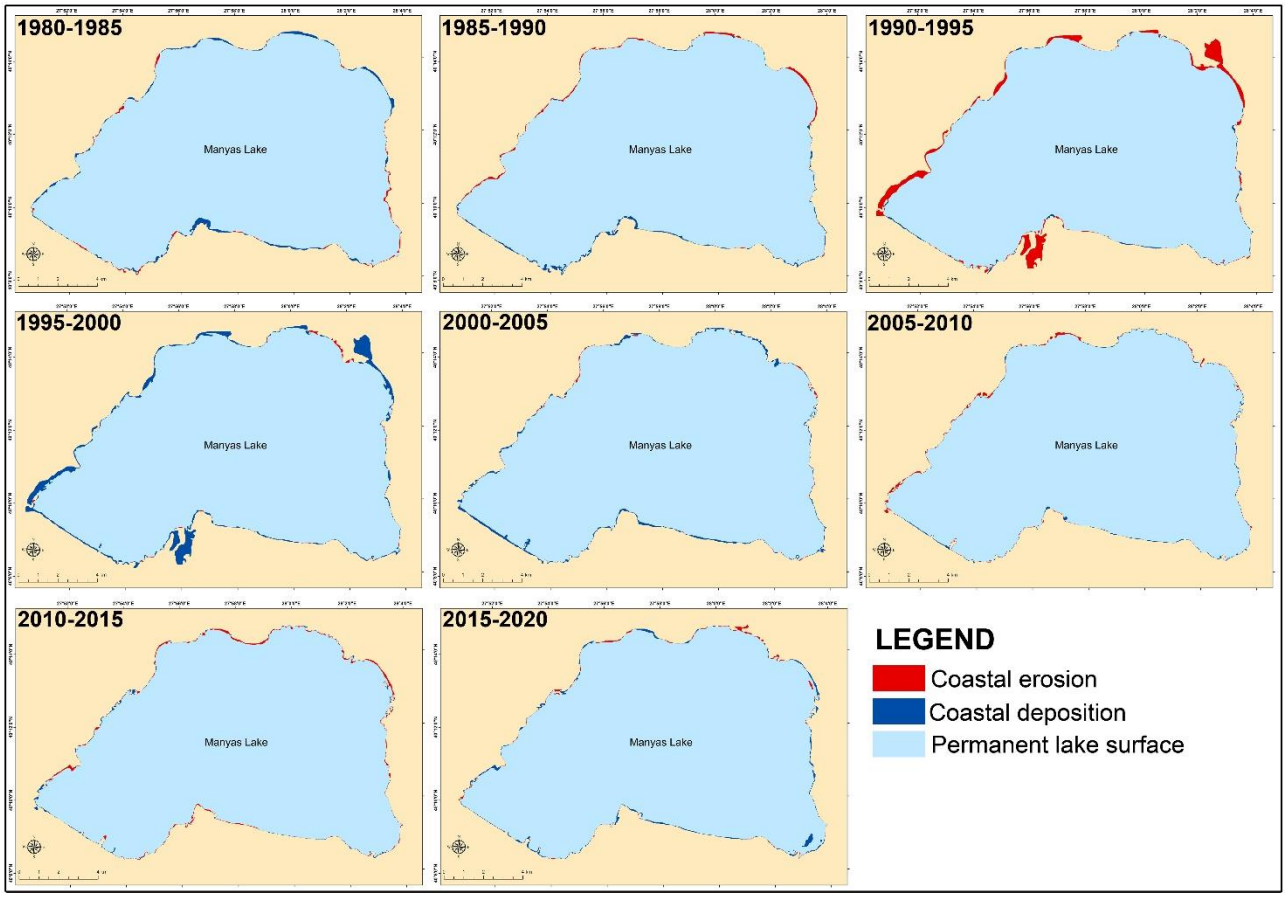

Figure 7. Distribution of coastal erosion and coastal deposition of Manyas Lake in 5-year periods between 1980-2020

The change in the surface area and shoreline of Manyas Lake between 1980 and 1985 resulted in 2.06 km^2 of coastal accumulation and 0.72 km^2 of coastal erosion (Figures 7 and 8). During this period, the permanent lake surface area was calculated as 150.3 km^2. During this period, coastal accumulation was observed most prominently in the Manyas Creek delta and in the reed areas in the north of the lake.

Coastal erosion was observed at various places on the eastern and western shores of the lake. Between 1985 and 1990, 1.3 km^2 of shore accumulation, 1.04 km^2 of shore erosion and 149.7 km^2 of permanent lake surface area were calculated (Figures 7 and 8). During this period, coastal accretion was completely observed in the southern and eastern parts of the lake, while coastal erosion intensity was detected on the northern and western shores. Between 1990-1995, 0.71 km^2 of coastal accumulation, 5.02 km^2 of coastal erosion and 150.1 km^2 of permanent lake surface area were determined in Manyas Lake (Figures 7 and 8). The observation of a large area of water surface spread in Manyas Creek and Sığıcı Creek deltas in this period is due to the fact that the satellite data of 1995 was temporally in May and the lake water input was higher in this period compared to the summer months. In the period between 1995 and 2000, 5.67 km^2 of coastal accumulation, 0.28 km^2 of coastal erosion and 149.4 km^2 of permanent lake surface area were detected (Figures 7 and 8). In contrast to the previous period, the fact that the coastal accumulation was observed at a value much higher than the general trend in this period is related to the fact that the satellite data coincides with the time that provides more hydrographic input periodically. In the period between 2000-2005, 2.2 km2 of coastal accretion, 0.27 km^2 of coastal erosion and 147.5 km^2 of permanent lake surface area were detected in Manyas Lake (Figure 8). In this period, the most prominent coastal accumulation was observed in the delta area and reeds in the southern part, while coastal erosion was observed in various areas on the east and west coasts (Figure 7). In the period between 2005 and 2010, 0.76 km2 coastal accumulation, 0.81 km^2 coastal erosion and 147.06 km^2 permanent lake surface area were determined. In this period, narrow shore deposits were detected in the southern part of the lake and shore erosion was detected in the reeds and wetlands in the west. Between 2010 and 2015, 0.62 km^2 of coastal accumulation, 1.34 km^2 of coastal erosion and 147.2 km^2 of permanent lake surface area were detected (Figure 7 and 8). In this period, the change in the satellite data dates increased the lake surface area and coastal erosion areas. In the period between 2015-2020, 1.66 km^2 of coastal accumulation, 0.63 km^2 of coastal erosion and 146.9 km^2 of permanent lake surface area were detected in Manyas Lake. During this period, accumulation areas were found on the southern shores of the lake and coastal erosion was found on various shores in the north (Figure 7).

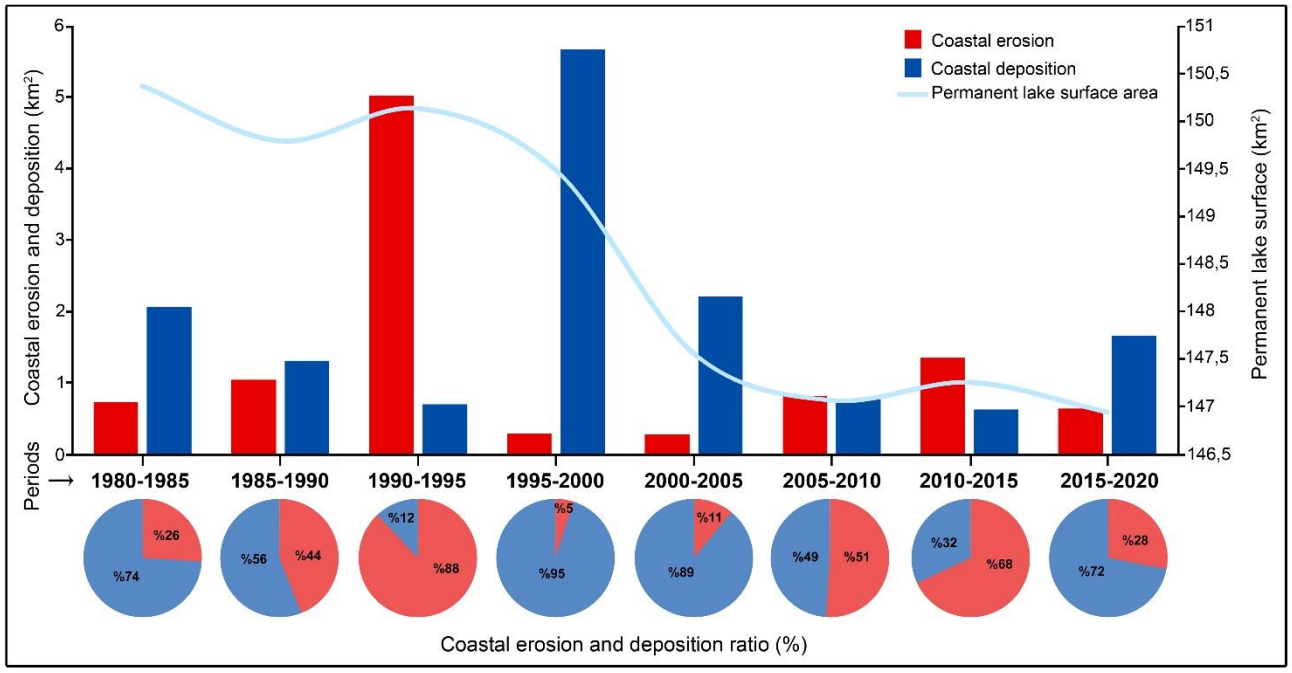

Figure 8. Numerical values of coastal erosion and coastal accretion of Manyas Lake in 5-year periods between 1980-2020

Although coastal erosion and coastal accretion show periodic differences in the surface area and shoreline of Manyas Lake between 1980 and 2020, it is understood from the analyses that the trend is in the direction of coastal accretion. In addition, it was determined that the trend of permanent lake surface area in the specified periods was in the direction of decrease (Figure 8). This situation quantitatively reveals that there is a decreasing trend in the sources that make up the water budget of the lake. In addition, the expansion in the Manyas Creek delta and the coastal stretching in the Sığırcı Creek delta, which has a narrower basin area, show the role of natural dynamic geomorphological processes in the coastal change of Manyas Lake. The change in the water budget due to the seasonal variation of the climatological conditions in Lake Manyas and its

basin was also observed in the change data on certain dates (Figure 7 and 8).

3.2. Long-term Change Analysis of Manyas Lake Surface Area and Shoreline between 1980-2020

NSM, EPR, SCE and LRR statistics were analysed on 9 shorelines of Manyas Lake between 1980 and 2020 (Figure 9 and Table 4). According to the results of NSM statistics, the maximum distance change of 1585.5 m, the minimum distance change of -403.7 m and the average distance change of 139.8 m were determined on the shoreline of Manyas Lake as in the long period between 1980-2020 (Table 4). In the 40-year long term interval, the change in the shoreline of Manyas Lake was realised in the form of coastal accretion in the Manyas Creek delta and in the reedy area extending NW-SE to the west, in the reedy islets around the Karaçay gorge and in small deltas on the eastern shores (Figure 9). During this period, the changes were concentrated on the western and northern shores of Manyas Lake, and coastal erosional changes occurred in the Sığırcı Creek delta and Soğuklar Creek delta. The quantitative data of the NSM analysis show that the surface area of Manyas Lake has shrunk over the 40-year period and an average coastal advance of 134 metres has occurred.

When the graph of the NSM statistics of the shoreline change of Manyas Lake between 1980-2020 is analysed, it is seen that the coastal accumulation is more intense and wider in terms of dimension (Figure 10). It is understood that the coastal accumulation above 1000 metres, especially on the southern shores of the lake, is concentrated around the Manyas Creek delta, reedbed area and Karaçay Creek gorge. While the accumulation and erosion areas on the eastern shore of the lake form the geomorphological process together, erosion areas on the northern and western shores attract attention.

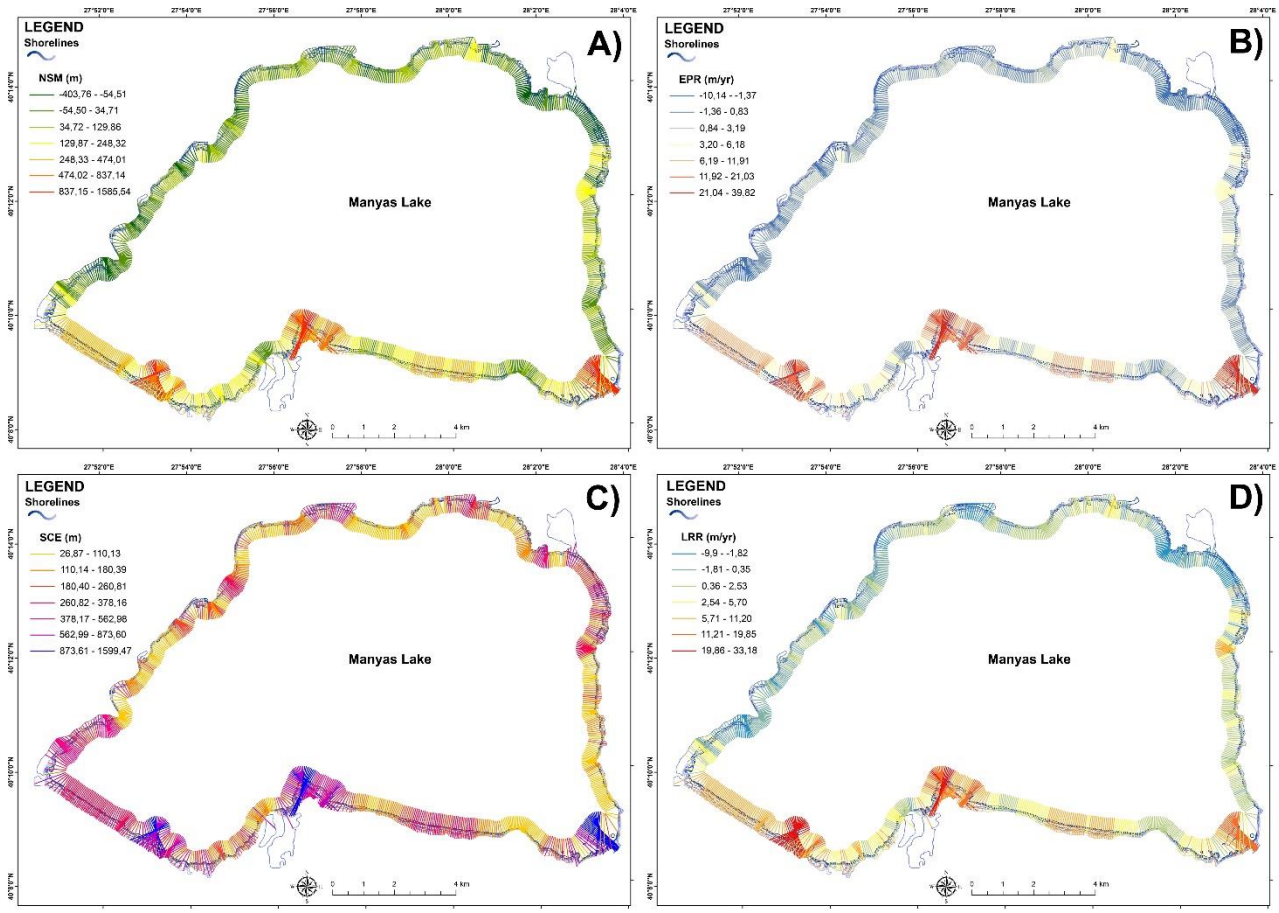

Figure 9. Analysis of all shorelines of Manyas Lake determined between 1980-2020 with DSAS tool. A) NSM, B) EPR, C) SCE and D) LRR

According to the results of EPR statistics in the long term between 1980 and 2020, maximum 39.82 m/year, minimum -10.14 m/year and average 3.51 m/year changes in the shoreline of Manyas Lake were calculated (Table 4). During this period, it was determined that changes were experienced in the form of coastal advancement on the southern shores of Manyas Lake, especially in the Manyas Creek delta, the shores of Karaçay gorge and the reeds in the southwest, and coastal retreat on the western and northern shores of the lake (Figure 9).

According to the SCE statistics, the maximum, minimum and average distance change of 1599.4, 26.8 and 243.1 metres, respectively, were determined in the shoreline of Manyas Lake between 1980 and 2020 (Table 4). The highest shore advance

was found in the Manyas Creek delta, the reed area in the west and the reed area in the southeast of the lake. Minimum values were observed in various areas on the north, east and west coasts (Figure 9). According to LRR statistics, the maximum change of 33.18 m/year, minimum change of -9.9 m/year and average change of 3.44 m/year were calculated for the period between 1980 and 2020 (Table 4). The areas with the highest change are the southern shores of the lake, especially the Manyas Creek delta and reed areas (Figure 9). According to the LRR statistic, the areas with minimum change in the long term are the Sığırcı Creek delta and the western shores of the lake.

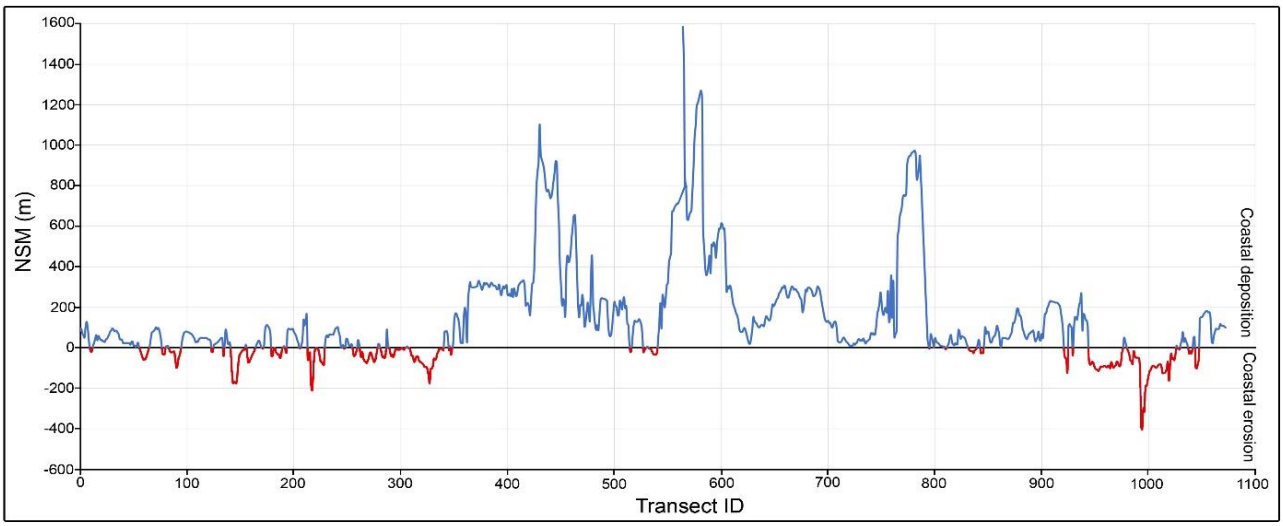

Figure 10. NSM graph of the shoreline change of Manyas Lake between 1980-2020

Table 4. Numerical data of NSM, EPR, SCE, LRR statistics of shoreline change of Manyas Lake between 1980-2020

	NSM (m)			EPR (m/year)		
Period	**Mean**	**Maximum**	**Minimum**	**Mean**	**Maximum**	**Minimum**
1980-2020	139,8	1585,5	-403,7	3,51	39,82	-10,14
	SCE (m)			**LRR (m/year)**		
Period	**Mean**	**Maximum**	**Minimum**	**Mean**	**Maximum**	**Minimum**
1980-2020	243,1	1599,4	26,8	3,44	33,18	-9,9

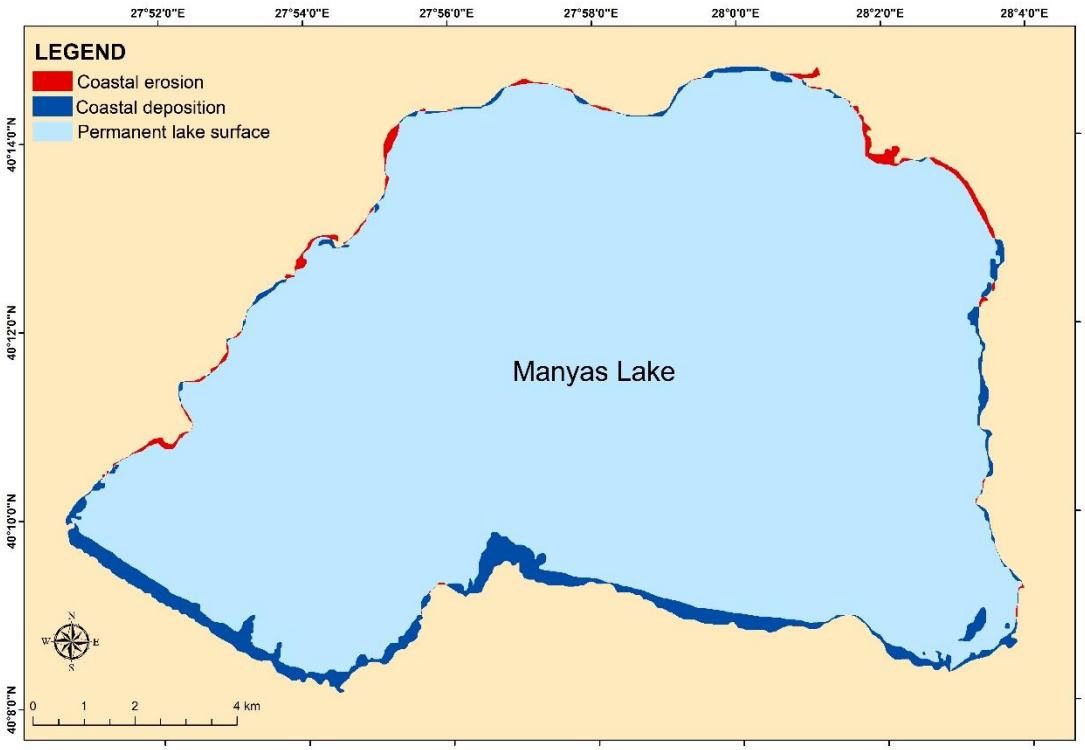

Figure 11. Distribution of coastal erosion and coastal deposition on the shores of Manyas Lake in the 40-year period between 1980-2020

From 1980 to 2020, 5.85 km² of coastal accretion and 1.03 km² of coastal erosion were determined on the surface area and coasts of Manyas Lake. Permanent lake surface area data of 146.5 km² was determined from the long-term analysis. From the change analysis, coastal accumulation areas are observed on the entire southern shores of the lake and in various places on the other shores (Figure 11). Coastal erosion is concentrated in the small deltas in the west of the lake and in and around the Sığırcı Creek delta in the north. During the 40-year temporal period, the surface area of Manyas Lake has shrunk and accumulation areas have occurred on the shores (especially the southern shores). The reason for the shrinkage of the surface area of the lake is the decrease in the water budget of the lake due to anthropogenic and natural causes, the increase in reed areas with the delta development in the south of the lake, anthropogenic interventions on some coasts and illegal water use in the surrounding agricultural areas.

3.3. Monthly Change Analysis of Manyas Lake Surface Area and Shoreline

In the long-term changes of the surface area and shoreline of Manyas Lake, even the recent changes in the dates of satellite data caused differences in areal and linear changes. For this reason, satellite images of Manyas Lake for each month in 2022 were obtained from Landsat and analysed (Figure 12). However, due to seasonal conditions, high cloudiness in some satellite images may cause some errors. For this reason, linear and areal calculations were made based on the months of February, April, June, August, August, October and December of Manyas Lake in the analyses in the DSAS tool.

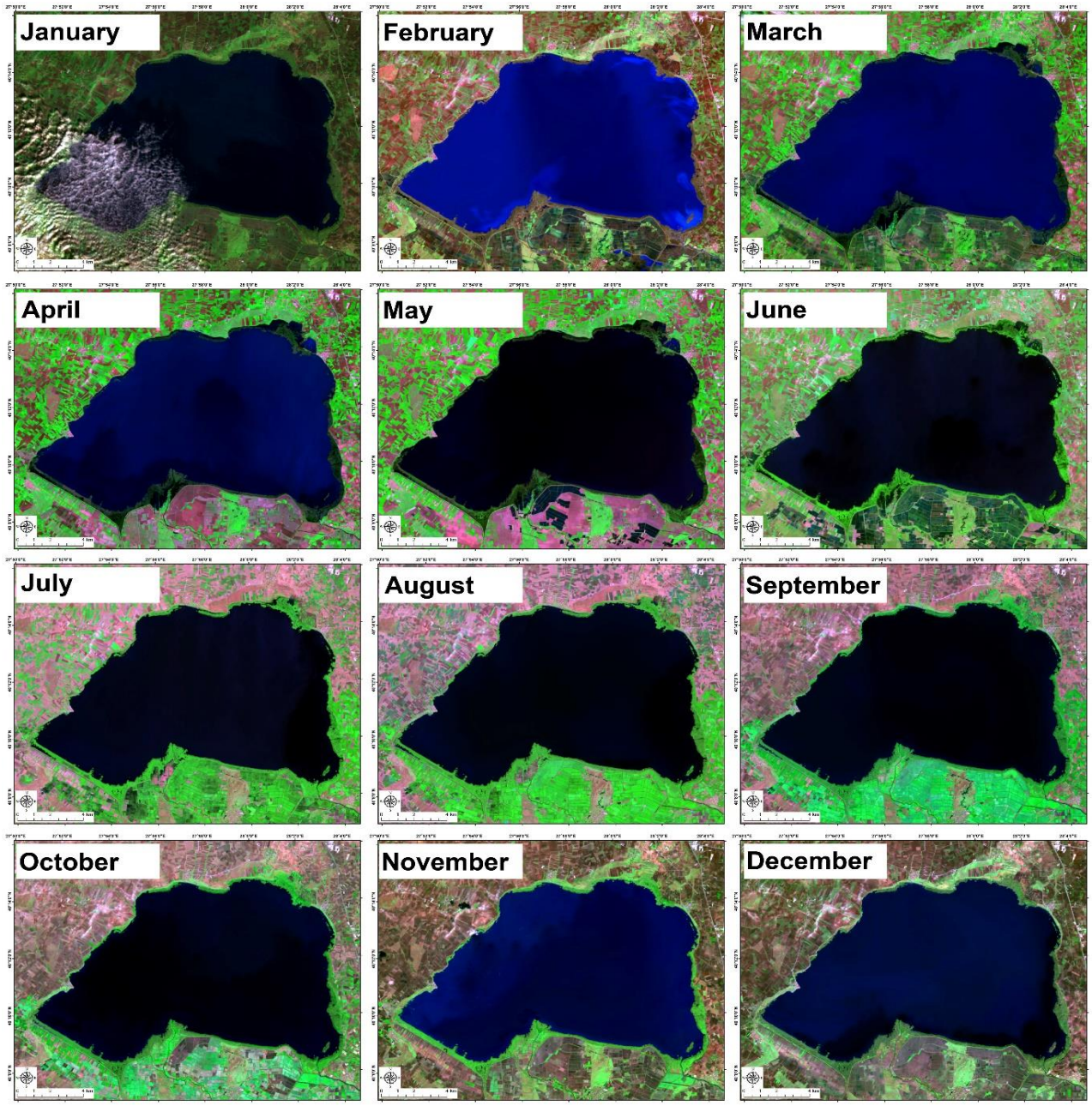

Figure 12. Satellite images of Manyas Lake for each month in 2022 used in the study

The shoreline length of Manyas Lake was calculated as 77.52 km in February 2022, 73.58 km in April, 78.87 km in June, 80.67 km in August, 79.96 km in October and 78.47 km in December. The obtained data reveal that the shoreline lengths decrease in winter and spring seasons and increase in summer season. Factors such as the increase in the water budget of the lake especially in the spring season, the productive structure of the wetland ecosystem, and the amount of evaporation play a role in this situation.

It is understood from the analyses that the monthly shoreline change of Lake Manyas is concentrated in certain areas (Figure 13). Especially in the southwest, northeast and north lagoon areas and delta areas, shoreline distance changes are observed. This situation can be explained by factors such as the wetland characteristic of the shores of Lake Manyas, the presence of reed marsh areas, the water budget of the lake, and the lake's outflow.

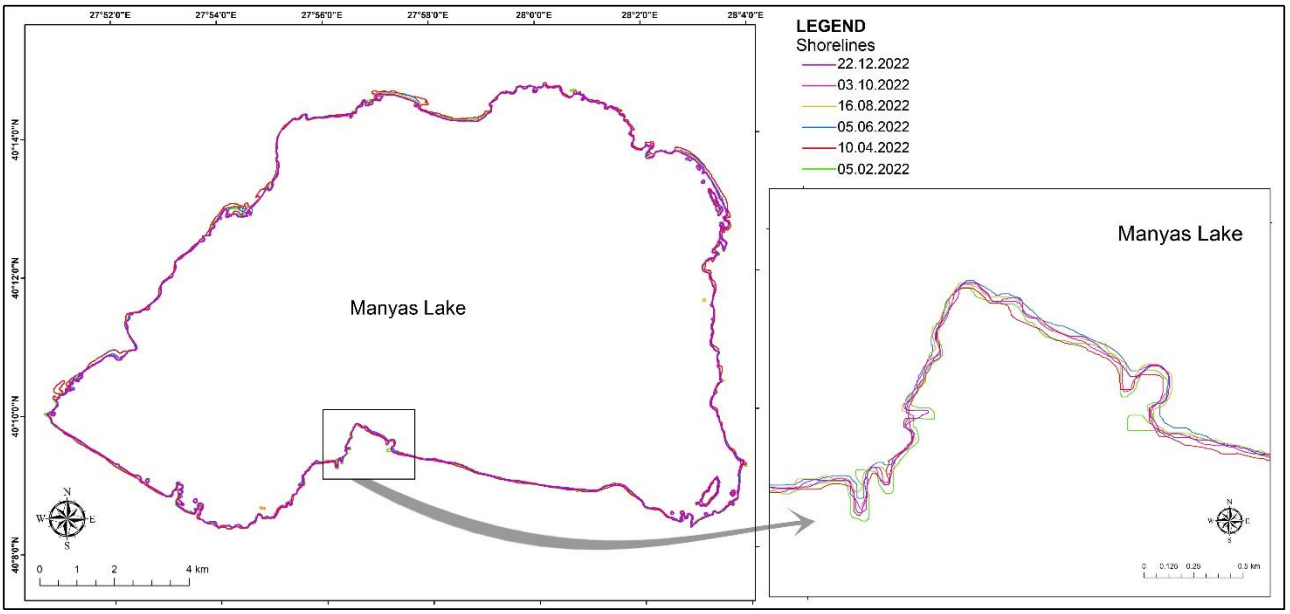

Figure 13. The shoreline of Manyas Lake in certain months determined in 2022

NSM, EPR, SCE and LRR statistical analyses were performed on the monthly shorelines of Manyas Lake in 2022 and the quantitative and spatial status of the change was explained (Figure 14 and Table 5). According to NSM statistics, the maximum change of 514.4 m, minimum change of -77.4 m and average change of 18.9 m were determined in the 2022 monthly shorelines of Manyas Lake (Table 5). According to the NSM analysis, in the monthly data, coastal advancement is observed in the reed area in the southwest of the lake, in all deltas on the lake shore, and coastal retreat is observed especially on the eastern and western shores of the lake (Figure 14). According to the EPR statistics, maximum 587.1 m/year, minimum -88.3 m/year and average 21.6 m/year changes were determined in the shorelines of the lake in 2022 (Table 5)

Table 5. Numerical data of the results of NSM, EPR,) SCE and LRR statistics over all shorelines of Manyas Lake determined in 2022

	NSM (m)			EPR (m/year)		
Period	**Mean**	**Maximum**	**Minimum**	**Mean**	**Maximum**	**Minimum**
2022	18,9	514,4	-77,4	21,6	587,1	-88,3
	SCE (m)			**LRR (m/year)**		
Period	**Mean**	**Maximum**	**Minimum**	**Mean**	**Maximum**	**Minimum**
2022	74,3	829,6	8,3	43,1	667,6	-156

When the distribution of EPR data was analysed, it was found that the changes were concentrated in delta and reed areas. The shoreline changes of Manyas Lake in 2022 was calculated as 829.6 m, minimum 8.3 m and average 74.3 m according to the SCE statistical analysis (Table 5). SCE is always positive as it reveals the maximum and minimum values of the profiles in shoreline change. In the distribution of SCE data, as in other data, it was determined that there is a density of change in reed areas and delta areas (Figure 14). According to the LRR statistic results of the monthly shorelines of Manyas Lake in 2022, a change value of 667, 6 m/year, a minimum of -156 m/year and an average change value of 43.1 m/year were calculated (Table 5). Numerical data reveal that the annual shoreline and surface change of the lake is quite high (Figure 14). Especially the changes in the reed and delta

areas revealed in all analyses show that the geomorphological, climatological, hydrographic and floristic features of the lake are affected by the distribution and dynamic processes. This situation reveals the basis of the wetland feature that makes the lake different and the productive-variable structure of the wetland ecosystem through annual and monthly data.

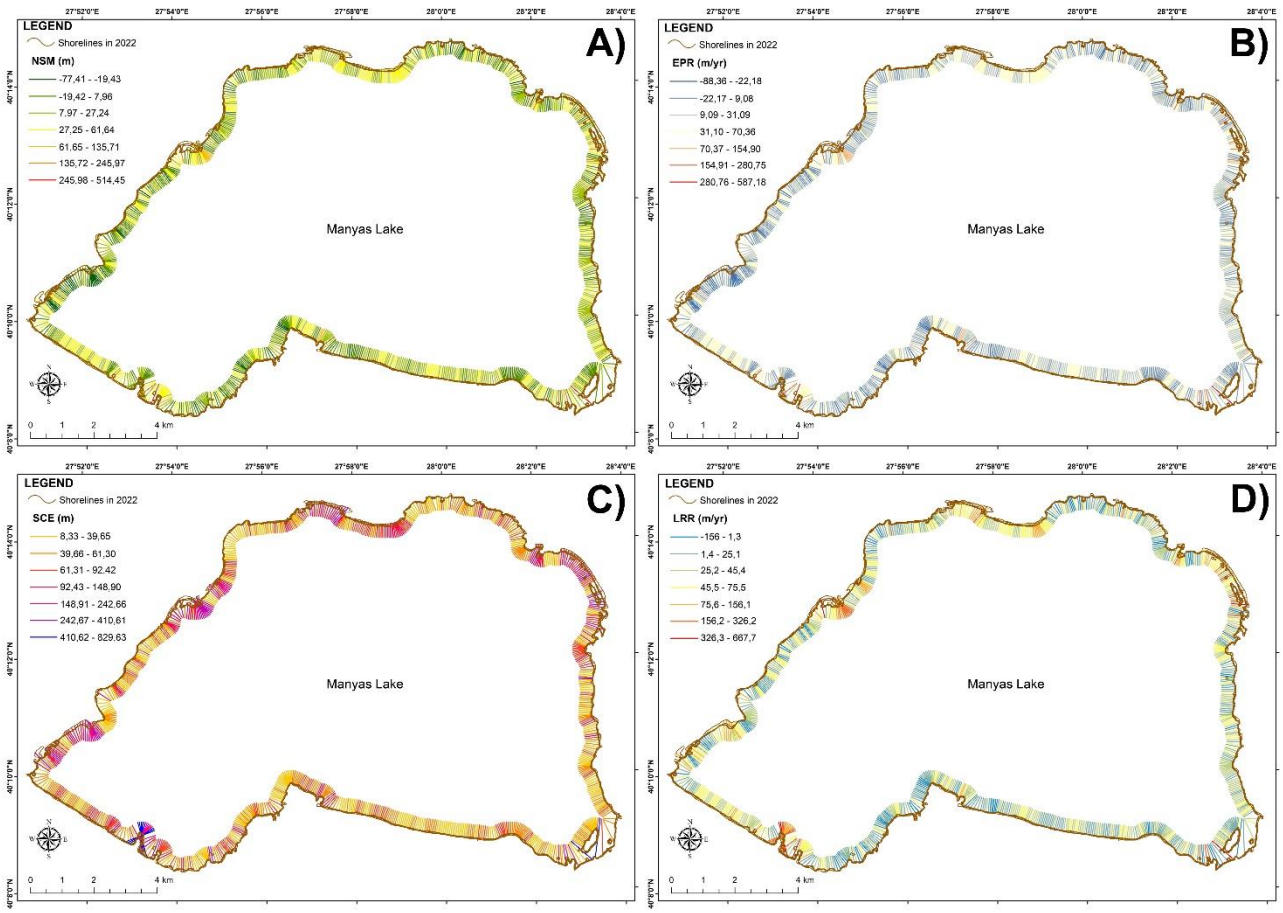

Figure 14. Distribution of the results of A) NSM, B) EPR, C) SCE and D) LRR statistics over all shorelines of Manyas Lake determined in 2022

Analyses of the monthly shoreline change of Manyas Lake also show that the surface area of the lake changes throughout the year (Figures 15 and 16). The surface area of the lake was 147.6 km^2 in February, 149.01 km^2 in April, 146.2 km^2 in June, 146.05 km^2 in August, 146.2 km^2 in October and 146.4 km^2 in December (Figure 16). The maximum value of the lake surface area is in April and the minimum value is in August. When the surface area change between April and August was analysed, it was found that coastal accumulation was 2.98 km^2, coastal erosion was 0.03 km^2 and permanent lake surface area was 146.02 km^2 (Figure 15). The findings show that the reedbed and terrestrial areas increased due to the decreasing water input from April onwards and 99% of the change was in the form of coastal accumulation. The areas of change extend as a narrow strip on the shore and consist of reed areas formed by the lagoonal environment (Figure 15).

When the monthly surface area changes of Manyas Lake in 2022 was modelled, it was found that peak values were observed in April, the lake surface area decreased to the minimum level in the summer season and then started to increase again (Figure 16). From the data obtained, the average surface area of the lake was found to be 146.91 km^2. According to the lake surface area change model, 4 months (February, March, April and May) were above the average value, while the surface area remained below the average value in the other months.

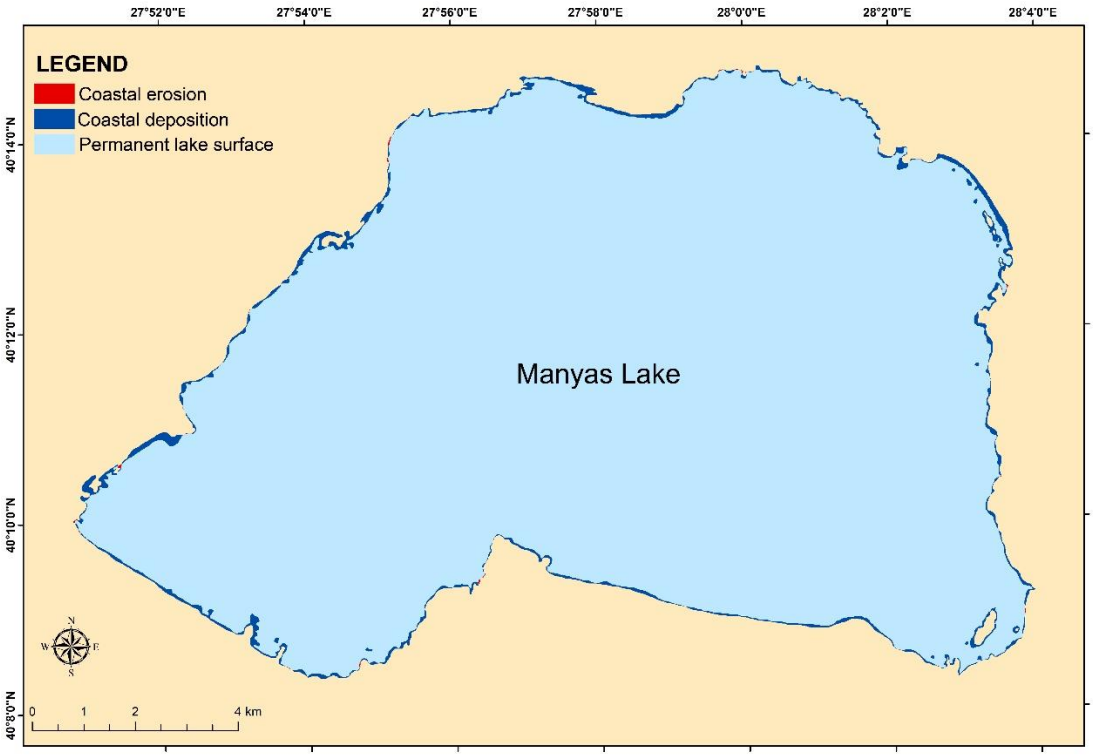

Figure 15. Coastal accretion and coastal erosion of Manyas Lake from April to August 2022

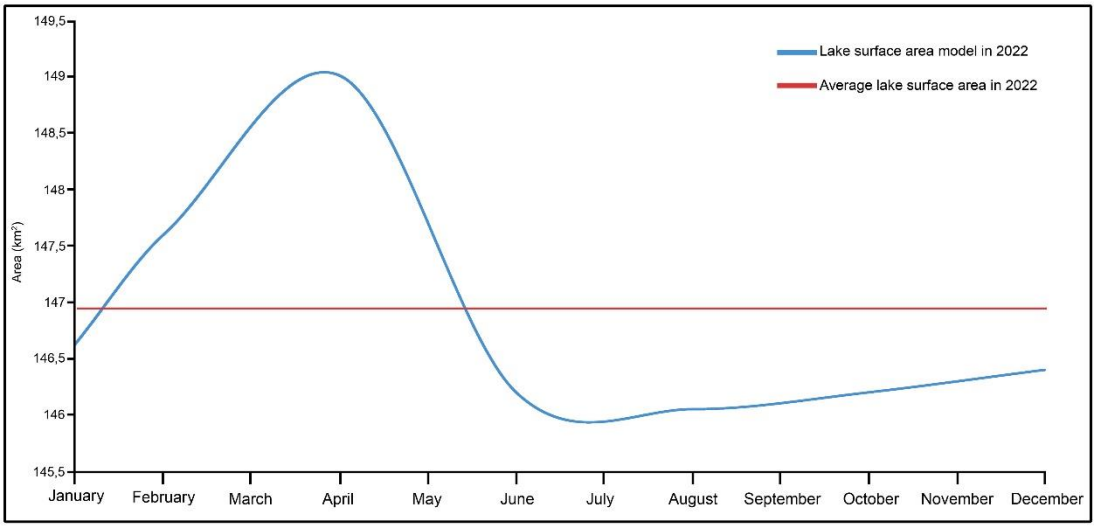

Figure 16. Change model of Manyas Lake surface area for the year 2022

4. DISCUSSION

In many studies on lake surface area and shoreline change in Turkey, it has been determined that the surface areas of lakes have shrunk from the past to the present, changes in the shoreline have been experienced, and this situation has occurred due to natural and anthropogenic factors (Bahadır, 2013; Duru, 2017; Aksoy et al., 2019; Aydın et al., 2020; Dereli & Tercan, 2020; Ataol & Onmuş, 2021; Topçu & Atatanır, 2021; Alevkayalı et al., 2023; Dinç, 2023). However, in some lakes in wetlands, changes occur at a large scale, while in others, changes occur at a more micro scale (Ataol & Onmuş, 2021; Sakaoğlu & Çepni, 2022). At the same time, many of the lakes change during the year by being affected by geomorphological, climatological, hydrographic and anthropogenic factors in their catchment basins. Manyas Lake, on the other hand, has been found to have a narrower long-term change dimension among the wetland lakes and other lakes in Turkey (Ataol & Onmuş, 2021). However, some previous studies have obtained different data on lake surface area and shoreline (Sakaoğlu & Çepni, 2022). In obtaining these data, the resolution of the data source and satellite image, the techniques and methods used may cause differences in the change results (Himmelstoss et al., 2018; Khorshiddoust et al., 2022). For this reason, in order to ensure that coastal flora is taken into account in wetland lakes and to determine the water surface and shoreline more accurately, a formula that provides water-land

separation specific to the study was produced by using 3 different water indices and 4 different vegetation indices. Based on this formula, the long-term (1980-2022) and monthly change of Manyas Lake in 2022 was determined. From the findings obtained, it was determined that the surface area of the lake decreased by 4.9 km^2 over a long period of 40 years. When the change data are compared with the change in surface area in other lakes and wetlands in Turkey, it is understood that the decrease in Manyas Lake is narrower (Bahadır, 2013; Aksoy et al., 2019; Aydın et al., 2020; Ataol & Onmuş, 2021; Topçu & Atatanır, 2021; Sakaoğlu & Çepni, 2022; Alevkayalı et al., 2023; Kaya et al. 2023; Şenol et al., 2023). Especially the natural dynamic geomorphological process originating from the Manyas Creek delta has provided delta development within the lake. However, the dam constructed on Manyas Creek in recent years weakened the material transport and caused the delta progression to slow down. In addition, the development of reeds in many areas, especially in the southwest of the lake, has caused the shrinkage of the lake surface area. The fact that the Manyas Lake drainage basin harbours rivers of longer length than the southern part and the material transport of these rivers is of higher dimension has caused coastal accumulation to occur intensively in the southern part of the lake. When the changes occurring in the lake in a 40-year period were analysed by NSM statistics, it was found that there was an average shoreline advance of 139 m and 243 m in SCE analysis. According to EPR statistics, the annual shoreline change is 3.5 m and according to LRR statistics it is 3.4 m. DSAS statistical analyses show that in some areas of the lakeshore there is a shoreline advance of up to 1500 m and in some areas, there is a shoreline retreat of 400 m. While the highest coastal advancement is observed in Manyas delta and the reed areas to the west, coastal retreat is intensely experienced in the Sığırcı Creek delta in the north of the lake. When Manyas Lake shore change and lake surface area are modelled through monthly analyses, it is found that the lake surface area reaches the largest dimensions in April, while the lake surface area reaches the smallest size in July and August. This situation shows that climatic conditions affect the hydrographic budget of the lake like many lakes in Turkey (Ataol & Onmuş, 2021). The mentioned situations reveal that the shoreline change may be different in morphological elements that show wetland characteristics such as Manyas Lake. For this reason, the use of more than one index and method in the determination of the shoreline and lake surface area using GIS and UA techniques will give more accurate results. In addition, it was revealed in the study that the lake surface area and shoreline change during the year in wetlands, which have a productive structure as an ecosystem, will also differ and this can be modelled with the DSAS tool.

5. CONCLUSION

In order to determine the surface area and shoreline change of Manyas Lake, Landsat satellite images were analysed in 5-year periods between 1980-2020 and all months of 2022. Due to the wetland characteristic of the lake, problems may arise in determining the water-land distinction in the study. For this reason, a study-specific formula was created using NDWI, MDWI, WRI water indices and NDVI, RVI, NDMI, GCI vegetation indices. The formula was applied to 9 different satellite images between 1980-2020 and 6 different monthly satellite images in 2022 with favourable cloudiness conditions. According to the results obtained, the shoreline length of Manyas Lake was calculated as 63.1 km in 1980 and 73.5 km in 2020. The shoreline length also showed different changes in other time intervals. The increase in the length of the shoreline has been influenced by the delta progression and the formation of islets by reeds. The shore of Manyas Lake was analysed with the DSAS tool for each 5-year consecutive period using NSM and EPR statistics, and the long term between 1980-2020 was analysed with NSM, EPR, SCE and LRR statistics. According to the results, extreme coastal changes occurred between 1990-1995 and 1995-2000. Especially in 1995, the width of the lake surface area resulting from the satellite image in May was reflected in the data. According to the results of NSM statistics, maximum 1585.5 m, minimum -403.7 m and average 139.8 m distance change was determined in the shoreline of Manyas Lake in the 40-year long period between 1980-2020. According to the EPR statistic, maximum 39.82 m/year, minimum -10.14 m/year and average 3.51 m/year changes were calculated. According to the SCE statistic, a maximum distance change of 1599.4, a minimum distance change of 26.8 and an average distance change of 243.1 metres were determined on the shoreline of Manyas Lake. According to the LRR statistic, a maximum change of 33.18 m/year, a minimum change of -9.9 m/year and an average change of 3.44 m/year were calculated on the shoreline of Manyas Lake. From 1980 to 2020, 5.85 km2 coastal accretion, 1.03 km2 coastal erosion and 146.5 km2 permanent lake surface area data were determined on the surface area and shores of Manyas Lake. The data reveal that the lakeshore is progressing in the long term and the lake surface area is shrinking. Especially in the Manyas Creek delta and the reedbed area to the west, in the reed islets around the Karaçay drainage and in the small deltas on the eastern shores, coastal accumulation and coastal erosion in the north of the lake were detected. When the NSM, SCE, EPR and LRR analyses of the monthly satellite images of Manyas Lake in 2022 were examined, it was calculated that the change amplitude exceeded 800 m. The lake surface area reaches the peak width in April and the narrowest area in July-August for the year 2022. This situation is observed as the natural dynamic process of the wetland ecosystem structure of the lake. It was

determined that the average shore change distance of Manyas Lake in 2022 was 18 m and the average change in linear regression was 43 m/year. All the findings obtained show that Manyas Lake has experienced less water loss than other lakes in Turkey in the 40-year period, but the loss of lake surface area in the future may be higher. It was also determined in the study that shoreline changes in Manyas Lake are intensely experienced as a result of natural and anthropogenic processes. In particular, it was determined that the lake surface area narrowed in the long term and the shoreline progressed in the southern part. This situation shows that the lake, which is within the scope of Ramsar, is open to future threats and the ecological structure may be affected. In particular, water use originating from agricultural areas around the lake should be modelled and controlled accordingly, and basin-based planning should be made in the rivers that source the lake.

Author contributions

The study was conducted by a single author.

Conflicts of Interest

The author declares no conflict of interest.

Research and publication ethics statement

In the study, the author declares that there is no violation of research and publication ethics and that the study does not require ethics committee approval.

REFERENCES

Akdeniz, H. B. & İnam, Ş. (2023). Spatio-temporal analysis of shoreline changes and future forecasting: the case of Küçük Menderes Delta, Türkiye. *Journal of Coastal Conservation*, 27, 34. https://doi.org/10.1007/s11852-023-00966-8

Aksoy, T., Serhat, S. A. R. I., & Çabuk, A. (2019). Sulak alanların yönetimi kapsamında su indeksinin uzaktan algılama ile tespiti, Göller Yöresi (in Turkish). *GSI Journals Serie B: Advancements in Business and Economics*, 2(1), 35-48.

Alevkayalı, Ç., Atayeter, Y., Yayla, O, Bilgin, T. & Akpınar, H. (2023). Long-term coastline changes and climate relationship in Burdur Lake: Spatio-temporal trends and forecasts. *Turkish Geographical Review,* 82, 37-50. https://doi.org/10.17211/tcd.1287976

Ataol, M., Kale, M. M. & Tekkanat, İ. S. (2019) Assessment of the changes in shoreline using digital shoreline analysis system: a case study of Kızılırmak Delta in northern Turkey from 1951 to 2017. *Environ Earth Sci*, 78, 579. https://doi.org/10.1007/s12665-019-8591-7

Ataol, M. & Onmuş, O. (2021). Wetland loss in Turkey over a hundred years: implications for conservation and management. *Ecosystem Health and Sustainability,* 7(1), 1-13. https://dx.doi.org/10.1080/20964129.2021.1930587

Aydın, F., Erlat, E. & Türkeş, M. (2020). Impact of climate variability on the surface of Lake Tuz (Turkey), 1985–2016. *Reg Environ Change*, 20, 68. https://doi.org/10.1007/s10113-020-01656-z

Bahadır, M. (2013). Determination of Spatial Changes of Akşehir Lake with Remote Perception Techniques. *Marmara Geographical Review,* 28, 246-275.

Bombino, G., Barbaro, G., D'Agostino, D., Denisi, P., Foti, G., Labate, A. & Zimbone, S. M. (2022). Shoreline change and coastal erosion: the role of check dams. first indications from a case study in Calabria, Southern Italy. *CATENA*, 217. https://doi.org/10.1016/j.catena.2022.106494

Bird, E. (2008). Coastal geomorphology: An introduction Second edition. *John Wiley & Sons.*

Çoban, H., Koç, Ş. & Kale, M. M. (2020). Shoreline changes (1984 – 2019) in the Çoruh delta (Georgia/Batumi). *International Journal of Geography and Geography Education (IGGE),* 42, 589-601. https://doi.org/10.32003/igge.741573

Darwish, K., Smith, S. E., Torab, M., Monsef, H. & Hussein, O. (2017). Geomorphological Changes along the Nile Delta Coastline between 1945 and 2015 Detected Using Satellite Remote Sensing and GIS. *J. Coast. Res,* 33(4): 786–794. http://dx.doi.org/10.2112/JCOASTRES-D-16-00056.1

Davidson-Arnott, R. (2010). Introduction to Coastal Processes and Geomorphology. *University Press Cambridge.*

Davidson, N. C. & Finlayson, C. M. (2018). Extent, Regional Distribution and Changes in Area of Different Classes of Wetlands." *Marine and Freshwater Research,* 69, 1525–1533. http://dx.doi.org/10.1071/MF17377

Dereli, M. A. & Tercan, E. (2020). Assessment of Shoreline Changes using Historical Satellite Images and Geospatial Analysis along the Lake Salda in Turkey. *Earth Sci Inform*,13, 709–718. https://doi.org/10.1007/s12145-020-00460-x

Dinç, G. (2023). Unveiling shoreline dynamics and remarkable accretion rates in Lake Eğirdir (Turkey) using DSAS. The implications of climate change on lakes. *Tema. Journal of Land Use, Mobility and Environment*, 95-108. http://dx.doi.org/10.6092/1970-9870/10111

Duru, U. (2017). Shoreline change assessment using multi-temporal satellite images: a case study of Lake Sapanca, NW Turkey. *Environ Monit Assess,* 189, 385. https://doi.org/10.1007/s10661-017-6112-2

Erinç, S. (1986). Kıyılardan Yararlanmada Hukuki Düzenlemelere Jeomorfolojinin Katkısı. Jeomorfolojisi Dergisi, 14, 1-5 (in Turkish).

Erol, O. (1989). Türkiye'de Kıyıların Doğal Niteliği, Kıyı ve Kıyı Varlıklarının Korunmasına İlişkin Kıyı Kanunu ve Uygulamaları Konusunda Jeomorfolojik Yaklaşım. *İstanbul Üniversitesi Deniz Bilimleri ve Coğrafya Enstitüsü,* 6, 15-46 (in Turkish).

Gao, B. C. (1996). NDWI-A normalized difference water index for remote sensing of vegetation liquid water from space. *Remote Sensing of Environment,* 58(3), 257–266. https://doi.org/10.1016/S0034-4257(96)00067-3

Gómez-Pazo, A., Payo, A., Paz-Delgado, M. V. & Delgadillo-Calzadilla, M. A. (2022). Open digital shoreline analysis system: ODSAS v1. 0. *Journal of Marine Science and Engineering*, 10(1), 26. https://doi.org/10.3390/jmse10010026

Grottolli, H. Biausque, M. Jackson, D. & Cooper, J. A. (2023). Long-term drivers of shoreline change over two centuries on a headland-embayment beach. *Earth Surface Processes and Landforms,*, 1-21. https://doi.org/10.1002/esp.5641

Hakkou, M., Maanan, M., Belrhaba, T., El khalidi, K., El Ouai, D. & Benmohammadi, A. (2018). Multi-decadal assessment of shoreline changes using geospatial tools and automatic computation in Kenitra coast, Morocco. *Ocean & Coastal Management,* 163, 232–239. https://doi.org/10.1016/j.ocecoaman.2018.07.003

Himmelstoss, E. A., Henderson, R. E., Kratzmann, M. G. & Farris, A. S. (2018). Digital Shoreline Analysis System (DSAS) Version 5.0 User Guide (No. 2018-1179). *US Geological Survey*.

Hossain, S. Yasir, M. Wang, P. Ullah, S. Jahan, M., Hui, S. & Zhao, Z., (2021). Automatic shoreline extraction and change detection: A study on the southeast coast of Bangladesh. *Marine Geology,* 441, 1-15. https://doi.org/10.1016/j.margeo.2021.106628

Hoşgören, M. Y. (1994). Lakes of Turkey. *Turkish Geographical Review*, 29, 19-51.

Hu, X. & Wang, Y. (2020). Coastline Fractal Dimension of Mainland, Island, and Estuaries Using Multi-temporal Landsat Remote Sensing Data from 1978 to 2018: A Case Study of the Pearl River Estuary Area. *Remote Sensing*, 12, 2482. https://doi.org/10.3390/rs12152482

Janki, S., Klop, K. W., Dooper, I. M., Weimar, W., Ijzermans, J. N. & Kok, N. F. (2015). More than a decade after live donor nephrectomy: a prospective cohort study. *Transplant International,* 28(11), 1268-1275. https://doi.org/10.1111/tri.12589

Kale, M. M., Ataol, M. & Tekkanat, İ. S. (2019). Assessment of shoreline alterations using a Digital Shoreline Analysis System: a case study of changes in the Yeşilırmak Delta in northern Turkey from 1953 to 2017. *Environ Monit Assess,* 191, 398. https://doi.org/10.1007/s10661-019-7535-8

Kaya, Y., Sanli, F. B. & Abdikan, S. (2023). Determination of long-term volume change in lakes by integration of UAV and satellite data: the case of Lake Burdur in Türkiye. *Environ Sci Pollut Res*, 30, 117729–117747. https://doi.org/10.1007/s11356-023-30369-z

Kazı, H. & Karabulut, M. (2023). Monitoring the shoreline changes of the Göksu Delta (Türkiye) using geographical information technologies and predictions for the near future. International *Journal of Geography and Geography Education,* 50, 329-352. https://doi.org/10.32003/igge.1304403

Khorshiddoust, A. M., Patel, N., Khalilzadeh, E. Bostanaba, A. S. & Tajbar, S., (2022). A comparative study of the surface level changes of Urmia Lake and Aral Lake during the period of 1988 to 2018 using satellite images*. Front. Earth Science*. https://doi.org/10.1007/s11707-022-1010-5

Kılar, H. & Çiçek, İ. (2018). Shoreline Change Analysis in Göksu Delta by Using DSAS. *Turkish Journal of Geographical Sciences,* 16(1), 89-104. https://doi.org/10.1501/Cogbil_0000000192

Kılar, H. (2023). Shoreline change assessment using DSAS technique: A case study on the coast of Meriç Delta (NW Türkiye). *Regional Studies in Marine Science,* 57, 102737. https://doi.org/10.1016/j.rsma.2022.102737

Kuleli, T. (2010). Quantitative analysis of shoreline changes at the Mediterranean Coast in Turkey *Environ. Monit. Assess*., 167, 387–397. https://doi.org/10.1007/s10661-009-1057-8

Lazuardi, Z., Karim, A. & Sugianto, S. (2022). Analisis Perubahan Garis Pantai Menggunakan Digital Shoreline Analysis System (DSAS) di Pesisir Timur Kota Sabang. *Jurnal Ilmiah Mahasiswa Pertanian,* 7(1), 662-676.

Maltby, E. & Barker, T. (2009). The Wetlands Handbook. *John Wiley & Sons*. ISBN:978-0-632-05255-4.

McDonald, A. J., Gemmell, F. M. & Lewis, P. E. (1998). Investigation of the utility of spectral vegetation indices for determining information on coniferous forests. *Remote Sensing of Environment,* 66(3), 250-272. https://doi.org/10.1016/S0034-4257(98)00057-1

McFeeters, S. K. (1996). The use of the Normalized Difference Water Index (NDWI) in the delineation of open water features, *International Journal of Remote Sensing,* 17:7, 1425-1432, http://doi.org/10.1080/01431169608948714

Myneni, R. B., Hall, F. G., Sellers, P. J. & Marshak, A. L. (1995). The interpretation of spectral vegetation indexes. *IEEE Transactions on Geoscience and remote Sensing*, 33(2), 481-486. https://doi.org/10.1016/0034-4257(94)00073-V

Murray, J., Adam, E., Woodborne, S., Miller, D., Xulu, S. & Evans, M. (2023). Monitoring shoreline

changes along the southwestern coast of South Africa from 1937 to 2020 using varied remote sensing data and approaches. *Remote Sensing*, 15(2), 317. https://doi.org/10.3390/rs15020317

Nassar, K., Mahmod, W. E., Fath, H., Masria, A., Nadaoka, K. & Negm, A. (2019). Shoreline change detection using DSAS technique: Case of North Sinai coast, Egypt. *Marine Georesources & Geotechnology*, 37(1), 81-95. https://doi.org/10.1080/1064119X.2018.1448912

Pardo-Pascual, J. E., Almonacid-Caballer, J., Ruiz, L. A. & Palomar-Vázquez, J. (2012). Automatic extraction of shorelines from Landsat TM and ETM+ multi-temporal images with subpixel precision. *Remote Sensing of Environment*, 123, 1-11. https://doi.org/10.1016/j.rse.2012.02.024

Paz-Delgado, M. V., Payo, A., Gómez-Pazo, A., Beck, A. L. & Savastano, S. (2022). Shoreline Change from Optical and Sar Satellite Imagery at Macro-Tidal Estuarine, Cliffed Open-Coast and Gravel Pocket-Beach Environments. *Journal of Marine Science and Engineering,* 10(5), 561. https://doi.org/10.3390/jmse10050561

Pouye, I., Adjoussi, D.P., Ndione, J.A., Sall, A. (2023). Topography, Slope and Geomorphology's Influences on Shoreline Dynamics along Dakar's Southern Coast, Senegal. *Coasts*, 2023(3), 93–112. https://doi.org/10.3390/coasts3010006

Richardson, A. J. & Wiegand, C. L. (1977). Distinguishing vegetation from soil background information. *Photogrammetric engineering and remote sensing,* 43(12), 1541-1552.

Sakaoğlu, E. & Çepni, O. (2022). Türkiye'deki Tektonik Kökenli Ramsar Göllerinin Uzaktan Algılama Teknikleri ile Analizi (in Turikish). *İksad Pulished House. ISBN: 978-625-8377-54-5.*

Samra, R. M. & Ali, R. R. (2021). Applying DSAS tool to detect coastal changes along Nile Delta, Egypt. The Egyptian *Journal of Remote Sensing and Space Science*, 24(3-1), 463-470. https://doi.org/10.1016/j.ejrs.2020.11.002

Shen, L. & Li, C. (2010) Water body extraction from Landsat ETM+ imagery using adaboost algorithm 18th International *Conference on Geoinformatics, IEEE (2010),* 1-4. https://doi.org/10.1109/GEOINFORMATICS.010.5567762

Sikder, M. S., Wang, J., Allen, G. H., Sheng, Y., Yamazaki, D., Song, C., Ding, M., Crétaux, J. F. & Pavelsky, T. M. (2023). Lake-TopoCat: a global lake drainage topology and catchment database, *Earth Syst. Sci. Data*, 15, 3483–3511, https://doi.org/10.5194/essd-15-3483-2023

Singh, K. V., Setia, R., Sahoo, S., Prasad, A. & Pateriya, B. (2015). Evaluation of NDWI and MNDWI for assessment of waterlogging by integrating digital elevation model and groundwater level. *Geocarto International*, 1-12. https://doi.org/10.1080/10106049.2014.965757

Siyal, A. A., Solangi, G. S., Siyal, P., Babar, M. M. & Ansari, K. (2022). Shoreline change assessment of Indus delta using GIS-DSAS and satellite data. *Regional Studies in Marine Science*, 102405 http://dx.doi.org/10.1016/j.rsma.2022.10245

Song, Y., Shen, Y., Xie, R. & Li, J. (2021). A DSAS-based study of central shoreline change in Jiangsu over 45 years. *Anthropocene Coasts*, 4(1), 115-128. http://dx.doi.org/10.1139/anc-2020-0001

Şenol, H. İ., Kaya, Y., Yiğit, A. Y. & Yakar, M. (2023). Extraction and geospatial analysis of the Hersek Lagoon shoreline with Sentinel-2 satellite data. *Survey Review*, 1–16. https://doi.org/10.1080/00396265.2023.2257969

Tağıl, Ş. & Cürebal, İ. (2005). Remote Sensing and GIS Monitoring of Coastline in Altınova Coast Turkey. Fırat University Journal of Social Sciennces, 15(2), 51-68.

Tian, H., Xu, K., Goes, J. I., Liu, Q., Gomes, H. d. R. & Yang, M. (2020). Shoreline Changes Along the Coast of Mainland China—Time to Pause and Reflect? *ISPRS Int. J. Geo-Inf*, 9, 572. https://doi.org/10.3390/ijgi9100572

Topçu, H. & Atatanır, L. (2021). Determination of temporal changes in Bafa and Azap Lake Surface Areas. *Akademik Ziraat Dergisi*, 10(1), 115-122. https://doi.org/10.29278/azd.792589

Topuz, M. (2018) Investigations Occurred Changes in The Coastal Line of Sarikum Lagoon (Sinop) by Using the Remote Sensing Techniques. *International Journal of Social Science*, 71, 481-493. http://dx.doi.org/10.9761/JASSS7853

Tucker, C. J. (1979). Red and photographic infrared linear combinations for monitoring vegetation. *Remote Sensing of Environment,* 8(2), 127-150. https://doi.org/10.1016/0034-4257(79)90013-0

Turoğlu, H. (2009). The Coastal Law (number 3621) and Its Applied Problems. *Turkish Geographical Review*, 53, 31-40.

Turoğlu, H. (2017). Deniz ve Göllerde Kıyı, Yasal ve Bilimsel Boyutlarıyla Kıyı, *Jeomorfoloji Derneği Yayını,* 1 (in Turkish).

Uzun, M. (2021). Human-Induced Geomorphological Changes and Processes on the Coasts of the Gulf of Izmit. *Journal of Geomorphological Researches*, 7, 61-81. https://doi.org/10.46453/jader.983465

Uzun, S. M. (2023) Analysis of Changing Shoreline with Natural and Anthropogenic Factors in Riva (Istanbul) Coast with Dsas Tool. *Journal of Geomorphological Researches*, 2023(11), 95-113. https://doi.org/10.46453/jader.1335105

Xu, H. (2006). Modification of Normalised difference water index NDWI to enhance open water features in remotely sensed imagery. *International Journal of Remote Sensing*, 27(14), 3025-3033.

https://doi.org/10.1080/01431160600589179

Woolway, R. I., Kraemer, B. M., Lenters, J. D., Merchant, C. J., O'Reilly, C. M. & Sharma, S. (2020). Global lake responses to climate change. *Nature Reviews Earth & Environment*, 1, 388–403, https://doi.org/10.1038/s43017-020-0067-5

Wu, Q., Miao, S., Huang, H., Guo, M., Zhang, L., Yang, L. & Zhou, C. (2022). Quantitative Analysis on Coastline Changes of Yangtze River Delta based on High Spatial Resolution Remote Sensing Images. *Remote Sensing,* 14, 310. https://doi.org/10.3390/rs14020310

Yasir, M., Hui, S., Hongxia, Z., Hossain, S., Fan, H., Zhang, Li. & Jixiang, Z. (2021). A Spatiotemporal Change Detection Analysis of Coastline Data in Qingdao, East China. *Hindawi Scientific Programming,* 1-10. https://doi.org/10.1155/2021/6632450

Zuzek, P. J., Nairn, R. B. & Thieme, S. J. (2003). Spatial and Temporal Considerations for Calculating Shoreline Change Rates in the Great Lakes Basin. *Journal of Coastal Research*, 125–146.

Araştırma Makalesi/Research Article
https://doi.org/10.51489/tuzal.1484324

2024; 6(1); 57-67

Turkish Journal of Remote Sensing

https://dergipark.org.tr/en/pub/tuzal

e-ISSN 2687-4997

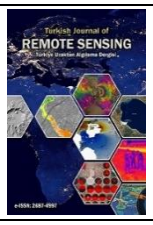

Monitoring and Analysis of Air Quality in Zonguldak Province by Remote Sensing

Nehir Uyar*[1]

[1]Zonguldak Bülent Ecevit University, Zonguldak Vocational School, Architecture and Urban Planning, Zonguldak, Turkey

Keywords
Sentinel-5P TROPOMI
Nitrogen Dioxide
Sulphur Dioxide
Ozone
Carbon Monoxide

ABSTRACT

While air pollution poses a major threat to environmental health, monitoring and understanding this problem is extremely important. Especially in industrial areas, it is a vital requirement to monitor the levels of pollutants such as Nitrogen Dioxide (NO_2), Sulphur Dioxide (SO_2), Ozone (O_3), Formaldehyde (HCHO) and Carbon Monoxide (CO) in the atmosphere. This situation becomes even more critical in areas such as Zonguldak where industrial activities are intense. In this study, the Sentinel-5P TROPOMI satellite and Google Earth Engine (GEE) platform were used to determine the air quality values in Zonguldak province. The study extracted data using coding method to determine the values of pollutants such as NO_2, SO_2, O_3, HCHO and CO in the atmosphere between 2020 and-2022. Coding was performed using satellite data on the GEE platform and thematic maps and graphs were created with the data obtained. According to the results obtained, it was observed that air pollution is intense especially in Ereğli district and Filyos town. Such analyses are extremely important in terms of understanding the pollution levels in certain regions and evaluating their possible environmental impacts. These findings can provide important clues for taking protective measures for environmental health and reducing the effects of industrial activities on the environment.

Uzaktan Algılama ile Zonguldak İlinde Hava Kalitesinin İzlenmesi ve Analizi

Anahtar Kelimeler:
Sentinel-5P TROPOMI
Azot Dioksit
Kükürt Dioksit
Ozon
Karbon Monoksit

ÖZ

Hava kirliliği, çevre sağlığı için büyük bir tehdit oluştururken, bu sorunun izlenmesi ve anlaşılması son derece önemlidir. Özellikle endüstriyel bölgelerde, Azot Dioksit (NO_2), Kükürt Dioksit (SO_2), Ozon (O_3), Formaldehit (HCHO) ve Karbon Monoksit (CO) gibi kirleticilerin atmosferdeki seviyelerini izlemek hayati bir gerekliliktir. Bu durum Zonguldak gibi endüstriyel faaliyetlerin yoğun olduğu bölgelerde daha da kritik bir hal alır. Bu çalışmada, Zonguldak ilindeki hava kalitesi değerlerini belirlemek amacıyla Sentinel-5P TROPOMI uydusu ve Google Earth Engine (GEE) platformunu kullanmıştır. Çalışma, 2020-2022 yılları arasında NO_2, SO_2, O_3, HCHO ve CO gibi kirleticilerin atmosferdeki değerlerini belirlemek üzere kodlama yöntemiyle veri çıkartmıştır. GEE platformunda uydu verileri kullanılarak kodlama yapılmış ve elde edilen verilerle tematik haritalar ve grafikler oluşturulmuştur. Elde edilen sonuçlarına göre özellikle Ereğli ilçesi ve Filyos beldesinde hava kirliliğinin yoğun olduğu gözlemlenmiştir. Bu tür analizler, belirli bölgelerdeki kirlilik seviyelerini anlamak ve olası çevresel etkilerini değerlendirmek açısından son derece önemlidir. Bu tespitler, çevre sağlığı için koruyucu tedbirler alınması ve endüstriyel faaliyetlerin çevreye olan etkilerinin azaltılması açısından önemli ipuçları sunabilir.

Article Info

Received:15/05/2024
Accepted: 28/06/2024
Published: 30/06/2024

Citation:

Uyar, N. (2024). Monitoring and Analysis of Air Quality in Zonguldak Province by Remote Sensing. Turkish Journal of Remote Sensing, 6 (1), 57-67.

***Corresponding Author:** Nehir Uyar, nehiruyar@beun.edu.tr, +90 372 265 6766 (131)

1. INTRODUCTION

Air pollution is the presence of high levels of harmful substances in the atmosphere. These harmful substances are usually caused by human activities such as industrial activities, vehicle emissions, agricultural processes, and energy production. Pollutants such as ozone, particulate matter, carbon monoxide, sulfur dioxide and, nitrogen dioxide can cause air pollution. Air pollution carries serious risks to the environment and human health. It can cause health problems such as respiratory system diseases, heart disease, lung damage, and even cancer. Air pollution also damages ecosystems and can have negative impacts on vegetation, water resources and biodiversity.

Air is a vital component for the survival of living organisms and its cleanliness is extremely important. However, human activities are the main source of environmental air pollution, which poses significant risks to public health. These activities contribute significantly to the emissions of various harmful pollutants (Gautam & Hens, 2020; Ghorani-Azam et al., 2016). Factors such as economic development, energy consumption, urbanization, motor vehicle use, transportation and rapid population growth are known to contribute significantly to air pollution (Kaplan et al., 2019). Particulate matter (PM), SO_2, O_3, NO_2 and CO are the main air pollutants we encounter in our daily lives (Chen et al., 2007). NO_2 plays a critical role in urban air pollution and PM acts as a precursor to acid rain and ground-level ozone (Bechle et al., 2013). Fossil fuel combustion, such as oil, coal, and gas, is the main source of NO_2 in the atmosphere. This highly reactive pollutant is emitted during fossil fuel combustion and is a primary contributor to transport emissions (Muhammad et al., 2020).

Increasing greenhouse gas emissions are a global concern of harmful consequences leading to climate change (Jain, 1993). Components such as sulfur dioxide and nitrogen oxides react with other chemicals in the atmosphere, leading directly to the production of greenhouse gases and indirectly affecting global warming. In addition, SO_2 emissions are known to reduce the atmosphere's oxidation capacity. Therefore, increased emissions accelerate the accumulation of greenhouse gases and other pollutants in the atmosphere (Ward, 2009).

O_3 is formed by the oxidation of CO, CH_4 (methane), non-methane hydrocarbons and other volatile organic compounds under the influence of sunlight in the troposphere (Badarinath et al., 2012). Assessing the level of ozone is quite complex because it depends on the presence of nitrogen oxides, cloud cover, level of exposure to sunlight and population density in each area. Furthermore, the effect of aerosols on the surface ozone is uncertain; this effect may vary depending on the optical properties, chemical composition, and loss of regional aerosols (Li et al., 2011).

HCHO (formaldehyde) is a carcinogenic trace gas and a toxic pollutant in the atmosphere (Tesfaye et al., 2020). The US Environmental Protection Agency (EPA) considers it one of the most important outdoor carcinogens among 187 harmful air pollutants (Scheffe et al., 2016; Blair et al., 1990). HCHO, the most common aldehyde in the atmosphere, is one of the main volatile organic compounds and pollutants in the troposphere (Jin et al., 2020).

About 40 percent of carbon monoxide (CO) in the atmosphere originates from natural sources, especially factors such as volcanic eruptions, natural gas emissions, degradation of vegetation and animals, and forest fires (Varma et al., 2009). The remaining 60 percent comes from anthropogenic factors such as fossil fuel consumption, garbage disposal, tobacco smoke and charcoal fires (Vreman et al., 2000).

Carbon monoxide in the troposphere is generally not perceived as a serious health problem outdoors. However, recent research suggests that exposure to high concentrations of carbon monoxide, especially in urban areas, may have a possible association with heart problems (Andre et al., 2010). This suggests that CO should be considered not only in terms of its environment but also in terms of its possible effects on human health.

The economy of the Zonguldak is mainly based on coal mining. Therefore, Zonguldak is one of the most problematic provinces in Türkiye in terms of air pollution. The main source of air pollution in Zonguldak is coal-fired thermal power plants. These power plants generate electricity by burning coal. During the coal burning process, harmful particles, gases and fumes are released into the air. These pollutants can cause respiratory diseases, heart diseases and cancer.

This study investigated the air quality in Zonguldak province, especially the changes in NO_2, SO_2, O_3, HCHO, and CO concentrations. Zonguldak, a region with intensive coal industrial activities, is particularly important to air quality problems.

In the data processing and analysis phase, the increase in large geographic data, cloud computing technologies and big data processing services are important factors shaping future Remote Sensing applications. Without the challenges of traditional data analysis methods, Google Earth Engine enables scientists, experts, and to extract meaningful information from large remote sensing datasets quickly (Amani et al., 2020). In this study, we investigated the changes in air quality and pollution in Zonguldak province using Sentinel-5P/TROPOMI satellite data on the GEE platform.

2. MATERIAL and METHOD

Zonguldak is an important industrial city located on the Black Sea coast of Türkiye. Figure 1 shows the location of Zonguldak province on the Google Earth platform. With the increase in

industrial activities, the problem of air pollution is also increasing. Many satellite data contain information from advanced sensors used to detect different pollutants in the atmosphere. These data can be used to determine the air pollution in Zonguldak and the sources of pollutants. In this way, authorities can better understand environmental risks and take preventive measures.

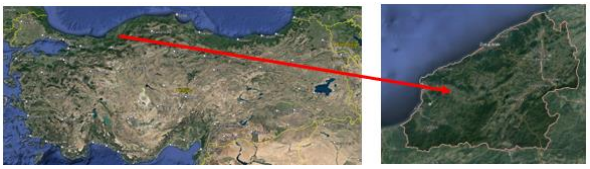

Figure 1. Location of Zonguldak province on the Google Earth platform.

Sentinel-5P, a satellite operated by the European Space Agency (ESA), is designed to measure air pollution parameters. Sentinel-5P is equipped with a sensor called TROPOMI (Tropospheric Monitoring Instrument). TROPOMI is a spectrometer operating in the UV-Vis (Ultraviolet-Visible) spectrum. This spectrometer measures the emission of pollutant molecules in the air and determines the concentration of these pollutants.

Launched on 13 October 2017, Sentinel-5 Precursor (Sentinel-5 P) is the first Copernicus mission satellite dedicated to monitoring the atmosphere. Sentinel 5P is equipped with a spectrometer called TROPOMI, which measures high spectral irradiances of ultraviolet earthlight. TROPOMI maps the global atmosphere daily with a resolution of 7 km × 3.5 km (Theys et al., 2019).

In this article, NO_2, SO_2, O_3, HCHO and CO parameters were analysed on the Google Earth Engine platform using Sentinel-5P, TROPOMI satellite.

NO_2, SO_2, O_3, HCHO and CO pose a serious threat to human health and the environment. These pollutants can cause respiratory diseases, heart diseases, cancer, and adverse effects on vegetation and the environment. The Sentinel-5P TROPOMI satellite is designed to monitor pollutant gases in the atmosphere with high resolution. Sentinel 5 data is readily available on the GEE platform, and data can be processed, analyzed, and visualized.

While air pollution is a major environmental health threat, it is extremely important to monitor and understand the problem. Figure 2 shows the workflow diagram. In this study, the Sentinel-5P TROPOMI satellite and the Google Earth Engine (GEE) platform were used to determine air quality levels in Zonguldak province. As a first step of the research, the relationship between air pollution and environmental health was focused and Zonguldak province was selected as the study area. As part of this study, the necessary tools such as satellite data and GIS software were identified and NO_2, SO_2, O_3, HCHO and CO were selected as the pollutants to be monitored in the atmosphere. Satellite data were collected by coding on the GEE platform and pollutant levels between 2020-2022 were extracted. The collected data were transferred to GIS software, spatial analysis was performed, and thematic maps and graphs were created. Air pollution risk map created based on satellite data. It was found that air pollution is intense in Ereğli and Filyos district pollution levels in specific regions were evaluated. Such analyses are extremely important in terms of understanding environmental impacts and taking protective measures. These findings, supported by GIS-based maps and graphics, can provide strategic guidance that is critical to environmental health.

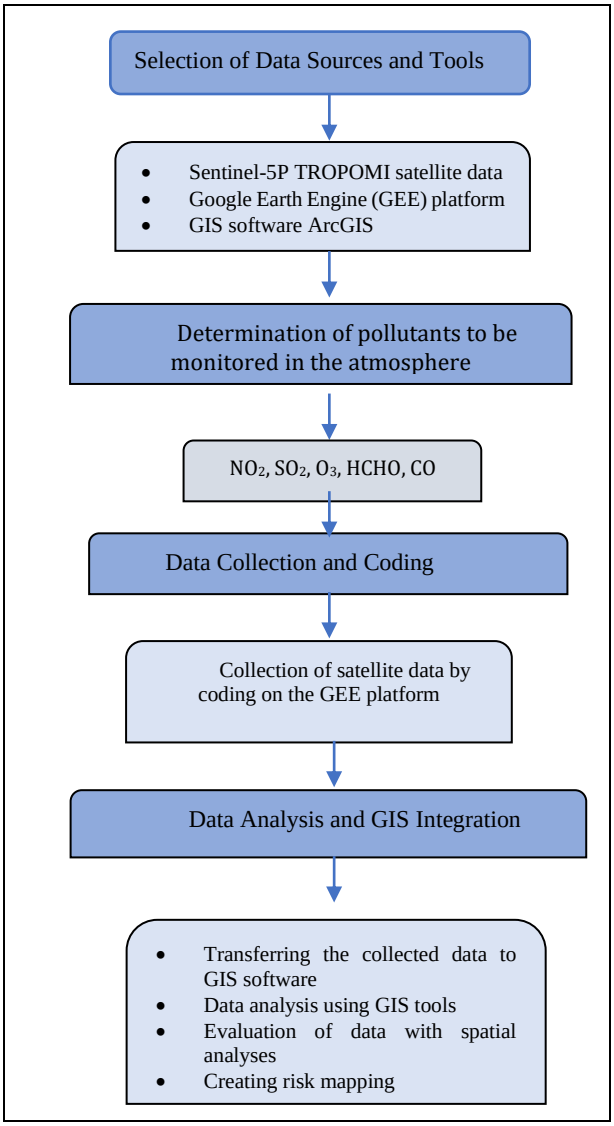

Figure 2. Work flow chart

3. RESULTS

In the study, Sentinel-5P satellite data designed to measure air pollution parameters (NO_2, SO_2, O_3, HCHO and CO) were used Google Earth Engine platform was used to extract these parameters from Sentinel-5P satellite data. In this platform, by writing coding; maps were created, and graphics were obtained to analyze the data.

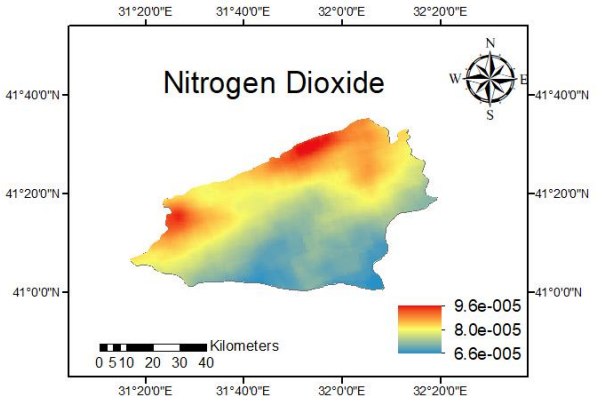

(a)

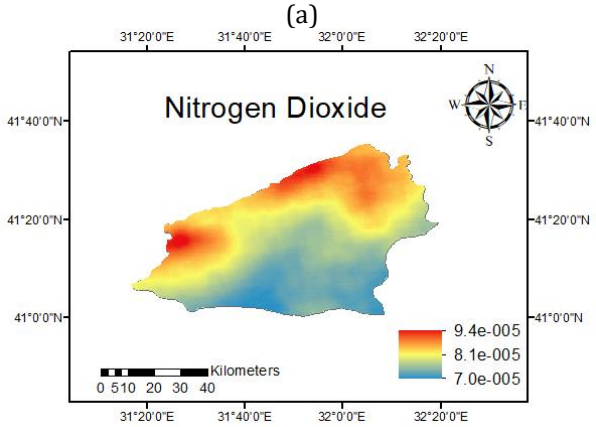

(b)

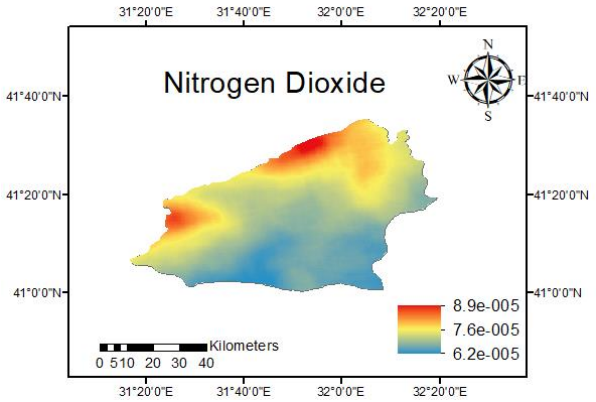

(c)

Figure 3. Thematic maps of NO_2 value for (a) 2022 (b) 2021 (c) 2020.

Figure 3 shows the thematic maps of the NO_2 parameter in 2020-2022. Values range from 9.6e-005 to 6.2e-005. For the year 2020, NO_2 values were observed to reach high values. For the year 2022, it was observed that NO_2 reached the lowest values. Especially in coastal areas, Alaplı, Ereğli, Zonguldak Centre, Kilimli districts and Filyos town, NO_2 parameter is observed to be intense.

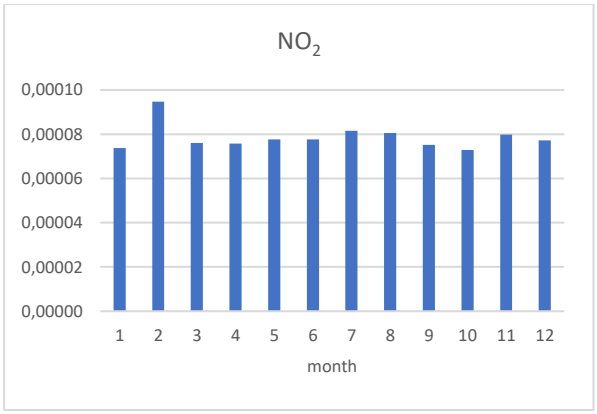

(a)

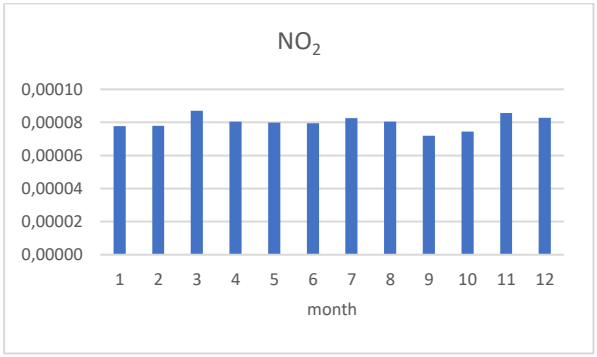

(b)

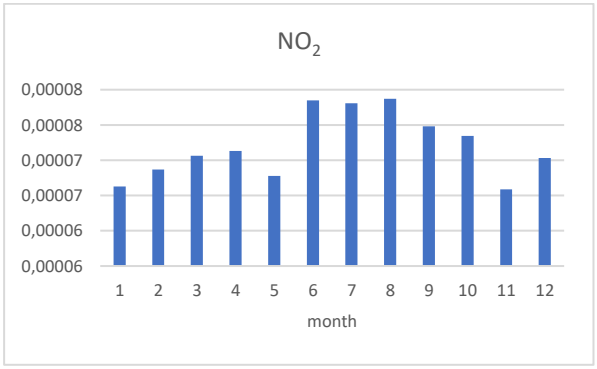

(c)

Figure 4. Charts of average values of NO_2 value for (a) 2022, (b) 2021, (c) 2020.

Figure 4 shows the maximum, minimum and average values of the NO_2 parameter in 2020-2022. For 2022, NO_2 values reached the highest values in February, while the lowest values were observed in May and July. For 2021, NO_2 values reached high values in November, December, and February, while the lowest values were observed in July and August. For 2020, it was observed that NO_2 reached the highest values in August and July, while it reached the lowest values in January and November.

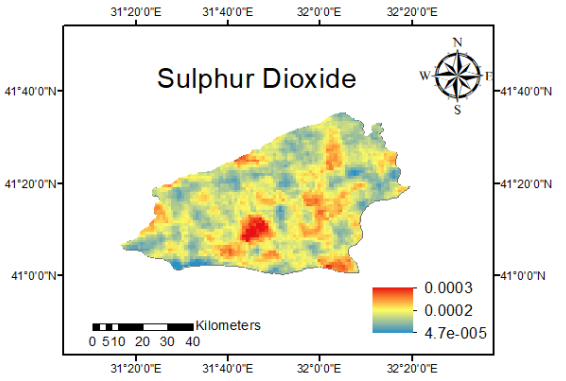

(a)

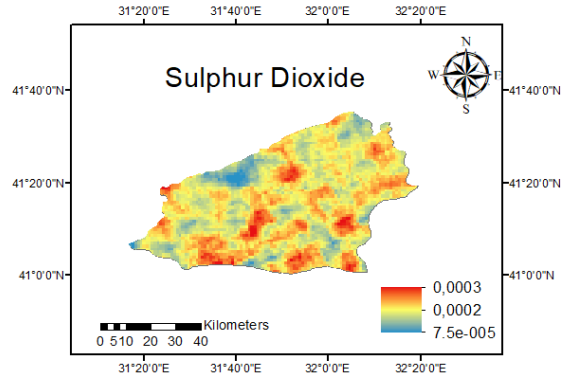

(b)

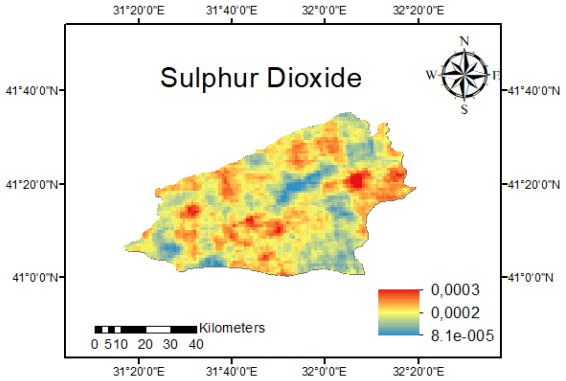

(c)

Figure 5. Thematic maps of SO_2 value for (a) 2022 (b) 2021 (c) 2020.

Figure 5 shows the thematic maps of the SO_2 parameter in 2020-2022. Values range from 0.0003 to 8.1e-005. For 2021, SO_2 values are observed to reach high values. For 2022, it was observed that the SO_2 value reached the lowest values. In 2020 and 2021, it was observed that the SO_2 value of the years 2020 and 2021 was widely observed in the districts of Zonguldak province.

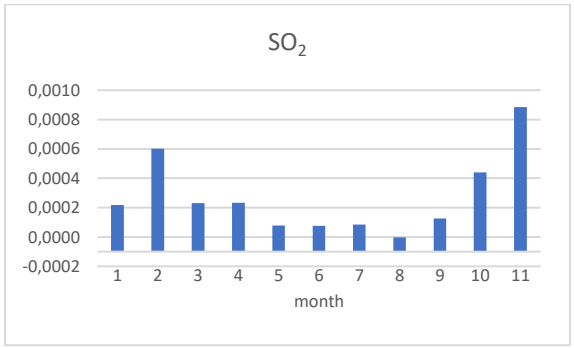

(a)

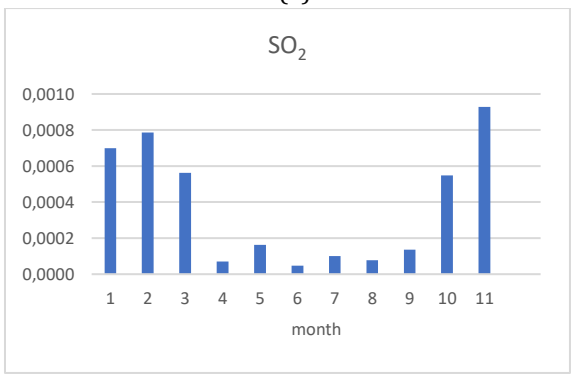

(b)

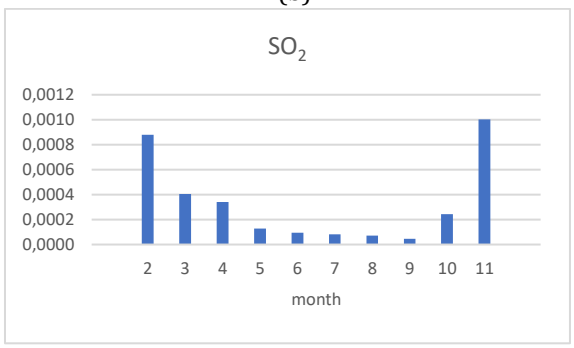

(c)

Figure 6. Charts of average values of SO_2 for (a) 2022, (b) 2021, (c) 2020.

Figure 6 shows the maximum, minimum and average values of SO_2 parameter in 2020-2022. For 2022, SO_2 values are observed to reach high values in November, while reaching the lowest values in August. For 2021, SO_2 values: It is observed that it reaches high values in November, while it reaches the lowest values in August. SO_2 values for 2020: It was observed that it reached high values in November, while it reached the lowest values in August.

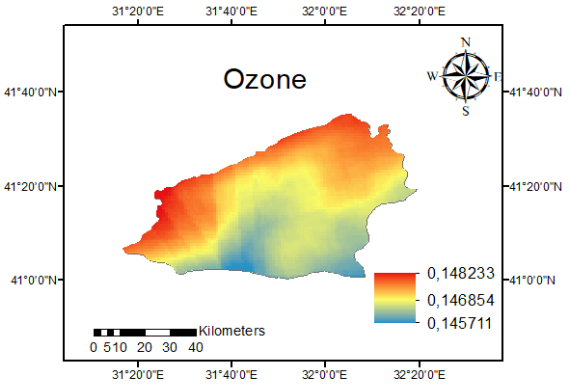

(a)

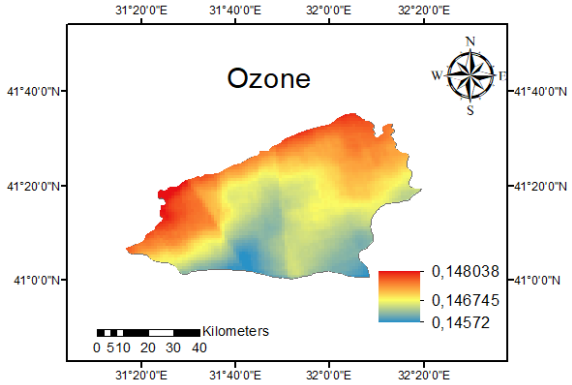

(b)

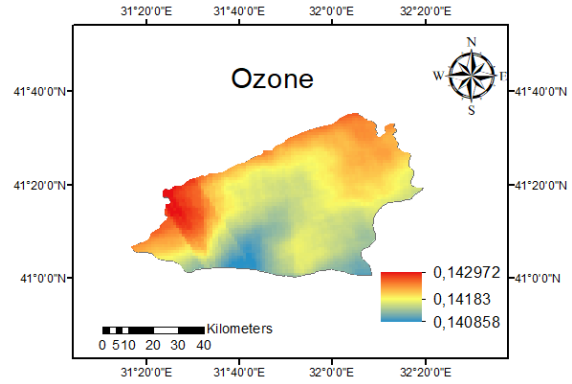

(c)

Figure 7. Thematic maps of O_3 value in (a) 2022 (b) 2021 (c) 2020

Figure 7 shows the thematic maps of the O_3 parameter in 2020-2022. Values range from 0.178 to 0.140. For 2021, O_3 values were observed to reach high values. For 2020, it was observed that O_3 reached the lowest values. The O_3 parameter is intense in the coastal areas of Alaplı, Ereğli, Zonguldak Centre, Kilimli and Çaycuma districts.

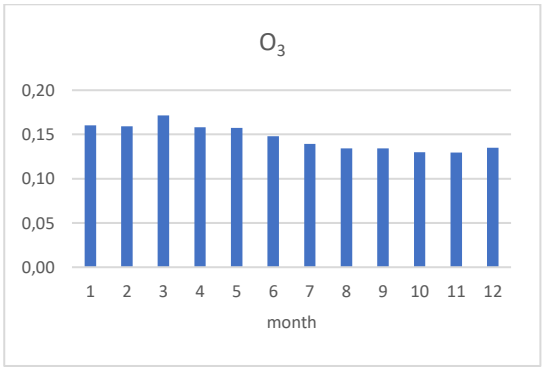

(a)

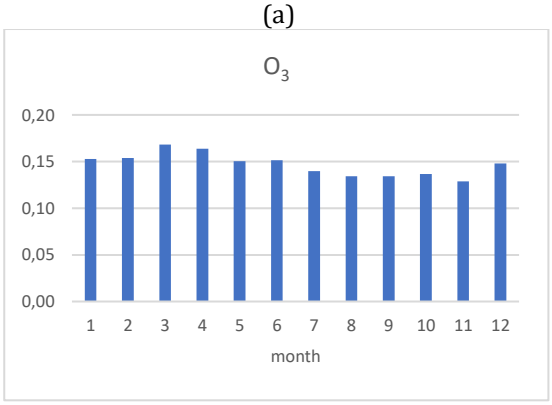

(b)

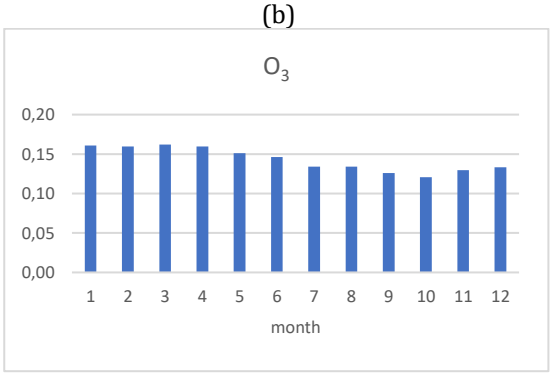

(c)

Figure 8. Schedules of the average values of O_3 in (a) 2022, (b) 2021 (c) 2020

Figure 8 shows the maximum, minimum and average values of the O_3 parameter in 2020-2022. For the year 2022, O_3 values reached high values in March, while they reached the lowest values in November. For the year 2021, O_3 values reached the highest values in March, and the lowest values in November. For 2020, O_3 values reached high values in March, and the lowest values in October.

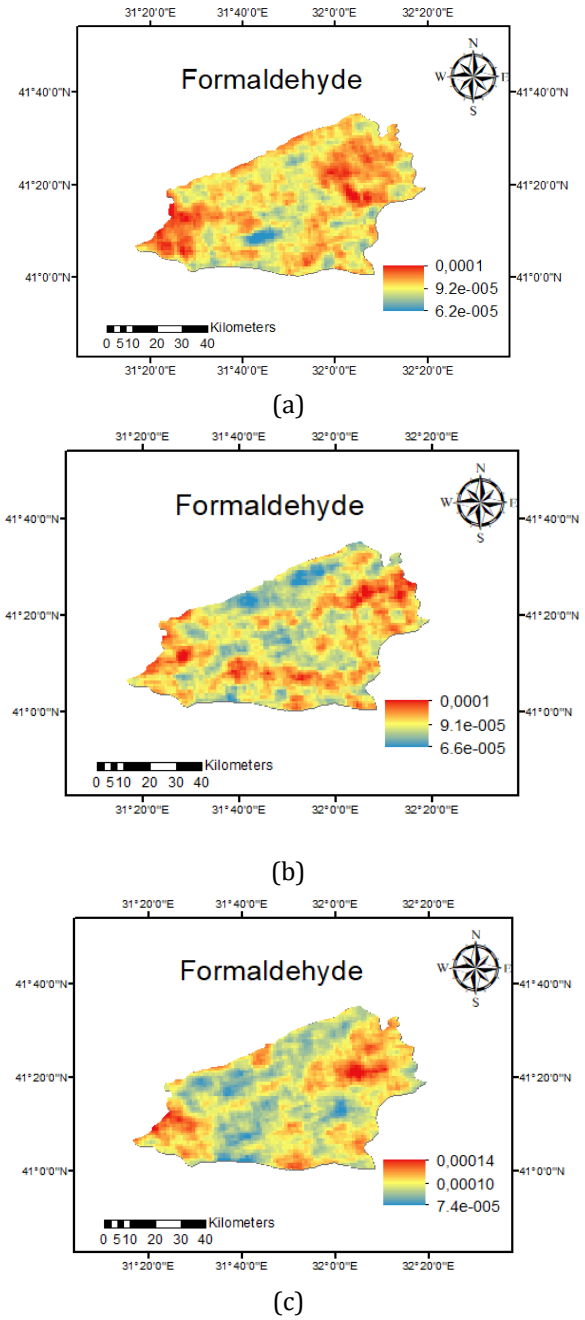

Figure 9. Thematic maps of HCHO value in (a) 2022 (b) 2021 (c) 2020

Figure 9 shows the thematic maps of the HCHO parameter in 2020-2022. Values range from 0.0001 to 7.4e-005. For 2022, it was observed that HCHO values reached high values. For 2021, HCHO reached the lowest values. Especially in Ereğli district and Filyos town, HCHO parameter was observed to be intense.

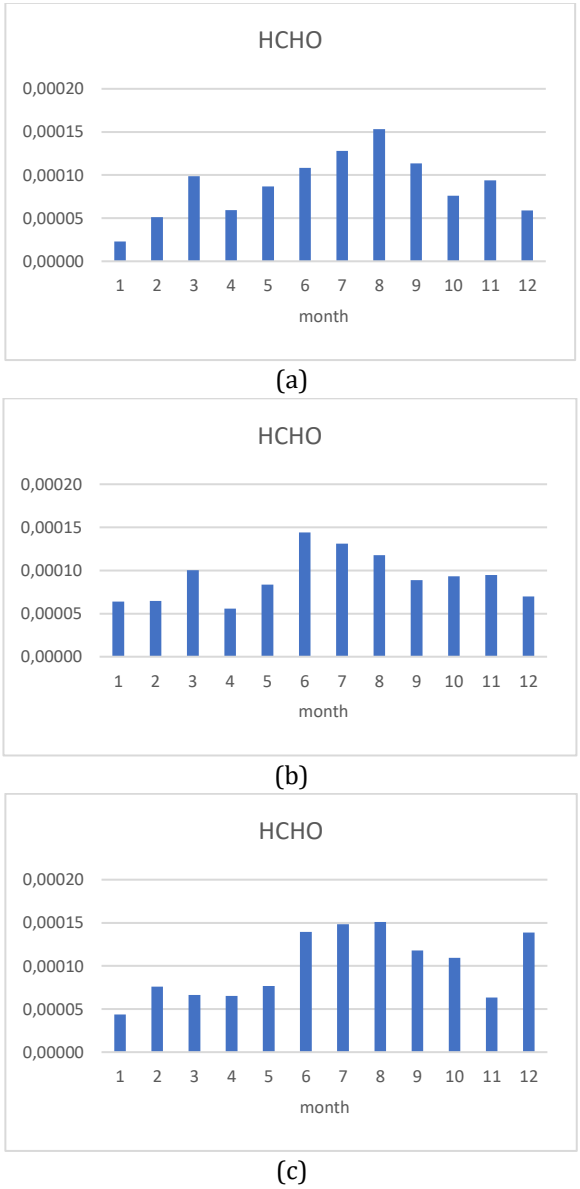

Figure 10. Plots of the average values of HCHO in (a) 2022, (b) 2021, (c) 2020

Figure 10 shows the maximum, minimum and average values of the HCHO parameter in 2020-2022. For 2022, HCHO values are observed to reach the highest values in August, and the lowest values in January. It was observed that HCHO values for 2021 reached the highest values in June and the lowest values in January. For 2020, it was observed that HCHO values reached the highest values in August, and the lowest values in January.

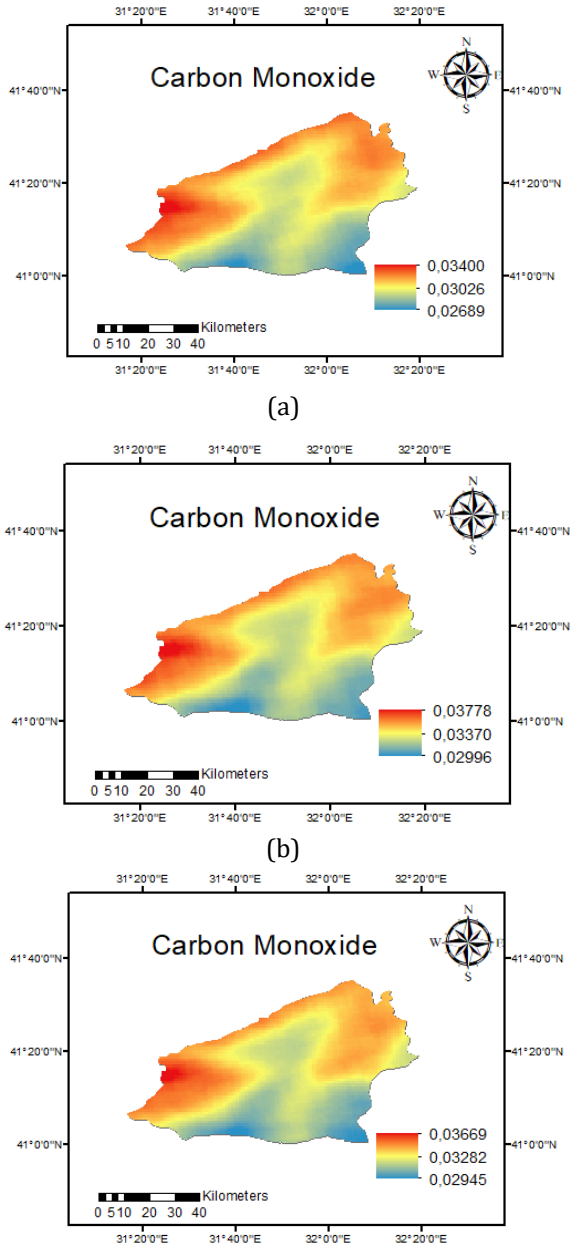

Figure 11. Thematic maps of CO value in (a) 2022 (b) 2021 (c) 2020

Figure 11 shows the thematic maps of the CO parameter in 2020-2022. Values range from 0.037 to 0.026. For 2021, it was observed that CO values reached high values. For 2022, it was observed that CO values reached the lowest values. It was determined that CO levels were high in Alaplı, Ereğli, Zonguldak Centre, Kilimli and Çaycuma districts, especially in coastal areas.

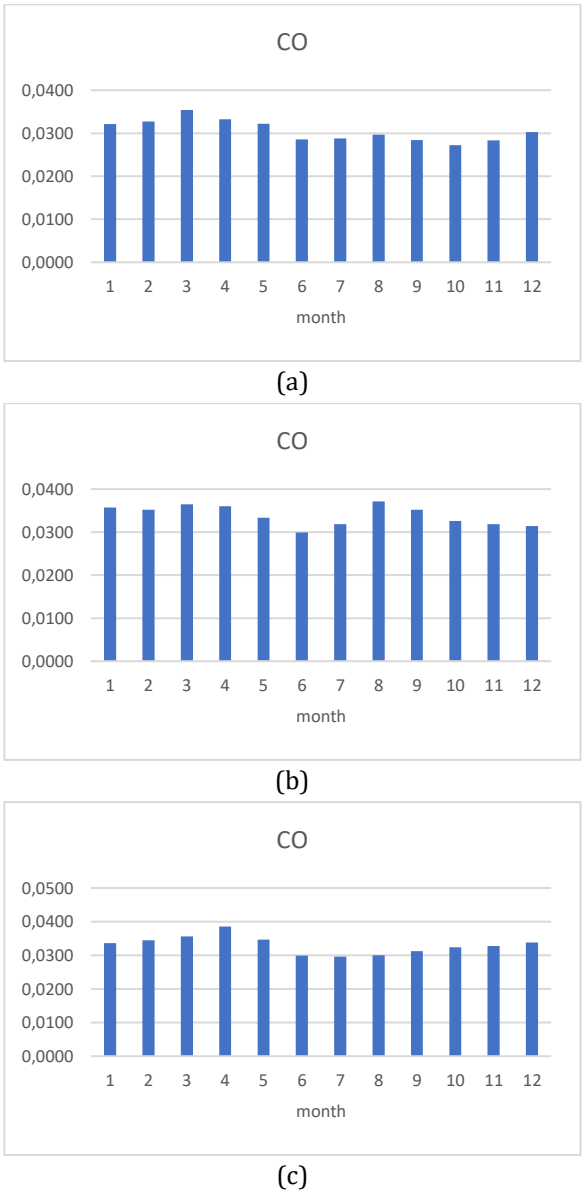

Figure 12. Charts of the average values of CO in (a) 2022, (b) 2021 (c) 2020

Figure 12 shows the maximum, minimum and average values of the CO parameter in 2020-2022. For 2022, CO values are observed to reach the highest values in March, and the lowest values in October. For the year 2021, CO values are observed to be highest in August, and lowest in June. For 2020, it was observed that CO values reached the highest values in April, and the lowest values in July.

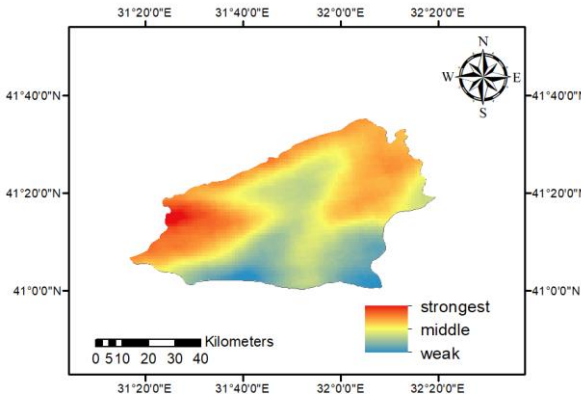

Figure 13. Air pollution risk map created based on satellite data.

Figure 13 shows an air pollution risk map based on satellite data. Air pollution risk map generation process based on satellite data was carried out using Multi-Criteria Decision Analysis (MCDA) model. In this process, the concentration data of NO_2, SO_2, O_3, HCHO, CO pollutants were collected and uploaded to ArcGIS software. Equal weights were assigned to each pollutant in line with their health and environmental impacts. This map helps environmental assessment and decision-making processes by visualizing air pollution risk levels in specific regions. It is critical for understanding the potential impacts of air pollution on human health and the environment, especially in areas with intensive industrial activities. The map consists of color-coded regions according to the concentrations of various pollutants (NO_2, SO_2, O_3, HCHO, CO) in the atmosphere. Red colors indicate areas with higher air pollution risk, while green color represents lower risk levels. According to the results obtained, it is observed that the risk of air pollution is high especially in Ereğli district and Filyos town of Zonguldak province. The intensity of industrial activities in these regions is one of the main factors that negatively affect air quality. The high-risk areas identified on the map emphasize the need for urgent intervention and continuous monitoring for environmental health.

4. CONCLUSION

Air pollution is a factor that seriously affects environmental quality and human health. In recent years, the use of satellite data has gained great momentum in air pollution detection and monitoring efforts. Satellite data have become an important tool for determining air pollution levels over a wide geographical scale, monitoring trends, and identifying pollution sources. These data have the potential to understand air quality in urban areas and support decision makers in environmental planning processes.

Many techniques are employed for space-based air quality and pollutant measurement, with Sentinel-5P being one of the most widely used satellites for this purpose. Sentinel-5P provides detailed data on various atmospheric pollutants, aiding in the comprehensive analysis and investigation of air quality on a global scale (Zheng et al., 1939; Hashim et al., 2021; Vîrghileanu et al., 2020).

The results of the analyses show the distribution of air quality values in Zonguldak province and change over time. This information is important for environmental management and health organisations to monitor air quality and take necessary measures. The Sentinel-5P TROPOMI satellite and the GEE platform are a powerful tool for monitoring and understanding the effects of air pollution. Determining air quality values in Zonguldak province using the Sentinel-5P TROPOMI satellite and GEE platform is important in protecting environmental health and combating air pollution. This method can be similarly applied in other regions and can be a useful resource for monitoring air quality. The results obtained with Sentinel-5P/TROPOMI data can make an important contribution to monitoring the air quality of Zonguldak province, identifying pollution sources and understanding environmental impacts.

Ereğli district and Filyos town stand out among the regions where air pollution is intense. Especially in these areas where industrial activities are intense, it can be associated with the activities of industrial facilities as well as environmental factors. Air pollutants such as NO_2, SO_2, O_3, HCHO and CO were detected at particularly significant levels in these regions.

This study shows that air pollution can be reduced by implementing systematic pollution source control measures within a given time interval. Furthermore, satellite remote sensing-based air pollution observations can provide complete measurements, considering the spatial extent and distribution of the study area. The pollution control decision maker can easily identify regions with high pollution levels and address regional control measures for these areas.

Furthermore, improving long-term data collection and analysis capabilities can be a critical step to identify and combat the impacts of air pollution. In this process, large-scale and remote sensing systems, such as satellite data, can provide a broad perspective on air pollution and, accordingly, can be used in environmental planning and policy-making processes. The use of satellite data for the detection and management of air pollution offers significant benefits to decision-makers in preserving the health and quality of the environment. Therefore, given the high resolution and extensive coverage of satellite imagery, it is critical that future research focuses on developing more efficient and predictive systems.

Acknowledgment

I would like to thank the anonymous reviewers and editors for their valuable comments and suggestions regarding this article.

Author contributions

The study was conducted by a single author.

Conflicts of Interest

The author declares no conflict of interest.

Research and publication ethics statement

In the study, the author declares that there is no violation of research and publication ethics and that the study does not require ethics committee approval.

REFERENCES

Amani, M., Ghorbanian, A., Ahmadi S. A., Moghimi, A., Mirmazloumi, S. M., Hamed, S., Moghaddam, A., Mahdavi, S., Ghahremanloo, M., Parsian, S., Wu, Q. & Brisco, B. (2020). Google Earth Engine cloud computing platform for remote sensing big data applications: a comprehensive review. *IEEE Journal of Selected Topics in Applied Earth Observations and Remote Sensing,* 13, 1-26. https://doi.org/10.1109/JSTARS.2020.3021052

Andre, L., Boissière J., Reboul, C., Perrier, R., Zalvidea, S., Meyer, G., Thireau, J., Tanguy, S., Bideaux P. & Hayot M. (2010). Carbon monoxide pollution promotes cardiac remodeling and ventricular arrhythmia in healthy rats. *American journal of respiratory and critical care medicine,* 181(6), 587-595. https://doi.org/10.1164/rccm.200905-0794OC

Badarinath, K., Kharol, S. K., Prasad, V. K., Sharma, A. R., Reddi, E., Kambezidis, H. & Kaskaoutis, D. (2008). Influence of natural and anthropogenic activities on UV Index variations–a study over tropical urban region using ground-based observations and satellite data. *J Atmos Chem.,* 59(3), 219–236. https://doi.org/10.1007/s10874-008-9103-4

Bechle, M. J., Millet, D. B. & Marshall, J. D. (2013). Remote sensing of NO2 exposure: Satellite and ground-based measurement in a large urban area. *Atmospheric Environment,* 69, 345-353. https://doi.org/10.1016/j.atmosenv.2012.11.046

Blair, A., Saracci, R., Stewart P. A., Hayes, R. & Shy, C. (1990). Epidemiologic evidence on the relationship between formaldehyde exposure and cancer. *Scand. J. Work. Environ. Health*, 16, 381–393.

Chen, T. M., Kuschner, W. G., Gokhale, J., & Shofer, S. (2007). Outdoor air pollution: nitrogen dioxide, sulfur dioxide, and carbon monoxide health effects. The American journal of the medical sciences, 333(4), 249-256. https://doi.org/10.1097/MAJ.0b013e31803b900f

Gautam, S. & Hens, L. (2020). SARS-CoV-2 outbreak in India: What can we expect? *Environment, Development and Sustainability,* 22(5), 3867-3869.

Ghorani-Azam, A., Riahi-Zanjani, B. & Balali-Mood, M. (2016). Effects of air pollution on human health and practical measures for prevention in Iran. *Journal of research in medical sciences*, 21(1), 65. https://doi.org/10.4103/1735-1995.189646

Hashim, B. M., Al-Naseri, S. K., Al-Maliki, A. & Al-Ansari, N. (2021). Impact of COVID-19 lockdown on NO2, O3, PM2. 5 and PM10 concentrations and assessing air quality changes in Baghdad, Iraq. *Science of the Total Environment*, 754, 141978. https://doi.org/10.1016/j.scitotenv.2020.141978

Jain, P. C. (1993). Greenhouse effect and climate change: scientific basis and overview. *Renew Energy,* 3, 403- 420.

Jin, X., Fiore, A., Boersma, K. F., Smedt, I. D. & Valin, L. (2020). Inferring changes in summertime surface Ozone–NO x–VOC chemistry over US urban areas from two decades of satellite and ground-based observations. Environmental science & technology, 54(11), 6518-6529. https://doi.org/10.1021/acs.est.9b07785

Kaplan, G., Avdan, Z. Y., & Avdan, U. (2019). Spaceborne nitrogen dioxide observations from the Sentinel-5P TROPOMI over Turkey. In International *Electronic Conference on Remote Sensing*, 18(1), 4. https://doi.org/10.3390/ECRS-3-06181

Li, G., Zavala, M., Lei W., Tsimpidi, A., Karydis, V., Pandis, S. N., Canagaratna, M. & Molina, L. (2011). Simulations of organic aerosol concentrations in Mexico City using the WRF-CHEM model during the MCMA-2006/MILAGRO campaign. *Atmos Chem Phys.,* 11(8), 3789–3809. https://doi.org/10.5194/acp-11-3789-2011

Muhammad, S., Long, X., & Salman, M. (2020). COVID-19 pandemic and environmental pollution: A blessing in disguise? *Science of the total environment,* 728, 138820. https://doi.org/10.1016/j.scitotenv.2020.138820

Scheffe R. D., Strum M., Phillips S. B., Thurman J., Eyth A., Fudge S., Morris M. & Palma T. (2016). Cook, R. Hybrid Modeling Approach to Estimate Exposures of Hazardous Air Pollutants (HAPs) for the National Air Toxics Assessment (NATA). *Environ. Sci. Technol.,* 50, 12356–12364. https://doi.org/10.1021/acs.est.6b04752

Tesfaye, S., Hamba, N., Gerbi, A. & Neger, Z. (2020). Oxidative Stress and Carcinogenic Effect of Formaldehyde Exposure: Systematic Review & Analysis. *Endocrinol. Metab. Syndr*. 9(6), 319-330.

Theys, N., Hedelt, P., Smedt, I., Lerot, C., Yu, H., Vlietinck, J., Pedergnana, M., Arellano, S., Galle, B., Fernandez, D., Carlito, C. J. M., Barrington, C., Taisne, B., Delgado-Granados, H., Loyola, D., Roozendael, V. M. (2019). Global monitoring of the volcanic SO2 degassing process with unprecedented resolution from TROPOMI on board the Sentinel-5 Precursor ship Science. *Representative*, 9, 2643.

Varma, D. R., Mulay, S. & Chemtob, S. (2009). Carbon monoxide: from public health risk to painless killer. In Handbook of toxicology of chemical warfare agents. *Academic Press*, 271-292.

Vîrghileanu, M., Săvulescu, I., Mihai, B. A., Nistor, C., & Dobre, R. (2020). Nitrogen Dioxide (NO2) Pollution monitoring with Sentinel-5P satellite imagery over Europe during the coronavirus pandemic outbreak. *Remote Sensing*, 12(21), 3575. https://doi.org/10.3390/rs12213575

Vreman, H. J., Wong, R. J. & Stevenson, D. K. (2000). Carbon monoxide in breath, blood, and other tissues. *Carbon monoxide toxicity*, 1, 19-60.

Ward, P. L. (2009). Sulfur dioxide initiates global climate change in four ways. *Thin solid films*, 517(11), 3188-3203. https://doi.org/10.1016/j.tsf.2009.01.005

Zheng, Z., Yang, Z., Wu, Z., & Marinello, F. (2019). Spatial variation of NO2 and its impact factors in China: An application of sentinel-5P products. *Remote Sensing,* 11(16), 1939. https://doi.org/10.3390/rs11161939